

The University of British Columbia

FACULTY OF GRADUATE STUDIES

PROGRAMME OF THE

FINAL ORAL EXAMINATION

FOR THE DEGREE OF

DOCTOR OF PHILOSOPHY

OF

KROVVIDI LALITA

B.Sc. Andhra University, Waltair, India, 1956

M.Sc. Andhra University, Waltair, India, 1959

IN ROOM 302, HENNINGS BUILDING

COMMITTEE IN CHARGE

Chairman: I. McT. Cowan

M. Bloom

J. Marko

B. G. Turrell

R. F. Snider

D. L. Williams

L. W. Reeves

External Examiner: J. S. Waugh
Massachusetts Institute of Technology
Cambridge, Mass.

Research Supervisor: M. Bloom

3:30 p.m., March 28, 1967

ABSTRACT

The spin-lattice relaxation time has been studied in normal H_2 as a function of density and temperature in the range $293^\circ K - 700^\circ K$. The measurements were made in the region where $T_1 \propto \rho$. The H_2 results have been interpreted using the Bloom-Oppenheim theory in which the transitions between different J states were taken into account. The analysis indicates that the resonant transitions $(1,3 \leftrightarrow 3,1)$ and quasi-resonant transitions $(1,2 \leftrightarrow 3,0)$ and $(1,4 \leftrightarrow 3,2)$ contribute significantly to the relaxation mechanism. The anisotropic intermolecular potential between the two H_2 molecules which depends on the orientation of both the molecules could be given by quadrupole-quadrupole interaction while the part that depends on the orientation of one of the molecules alone was found to be adequately represented by a Lennard-Jones potential.

T_1 was measured in $H_2 - He$ and $H_2 - CO_2$ mixtures as a function of density and composition in the temperature range $293^\circ K - 700^\circ K$. The analysis indicates that the interaction potential for $H_2 - He$ could be adequately described by a Lennard-Jones potential while the dominant interaction for $H_2 - CO_2$ could be given by quadrupole-quadrupole interaction. There were indications that the dependence of T_1/ρ in $H_2 - He$ mixture on the percentage of He is non-linear above $150^\circ K$. However, this was not found to be the case in $H_2 - CO_2$ mixtures.

T_1 was also measured in CH_4 and CH_4 - He mixture as a function of density and composition in the same temperature range. The data can be fitted by $\tau_1/\rho = AT^{-n}$ where n takes the value of 1.5 for pure CH_4 and 0.79 for CH_4 gas infinitely diluted in He. The analysis based on the existing theory for polyatomic gases shows that the intermolecular potential for CH_4 - CH_4 and CH_4 - He could be described by medium range potentials. The results indicate that the dependence of τ_1/ρ on the percentage of He is not linear below 400°K .

AWARDS

1956	University First:	Gold Medal
1959	University First:	Gold Medal
1962		Commonwealth Scholarship

GRADUATE STUDIES

Field of Study: Nuclear Magnetic Resonance

Elementary Quantum Mechanics	W. Opechowski
Electromagnetic Theory	G. M. Volkoff
Advanced Magnetism	M. Bloom
Statistical Mechanics	R. Barrie
Quantum Theory of Solids	W. Opechowski

NUCLEAR SPIN RELAXATION IN GAS MIXTURES

by

KROVVIDI LALITA

B.Sc., Andhra University, Waltair, 1956

M.Sc., Andhra University, Waltair, 1959

A THESIS SUBMITTED IN PARTIAL FULFILMENT OF
THE REQUIREMENTS FOR THE DEGREE OF
DOCTOR OF PHILOSOPHY

in the Department

of

PHYSICS

We accept this thesis as conforming to the
required standard

THE UNIVERSITY OF BRITISH COLUMBIA

MARCH, 1967

In presenting this thesis in partial fulfilment of the requirements for an advanced degree at the University of British Columbia, I agree that the Library shall make it freely available for reference and study. I further agree that permission for extensive copying of this thesis for scholarly purposes may be granted by the Head of my Department or by his representatives. It is understood that copying or publication of this thesis for financial gain shall not be allowed without my written permission.

Department of Physics

The University of British Columbia
Vancouver 8, Canada

Date March 31, 1967

ABSTRACT

The spin-lattice relaxation time has been studied in normal H_2 as a function of density and temperature in the range $293^\circ K - 700^\circ K$. The measurements were made in the region where $T_1 \propto \rho$. The H_2 results have been interpreted using the Bloom-Oppenheim theory in which the transitions between different J states were taken into account. The analysis indicates that the resonant transitions ($1,3 \leftrightarrow 3,1$) and quasi-resonant transitions ($1,2 \leftrightarrow 3,0$) and ($1,4 \leftrightarrow 3,2$) contribute significantly to the relaxation mechanism. The anisotropic intermolecular potential between the two H_2 molecules which depends on the orientation of both the molecules could be given by quadrupole-quadrupole interaction while the part that depends on the orientation of one of the molecules alone was found to be adequately represented by a Lennard-Jones potential,

T_1 was measured in $H_2 - He$ and $H_2 - CO_2$ mixtures as a function of density and composition in the temperature range $293^\circ K - 700^\circ K$. The analysis indicates that the interaction potential for $H_2 - He$ could be adequately described by a Lennard-Jones potential while the dominant interaction for $H_2 - CO_2$ could be given by quadrupole-quadrupole interaction. There were indications that the dependence of T_1/ρ in $H_2 - He$ mixture on the percentage of He is non-linear above $150^\circ K$. However, this was not found to be the case in $H_2 - CO_2$ mixtures.

T_1 was also measured in CH_4 and $CH_4 - He$ mixture as a function of density and composition in the same temperature

range. The data can be fitted by $T_1/\rho = A\tau^{-n}$ where n takes the value of 1.5 for pure CH_4 and 0.79 for CH_4 gas infinitely diluted in He. The analysis based on the existing theory for polyatomic gases shows that the intermolecular potential for $\text{CH}_4 - \text{CH}_4$ and $\text{CH}_4 - \text{He}$ could be described by medium range potentials. The results indicate that the dependence of T_1/ρ on the percentage of He is not linear below 400°K .

TABLE OF CONTENTS

	Page
Abstract.	ii
List of Tables.	vi
List of Illustrations.	vii
Acknowledgements.	xi
CHAPTER I. INTRODUCTION	1
CHAPTER II. APPARATUS AND EXPERIMENTAL TECHNIQUE	7
<u>2.1.</u> Measurement of Spin-lattice relaxation time.	7
<u>2.2.</u> N.M.R. Spectrometer	9
2.2.1. General Remarks	9
2.2.2. Timing Circuit	9
2.2.3. Transmitter	11
2.2.4. Sample Coil	12
2.2.5. Receiver	13
<u>2.3.</u> High-Pressure System	13
<u>2.4.</u> Heater	15
<u>2.5.</u> Mixing of gases: Determination of Concentration	17
CHAPTER III THEORY	25
<u>3.1.</u> Hydrogen	25
<u>3.2.</u> Theory of Relaxation in H ₂	29
3.2.1. Correlation functions of intra-molecular interactions	31
<u>3.3.</u> Application of the theory to some special cases	36
3.3.1. Infrequent transitions between different states of J.	36

	Page
3.3.2. Two-level System	37
<u>3.4.</u> Evaluation of $B_{\ell}(J, J')$ in terms of intermolecular anisotropic interactions.	39
CHAPTER IV EXPERIMENTAL RESULTS AND DISCUSSION	47
<u>4.1.</u> General Remarks	47
<u>4.2.</u> Hydrogen	47
4.2.1. Results	47
4.2.2. Interpretation	51
<u>4.3.</u> H ₂ - He Mixture	68
4.3.1. Results	68
4.3.2. Interpretation	72
<u>4.4.</u> H ₂ - CO ₂ Mixture	81
4.4.1. Results	81
4.4.2. Interpretation	85
CHAPTER V EXPERIMENTAL RESULTS AND DISCUSSION (contd.)	93
<u>5.1.</u> Methane	93
5.1.1. Results	93
5.1.2. Interpretation	98
<u>5.2.</u> CH ₄ - He Mixture	102
5.2.1. Results	102
5.2.2. Interpretation	105
CHAPTER VI CONCLUSIONS AND SUGGESTIONS FOR FURTHER WORK	110
APPENDIX A Circuit Diagrams	114
BIBLIOGRAPHY.	121

LIST OF TABLES

TABLE		Page
I	Fractional population of the rotational states for H ₂ .	28
II	Values of $I(p,n)$ for dilute H ₂ gas including the first quantum correction for a Lennard-Jones isotropic potential for $0.03 \leq \beta\epsilon \leq 0.09$	67
III	$(T_1/\rho)_{H_2-He}$ obtained from extrapolating the experimental data to 100% He.	71

LIST OF ILLUSTRATIONS

Figure		Page
1.	Block diagram of 30Mc. pulsed spectrometer	10
2.	Sample holder	14
3.	High pressure system	16
4.	Density of H ₂ -CO ₂ mixtures as a function of composition	21
5.	Signal strength vs. pressure for H ₂ -CO ₂ mixture at 293°K	23
6.	Signal strength vs. pressure for H ₂ -CO ₂ mixture at 400°K	24
7.	Block diagram of the nature of coupling between nuclear spins and the lattice	29
8a.	T ₁ vs. density at 293°K in H ₂	48
8b.	T ₁ vs. density at 738°K in H ₂	48
9.	T ₁ /ρ as a function of temperature in normal H ₂	50
10.	Theoretical plots of (T ₁ /ρ) _{0.p} /(T ₁ /ρ) _{0.0} as a function of η ₂ '/η ₁ ' as obtained from Eq.(4.2.14)	56
11.	Temperature dependence of (k ₁) ^{H₂-H₂} as obtained from Eq.(4.2.14) and the experimental values of (T ₁ /ρ) _{0.p} /(T ₁ /ρ) _{0.0} and (T ₁ /ρ) for normal H ₂	57
12.	Comparison of experimental values of [k ₁ (T)/k ₁ (200)] ^{H₂-H₂} with the theoretical values using Eq.(4.2.18)	59
13.	Comparison of the experimental values of T ₁ /ρ with the computed values using Eq.(4.2.14) and assuming that only quadrupole-quadrupole interaction is important	61
14.	Temperature dependence of (k ₀) ^{H₂-H₂} as obtained from Eq.(4.2.14) and the experimental values of (T ₁ /ρ) in normal H ₂	62

Figure		Page
15.	Comparison of experimental values of $[k_o(T)/k_o(200)]^{H_2-H_2}$ with the theoretical values using Eqs.(4.2.22) and (4.2.24)	64
16a.	T_1 vs. density at 293°K in H_2 -He mixture	69
16b.	T_1 vs. density at 738°K in H_2 -He mixture	69
17.	Dependence of T_1/ρ on Helium concentration in H_2 -He mixture	70
18.	Temperature dependence of $(k_o)^{H_2-He}$ as obtained from Eq.(4.2.14) and using the experimental values of (T_1/ρ) in H_2 -He mixture	75
19.	Theoretical plots of T_1/ρ vs. %He when Eq.(4.2.14) was normalised with the experimental values at 32.2% He, 77.0% He and 100% He	76
20.	Comparison of the extrapolated values of $(T_1/\rho)_{H_2-He}$ with the computed values using Eq.(4.2.14)	78
21.	Comparison of the experimental values of $[k_o(T)/k_o(293)]^{H_2-He}$ with the theoretical values using Eqs.(4.2.22) and (4.2.24)	79
22.	Dependence of T_1 on density at 293°K for H_2 -CO ₂ mixture	82
23.	Dependence of T_1/ρ on density at 293°K	83
24.	Dependence of T_1/ρ on the percentage of CO ₂ in H_2 -CO ₂ mixture	84
25.	Dependence of $\log(T_1/\rho)_{100\%CO_2}$ on $\log T^\circ K$ for H_2 -CO ₂ mixture	86
26.	Temperature dependence of $(k_o + Ck_1)^{H_2-CO_2}$ as obtained from Eqs.(4.2.14) and (4.4.7.) using the experimental values of T_1/ρ	89
27.	Theoretical plots of T_1/ρ vs. %CO ₂ in H_2 -CO ₂ mixture when Eq.(4.2.14) was normalised with the experimental values at different concentrations of CO ₂	90

Figure		Page
28.	Comparison of $[k_1(T)/k_1(293)]^{H_2-CO_2}$ with the computed values using Eq.(4.2.18)	92
29a.	Dependence of T_1 on density at 293°K for CH_4	94
29b.	Dependence of T_1/ρ on density at 293°K for CH_4	94
30a.	Dependence of T_1 on density at 720°K for CH_4	95
30b.	Dependence of T_1/ρ on density at 720°K for CH_4	95
31.	Dependence of T_1/ρ on temperature for CH_4	96
32.	$\log(T_1/\rho)$ as a function of $\log T^\circ K$ for CH_4	97
33.	Comparison of $[I(6,n)_T/I(6,n)_{293}]^{CH_4-CH_4}$ as obtained from Eq.(5.1.10) with the computed values using the numerical values of the integrals	101
34a.	Dependence of T_1 on density for CH_4 -He mixture at 293°K	103
34b.	Dependence of T_1/ρ on density for CH_4 -He mixture at 293°K	103
35a.	Dependence of T_1 on density for CH_4 -He mixture at 730°K	104
35b.	Dependence of T_1/ρ on density for CH_4 -He mixture at 730°K	104
36.	Dependence of T_1/ρ on Helium concentration in CH_4 -He mixture	106
37.	$\log(T_1/\rho)_{100\%He}$ as a function of $\log T^\circ K$ for CH_4 -He mixture	107
38.	Comparison of $[I(2,n)_T/I(2,n)_{293^\circ K}]^{CH_4-He}$ as obtained from Eq.(5.2.1) with the computed values using the numerical values of the integrals	109
A1.	Transmitter	115
A2.	Power supply	116
A3.	10Mc. crystal standard oscillator	117

Figure		Page
A4.	Wideband amplifier	118
A5.	30Mc. tripler	119
A6.	Pulse sequencer	120

ACKNOWLEDGEMENTS

I wish to express my sincere gratitude to Prof. Myer Bloom for his guidance and constant encouragement throughout this work.

I would like to thank Dr. John D. Noble for his valuable help in the design of the equipment and for many helpful discussions.

I am indebted to Mr. Basanta Sarkar who introduced me to the computer programming and who was always available for assistance in writing the programmes.

My thanks are due to Mr. William Morrison, for constructing the sample holder and for his ready help, to Peter Haas for doing the diagrams in this thesis, and to Mr. John Lees for his assistance in this work.

The scholarship provided by the Commonwealth Scholarship Scheme is gratefully acknowledged. I wish to thank Prof. Myer Bloom for the Research Assistantship from his N.R.C. grant. The financial help given by the P.E.O. Sisterhood is very much appreciated.

The Research was supported by the National Research Council of Canada.

I wish to thank the staff of the Computation Centre at the University of British Columbia for their services in running the programmes.

INTRODUCTION

The techniques of nuclear magnetic resonance are widely used to study the properties of matter in bulk samples. The rate at which the spin system approaches thermodynamic equilibrium with its surroundings, which is characterised by the time constant T_1 in the literature, can be measured experimentally and can be interpreted in terms of intermolecular forces that cause the spins to relax. The aim in this thesis is to extract quantitative information on the intermolecular forces between different molecules from the study of T_1 in gases.

The principles of magnetic resonance will be briefly discussed here and a more complete discussion can be found in the literature¹. The Zeeman energy of a nuclear spin with spin angular momentum $\hbar I$ and a magnetic moment $\mu = \gamma \hbar I$ when placed in an external magnetic field H_0 is given by

$$H = -\vec{\mu} \cdot \vec{H}_0 \quad (1.1.)$$

where H_0 is taken to be in the z-direction.

The energy levels of such a system are given by

$$E_m = -\gamma \hbar H_0 m_I \quad (1.2.)$$

where

$$m_I = I, I-1, \dots, -I$$

If there are N spins weakly interacting with each other and in thermal equilibrium with the "lattice" the fractional populations of these energy levels are given by

$$P_m = \frac{e^{-E_m/kT}}{\sum_{m=-I}^I e^{-E_m/kT}} \quad (1.3.)$$

where T is the "lattice" temperature. "Lattice" here refers to the other degrees of freedom of the sample in which the spins are located. The net magnetisation of the sample is then given by

$$M_0 = N \sum_{m=-I}^I P_m \gamma \hbar m_I$$

$$= N \gamma^2 \hbar^2 I(I+1) / 3 k T \quad (1.4.)$$

where the high temperature approximation $\frac{\gamma \hbar H_0}{k T} \ll 1$ has been made. Neglecting relaxation effects, the equation of motion of the magnetisation \vec{M} is given by

$$\frac{d \vec{M}}{dt} = \gamma \vec{M} \times \vec{H} \quad (1.5.)$$

where \vec{H} is the total magnetic field applied to the sample.

Transforming equation (1.5.) to a reference frame rotating with an angular velocity $\vec{\omega}$, the equation of motion for \vec{M} can be written as

$$\frac{\partial \vec{M}}{\partial t} = \gamma \vec{M} \times \left[\vec{H} + \frac{\vec{\omega}}{\gamma} \right] \quad (1.6.)$$

If $\vec{H} = H_0 \vec{k}$, $\frac{\partial \vec{M}}{\partial t} = 0$ when $\vec{\omega} = -\gamma H_0 \vec{k}$. i.e.

\vec{M} is fixed in the rotating reference frame. In the laboratory reference frame the magnetisation \vec{M} precesses about H_0 at a frequency $\omega = -\gamma H_0$. The angular frequency γH_0 is called "Larmor frequency".

The effect of an additional alternating field $H_1(t) = 2H_1 \cos \omega t$ perpendicular to H_0 can be analysed by breaking the alternating field into two rotating components of amplitude H_1 , one rotating clockwise and the other anti-clockwise. Since one of the two components rotates in the same sense as the precession of the magnetic moment and the other in the opposite direction, it can be

shown that the counter rotating component can be neglected at resonance. Therefore, the total magnetic field can be written to a good approximation as

$$\vec{H} = \vec{H}_0 + H_1 (\vec{i} \cos \omega t + \vec{j} \sin \omega t) \quad (1.7)$$

where $\vec{H}_1(t) = H_1 [\vec{i} \cos \omega t + \vec{j} \sin \omega t]$

If the x-axis of the rotating reference frame is chosen to be along H_1 , then H_1 is fixed in this frame of reference and the equation of motion of \vec{M} is given by

$$\begin{aligned} \frac{\partial \vec{M}}{\partial t} &= \gamma \vec{M} \times \left[\left(H_0 + \frac{\omega}{\gamma} \right) \vec{k} + H_1 \vec{i} \right] \\ &= \gamma \vec{M} \times \vec{H}_{\text{eff}} \end{aligned} \quad (1.8)$$

where $\vec{H}_{\text{eff}} = \vec{k} \left(H_0 + \frac{\omega}{\gamma} \right) + \vec{i} H_1$ (1.9)

and \vec{i} is a unit vector in the x-direction in the rotating reference frame. From equation (1.9) it is obvious that \vec{M} precesses about \vec{H}_{eff} with an angular velocity γH_{eff} . The effect of H_1 on H_{eff} is predominant when $\omega \approx -\gamma H_0$ in which case the magnetic moment precesses about H_1 with an angular velocity γH_1 . This phenomenon is called Nuclear Magnetic Resonance (N.M.R.). If H_1 were applied only for a duration of time t_ω , then the moment would precess through an angle θ given by

$$\theta = \gamma H_1 t_\omega \quad (1.10)$$

If t_ω and H_1 were chosen such that $\theta = \pi$ the pulse would invert the magnetisation and is referred to as a "180° pulse". Similarly, if $\theta = 90^\circ$ (90° pulse), the magnetisation would rotate through 90° and it would precess about H_0 in the x-y plane after the pulse.

In practice the sample is placed in a coil which is placed perpendicular to the magnetic field H_0 . An alternating field is

produced perpendicular to H_0 by passing r.f. current through the coil. The magnetisation precessing in the x-y plane after the application of a 90° pulse induces an e.m.f. in the coil which can be detected and observed and this is normally referred to as the free induction decay.

The preceding paragraphs indicate a method of preparing a non-equilibrium sample. The approach to equilibrium of such a system can be described by the phenomenological Bloch equations² as given below

$$\frac{d\vec{M}}{dt} = \gamma \vec{M} \times \vec{H} - \frac{M_x}{T_2} \vec{i} - \frac{M_y}{T_2} \vec{j} + \frac{M_0 - M_z}{T_1} \vec{k} \quad (1.11)$$

where \vec{i} , \vec{j} and \vec{k} are unit vectors in the x, y and z directions, T_1 and T_2 are longitudinal and transverse relaxation times, M_0 is the equilibrium magnetisation in the static field H_0 and \vec{H} is given by

$$\vec{H} = H_0 \vec{k} + 2H_1 \cos \omega t \vec{i} \quad \text{where } H_1 \ll H_0 \quad (1.12)$$

The solutions to the equation (1.11) ^{with $H_1=0$} can be written as

$$\begin{aligned} M_x(t) &= M_{xy}(0) \left[\cos \omega t + \phi \right] e^{-t/T_2} \\ M_y(t) &= M_{xy}(0) \left[\sin \omega t + \phi \right] e^{-t/T_2} \\ M_z(t) &= M_0 + \left[M_z(0) - M_0 \right] e^{-t/T_1} \end{aligned}$$

$$\text{where } M_{xy} = \left[M_x^2 + M_y^2 \right]^{1/2}$$

M_x , M_y and M_z can be monitored experimentally and hence T_1 and T_2 can be obtained.

Since T_1 is a measure of the rate at which the spin system exchanges energy with the lattice, it is possible to relate T_1 to the molecular properties of the gas. The spins relax as a result of fluctuations in the magnetic fields at the sites of the nuclei. In diatomic and polyatomic gases the contributions to these local

fields come from the interaction of the spin with the rotational angular momentum of the molecule and from the dipole moments of the other nuclei in the same molecule. The fluctuations in these intramolecular interactions are produced by those collisions which reorient the molecule. Thus the study of spin-lattice relaxation can give information on the intermolecular interactions which produce molecular reorientations.

The mechanism by which the spins relax was first proposed by Schwinger³ and then extended by Needler and Opechowski⁴ and Johnson and Waugh⁵. They have obtained expressions relating the spin lattice relaxation time to the correlation times of the intramolecular interactions.

Bloom and Oppenheim⁶ have treated the dynamics of the system with the "Constant Acceleration Approximation" (C.A.A.) and obtained expressions for the correlation times of the intramolecular interactions in terms of the intermolecular interactions. They have also assumed that the transitions between different J states are negligible compared with the transitions between different M_J states of the same J -manifold. This theory was used in interpreting the data below room temperature in their subsequent paper.⁸

Recently Bloom and Oppenheim⁹ have extended their theory to include the transitions between different J states which is more suitable to interpret the results at higher temperatures. This theory has been used in interpreting the data on H_2 in this thesis and is presented in detail in Chapter III.

The apparatus and experimental techniques that were used in obtaining the data are presented in Chapter II. Chapter IV pre-

sents the results in H_2 and $H_2 - He$, $H_2 - CO_2$ mixtures and their interpretation using the theory presented in Chapter III. Chapter V contains the results and interpretation of CH_4 and $CH_4 - He$ mixtures. In Chapter VI the results are summarised and some suggestions are made for further work. The circuit diagrams for various parts of the electronics are presented in Appendix A.

CHAPTER II

APPARATUS AND EXPERIMENTAL TECHNIQUE2. 1. Measurement of Spin-lattice Relaxation Time.

The measurement of the spin-lattice relaxation time T_1 will be described very briefly here since the technique is well established and is available in the literature. 1,10,11.

When a sample is placed in an external magnetic field \vec{H}_0 , the nuclear moments will have a net magnetisation aligned with the field under equilibrium conditions. In order to measure T_1 , the magnetisation of the spin system has to be disturbed from its equilibrium position. From the discussion in Chapter I it is evident that the magnetisation can be rotated through any desired angle θ from its equilibrium position by the application of a r.f. field H_1 at the Larmor frequency perpendicular to the static field H_0 . The r.f. field must be sufficiently intense to rotate the spin system through the desired angle in a time much shorter than T_1 or T_2 so that the relaxation effects can be neglected during this time. Referring to a coordinate system whose z-axis is chosen along \vec{H}_0 , a 90° pulse rotates the magnetisation to the x-y plane and when the pulse is removed the magnetisation precesses about H_0 in the x-y plane, thus inducing an e.m.f. in the sample coil. Due to the inhomogeneity of the magnetic field, all the spins do not precess with the same Larmor frequency. As a result the spins dephase among themselves and the induced signal decays in a time of the order of $(\gamma\Delta H)^{-1}$, where ΔH is the measure of inhomogeneity of the field across the sample. If a 180° pulse is

applied to the system after a time τ from the 90° pulse, the spins fall in phase again and the signal builds up to its maximum at a time 2τ from the 90° pulse and decays again for the same reasons. This second signal is called "spin echo".

In the experiments to be described in this thesis \vec{M} was inverted by a 180° pulse and the recovery of M_z was monitored from $-M_0$ to $+M_0$ by a subsequent $90^\circ - 180^\circ$ pulse sequence. If the time between 90° and the second 180° pulses is kept constant throughout the experiment, the magnitude of the echo is proportional to the value of M_z preceding the 90° pulse.

The measurements were made with a 30 Mc coherent pulsed spectrometer using phase sensitive detection. The Box-Car integrator¹² was used to improve the signal to noise ratio. The pulse sequence was repeated after every time interval $T \gg 10T_1$ so that the spins relax in between the sequence. During a measurement the time between the first 180° pulse and the 90° pulse was swept very slowly to several times T_1 keeping the time between the 90° pulse and the 180° pulse constant. The box-car was triggered by the 90° pulse and the sampling gate was adjusted to sample the echo formed by the 90° and the second 180° pulses. The magnitude of the echo and hence the recovery of M_z was plotted on a Varian Chart recorder. The time t between the first 180° pulse and the 90° pulse was measured with a Hewlett-Packard 524-C electronic counter and the time was printed out automatically by a Hewlett-Packard 526-B digital recorder. An event marker on the Varian chart recorder made a mark whenever the time was printed out by the digital recorder and proper times to those marks were assigned later. M_∞ was obtained by making $t \gg 10T_1$. If $A(t)$ is the height

of the signal at time t and A_∞ at $t=\infty$, then it can be seen that

$$A(t) = A_\infty (1 - e^{-t/T_1})$$

The slope of the straight line $\log (A_\infty - A(t))$ vs. t gives the value of T_1 .

2. 2. N.M.R. Spectrometer.

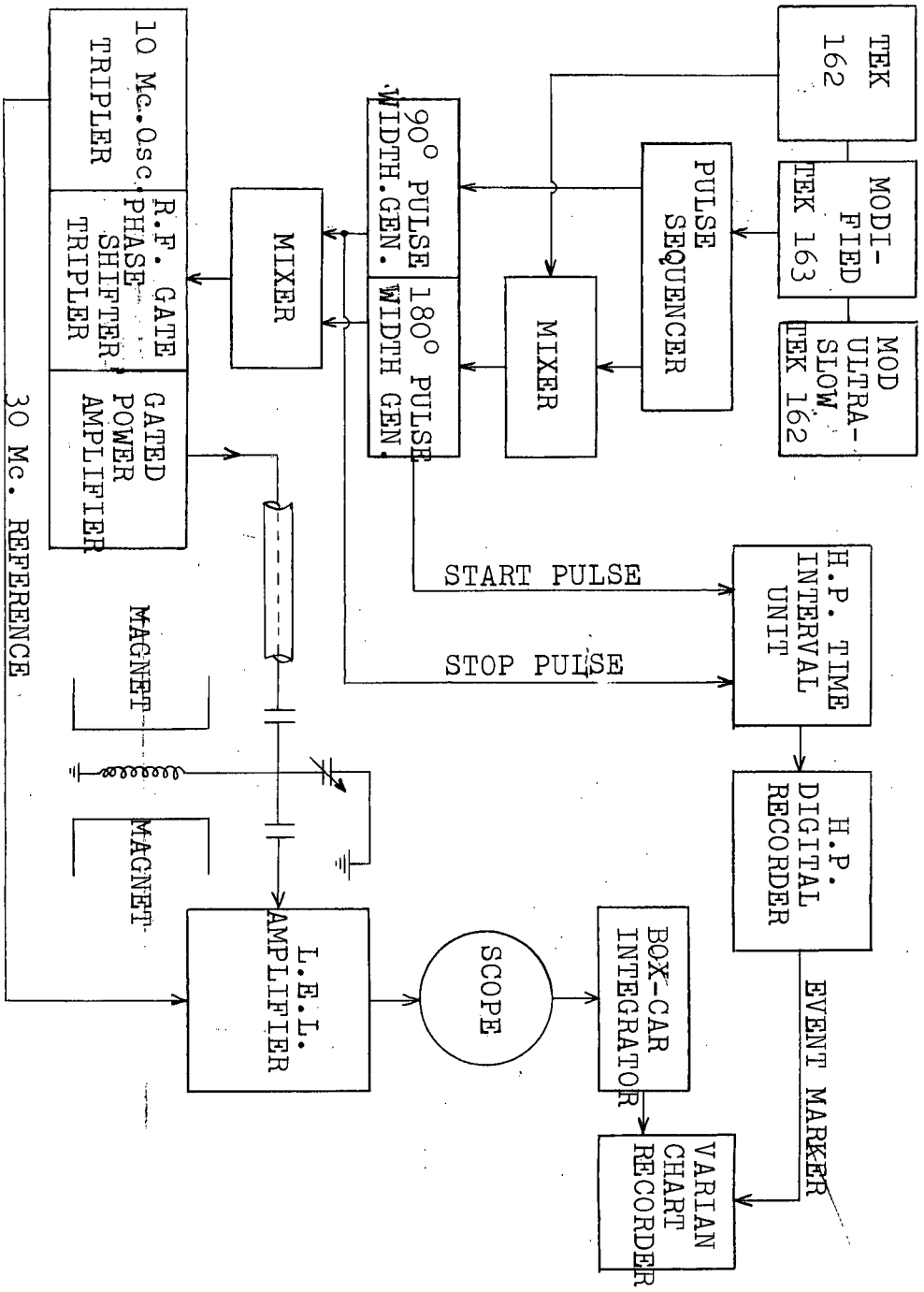
2.2.1. General Remarks.

The spectrometer, originally built by John D. Noble¹³, was modified to detect weak N.M.R. signals. A coherent 30Mc transmitter was built to use phase sensitive detection and the timing circuit was modified to make use of the box-car integrator. The box-car integrator was constructed by Walter N. Hardy¹⁴ based on the design of R.J. Blume¹² and a detailed analysis was reported in his Ph.D. thesis. A block diagram of the spectrometer is given in fig. (1)

2.2.2. Timing Circuit.

The timing circuit consisted of a collection of Tektronix wave-form and pulse generator units. A Tek. 162 wave-form generator was used in recurrent mode to provide the first 180° pulse. The sawtooth from the same generator started running down at the same time and was fed to a modified Tek. 163 pulse generator whose triggering level was set by the sawtooth of a modified "ultra-slow" Tek 162 wave-form generator. The pulse from the modified Tek. 163 pulse generator was taken to a pulse sequencer to produce two pulses whose separation was controlled by the pulse width of the input pulse. The first 180° pulse and the second pulse from the pulse sequencer were added together in a mixer circuit. These pulses were taken to a 180° pulse-width generator whereas the first pulse from

FIG. 1. BLOCK DIAGRAM OF 30MC PULSED SPECTROMETER



the pulse sequencer was taken to a 90° pulse-width generator. These two pulse-width generators were identical and were designed using phantatron circuits.¹³ The pulse-widths could be varied from a microsecond to about 100 microseconds. The pulses were then mixed and were used to gate the transmitter. The 90° pulse from the pulse sequencer was also used to trigger the Box-car.

2.2.3. Transmitter.

The transmitter was designed to make use of phase-sensitive detection since it was known from the beginning that the signals would be small. The phase-sensitive detection requires a coherent pulse system and a reference voltage at 30Mc. A transistorised crystal controlled oscillator was built to supply the r.f. at 10Mc and was shielded by a copper can. The output from this amplifier was taken out through a shielded cable to provide the reference voltage. The tripler as well as the 30Mc amplifier were transistorised which made it possible to build them inside the copper can. A transistorised power supply regulated by Zener diodes was also built inside the can. Thus only one lead at 6.3V a.c. was taken inside the can to supply the power transformer. This helped in keeping the r.f. leak to a minimum when the r.f. gate was closed.

The r.f. from the gate was taken to a conventional phase-shifting circuit¹⁵ and a tripler. The tripler was a push-pull amplifier at 30Mc. The output from the tripler was taken to a gated power amplifier stage tuned to 30Mc. The power amplifier produced reasonably rectangular r.f. pulses of 1200 volts peak to peak. With this power output the pulse widths needed to produce 90° and 180° pulses were about 6 microseconds and 13 microseconds respectively. The output power from the transmitter was taken to

the sample coil tuned to 30Mc through a small capacitor of about 3 pf.

2.2.4. Sample Coil

The sample coil was made of approximately twelve turns of 22 S.W.G. wire with a spacing in between the turns equal to the diameter of the wire and was about $1\frac{1}{4}$ " long. Since the sample coil was immersed in the sample (fig. 2) the enamel came off the wire and introduced impurity in the sample when the temperature of the sample holder was raised above room temperature. This resulted in a very sharp increase in T_1 because of the collisions of H_2 molecules with heavier impurity molecules. Therefore, the insulation on the wire was completely stripped off and the wire was thoroughly cleaned before use. Also the coil was pre-heated to the highest temperature along with the sample-holder and the gases were pumped out. When these precautions were taken no trace of impurity was noticed and the results were reproducible to within 3%. A thin walled glass tube was fitted tightly inside the pressure vessel to insulate the coil from the wall of the vessel. In order to get an ideal 180° pulse it is necessary to have all the sample inside the coil. So the coil was wound to fit almost exactly inside the glass tube so that most of the sample was inside the coil.

The r.f. lead was just the extension of one end of the coil and was taken through a stainless steel tube to plug A in fig. 2 where it was sealed against pressure with teflon washers at room temperature. The other end of the coil was fastened to the stainless steel plug by means of a screw. Glass was used for insulation wherever it was necessary. The r.f. lead was connected to a tuning capacitor through a 12 p.f. capacitor.

2.2.5. Receiver.

The receiver was a L.E.L. amplifier model 1.F.21.B.S. This is a wide band amplifier with a maximum gain of 100 db and a bandwidth of 2Mc. centered around 30Mc. A 1N295 diode detector was supplied with this and was used in the measurements. Ordinary diode detection is not linear over the entire region and the non-linearity becomes very important while dealing with small signals. Phase-coherent detection was used which allowed operation in the linear region of the diode. The 30Mc reference voltage was added to the signal at a stage in the receiver where the stagger tuned triplet stages were coupled together. The diode detects the "sum" of the reference voltage and the signal. The signal was kept below about 1/10 of the reference voltage to avoid distortion.

2.3. High-Pressure System.

The high-pressure apparatus used in the experiments is shown in fig. 2. It consists of a thick walled Be-Cu vessel (O.D. 17/16" and I.D. 3/8") and a stainless steel plug sealed in the vessel by means of Bridgmann's arrangement of packing washers.^{16,17} The central washer was annealed copper instead of lead. Copper, when annealed, is quite soft and hence makes a good seal. Also, since the thermal expansion of copper is the same as that of Be-Cu, the seal, when made at room temperature, maintains itself at higher temperatures. The other two washers were made of Be-Cu instead of Everdur. The outside edge of the washer D₁ was tapered to the inside to fit on to the taper of the stainless steel plug. This provided more area of contact between the stainless steel plug and the Be-Cu washer and hence the pressure was applied uniformly on

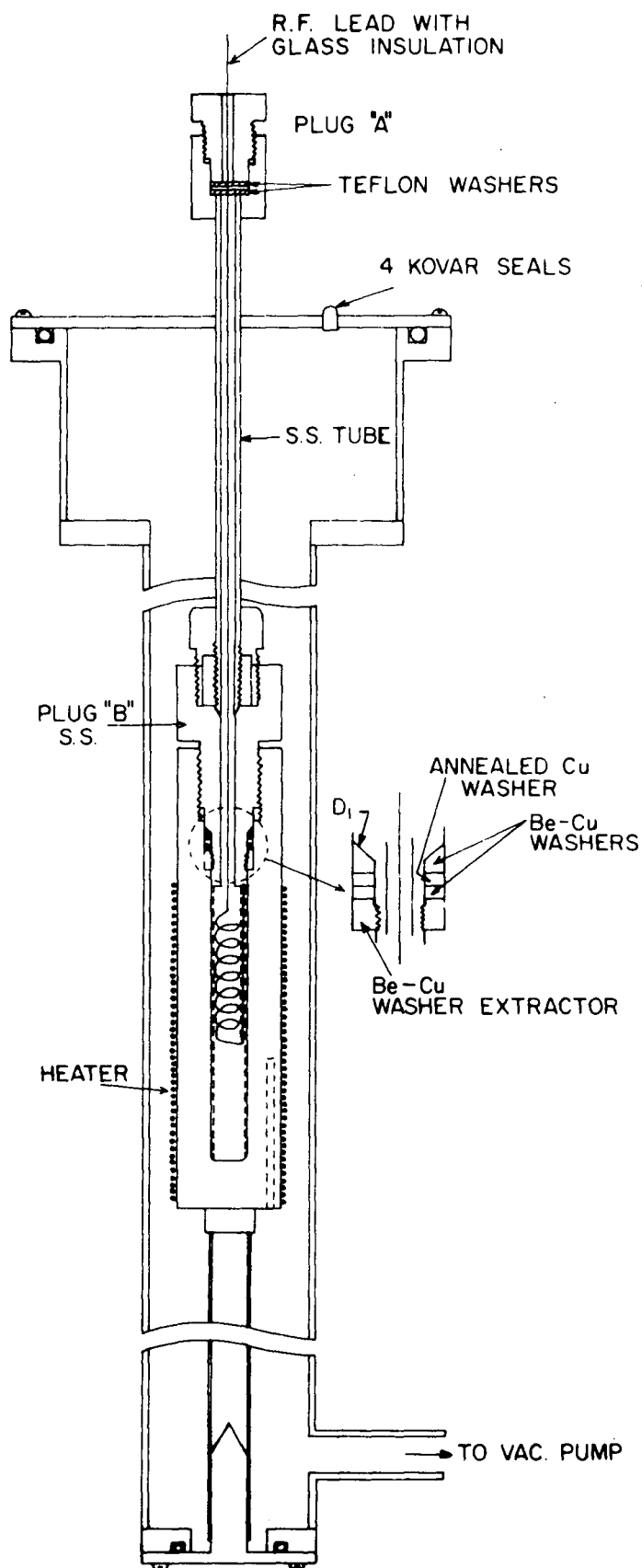


FIG. 2. SAMPLE HOLDER

the central washer when the stainless steel plug was tightened to make the seal.

The r.f. lead was sealed against pressure at room temperature in plug A with teflon washers and then brought into the high pressure region through a $\frac{1}{4}$ " stainless steel tube. The stainless steel tube was pressure sealed inside the plug using the same technique as that of standard high pressure equipment and was quite satisfactory throughout the temperature range.

The schematic of high pressure system is given in fig. 3. All the high pressure connectors were purchased from Autoclave Eng. Inc. and were designed to withstand pressures up to 30,000 p.s.i. P.S I.

2.4. Heater.

The heater was wound on the high-pressure vessel using a thin mica sheet to insulate it from the vessel. To avoid multi-layer winding, a commercial 600 watts spiral element was used instead of a straight nichrome wire. It was wound non-inductively with a spacing in between the windings approximately equal to the diameter of the element. A liquid porcelain called "Saureisen" was used to keep the windings in place.

The high-pressure vessel along with the heater was kept inside a vacuum jacket to keep the radiation and convection current losses to a minimum. The leads from the heater were taken outside the vacuum jacket through Kovar seals. The heater current was regulated by a variac. About 150 watts of power was supplied to maintain the sample holder at 750° K.

The temperature was measured with a chromel-allumel thermo-

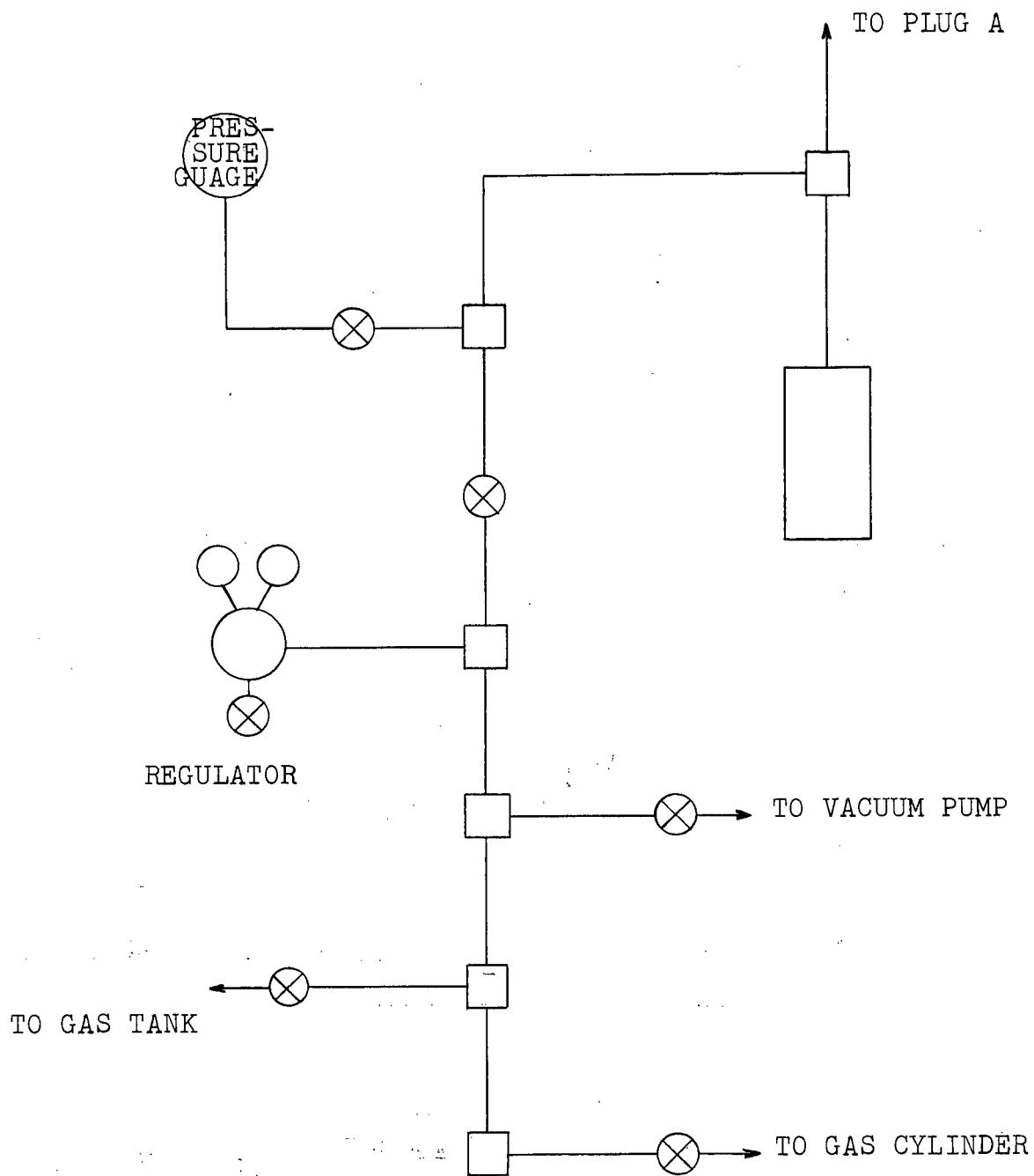


FIG. 3.

HIGH PRESSURE SYSTEM

couple. The "Hot-Junction" of the thermo-couple was placed in the hole provided for it in the vessel. The leads were taken outside the vacuum jacket through Kovar seals. The thermal E.M.F. was measured with a "Honey-Well" potentiometer using a null detector. No special effort was made to control the temperature automatically because once the current was adjusted the temperature was steady to within a degree after reaching the equilibrium. Whenever the temperature was changed at least 8 or 10 hours was allowed before taking the measurements to make sure that the sample was at equilibrium with the vessel. The temperature measurements were accurate to within $\pm 0.5\%$.

2.5. Mixing of Gases: Determination of Concentration.

The gases that were used in the experiments were of research grade and were obtained from Matheson Company. The mixture of two gases was prepared in a third cylinder by letting in one component at lower pressure first and then the other component. The total pressure was noted before and after the introduction of the second component. Knowing the partial pressures of the individual components and the temperature, the density of each component gas in ideal amagat units can be found from the equation of state data ¹⁸ and hence the composition of the mixture can be determined. _{One} Ideal Amagat is the number density of the gas at N.T.P.

The calculated value of the concentration can be verified experimentally by comparing the height of the echo of the mixture with that of pure gas containing protons under identical conditions. In the case of hydrogen and its mixtures the

height of the echo has to be corrected for the effects of T_2 and diffusion.

The height of the echo $A(2\tau)$, where τ is the time between 90° and 180° pulses, is given by

$$A(2\tau) = A(0) \exp \left[-2\tau/T_2 - k(2\tau)^3 \right] \quad (2.5.1.)$$

where $k = \frac{1}{12} \gamma^2 G^2 D$

$$T_2 \propto \rho ; \quad D \propto 1/\rho$$

and ρ is the density of gas in amagat units, where an "amagat" is 2.69×10^{19} molecules/cm³

Neglecting the diffusion effects

$$A(2\tau) = A(0) \exp(-2\tau/T_2) \quad (2.5.2.)$$

If the number of spins per molecule is denoted by n_I ,

then

$$A(0) \propto M(0) \quad \text{where} \quad M(0) = \rho \frac{n_I \gamma^2 \hbar^2 I(I+1)}{3 k T} \quad (2.5.3.)$$

$$\text{or} \quad A(0) = C \rho \quad \text{where } C \text{ is a constant} \quad (2.5.4.)$$

Equation (2.5.2.) becomes

$$A(2\tau) = C \rho \exp(-2\tau/T_2) \quad (2.5.5.)$$

Since in the high density region $T_1/\rho = T_2/\rho$

$$C \rho = A(2\tau) \exp(2\tau/T_1) \quad (2.5.6.)$$

Therefore $\frac{(C\rho)_{\text{mixture}}}{(C\rho)_{\text{H}_2}}$ gives the fractional composition of the mixture.

In the case of CH_4 and its mixtures the correction is very small since T_1 is much longer than 2τ , which is approximately a milli-second in all the measurements.

For an ideal gas the density in amagats of the mixture at any intermediate pressure P is given by

$$\rho = \frac{273}{T} P \text{ (in atmospheres)} \quad (2.5.7.)$$

The CO₂ - H₂ mixture presents a different problem. The dependence of ($C\rho$) ^{mixture} on total pressure is linear at high temperatures, but not at room temperature and this effect is more prominent at higher concentrations of CO₂. This is due to the fact that room temperature is not high enough to describe the equation of state of CO₂ by ^{the} ideal gas law. From the equation of state data for CO₂ it can be seen that the density has increased from 9.5 to 47.5 amagats when the pressure has increased from 10 atmospheres to 40 atmospheres at room temperature i.e. the density at 40 atmospheres is about 25% higher than what the ideal gas law predicts. Similar study at 400°K shows that the density at 40 atmospheres is about 6% higher than the density obtained by ideal gas law and at higher temperatures the ideal gas equation is found to be a good approximation to within 2%. As a result of this, comparison of signal strengths at room temperature does not give the fractional composition of the mixture nor could it be determined by noting the pressures before and after the introduction of the second component when the pressures involved are high (i.e. >10 atm.). Hence a different procedure was adopted to determine the fractional composition as well as the density at any other pressure P¹ which is described below.

Let the pressure of CO₂ introduced into the cylinder be P₁ and let H₂ be added to this to bring the total pressure to P. The gases were left together for about 24 hours to mix by diffusion.

The signal strength was calibrated in units of proton density by noting the signal strengths at various pressures for H_2 . The sample holder was evacuated and the mixture was let into the sample holder at pressure P . Keeping the gain of the spectrometer the same, the signal strength of the mixture was noted at pressure P as well as at several other pressures between 0 and P . The strength of the signal at pressure P gives the density of hydrogen in amagats. The density of CO_2 was obtained from the equation of state data for CO_2 knowing P_1 and temperature. If ρ_{CO_2} is the density of CO_2 and ρ_{H_2} is the density of H_2 , $\rho_{CO_2}/(\rho_{CO_2} + \rho_{H_2})$ gives the fractional composition of the mixture. The density of the mixture at any intermediate pressure P' was obtained from the signal strength S' of the mixture at pressure P' . S' was converted to the density of H_2 , ρ_{H_2}' , and since the ratio ρ_{CO_2}/ρ_{H_2} is a constant K ,

$$\rho_{CO_2}' = K \rho_{H_2}'$$

The density of the mixture at pressure P' was obtained as $(\rho_{CO_2}' + \rho_{H_2}')$.

Fig. 4 shows the density of the mixture as a function of composition at different pressures. At higher concentrations of CO_2 the density is proportional to the percentage of CO_2 but at lower concentrations it is non-linear. The values extrapolated to 100% CO_2 are in agreement with the values obtained from the equation of state data for CO_2 within experimental errors.

The density of the mixture was obtained experimentally as a function of pressure at other temperatures of interest also. At 350°K it was found that the density obtained from the ideal gas equation differs from the experimental value by 5%

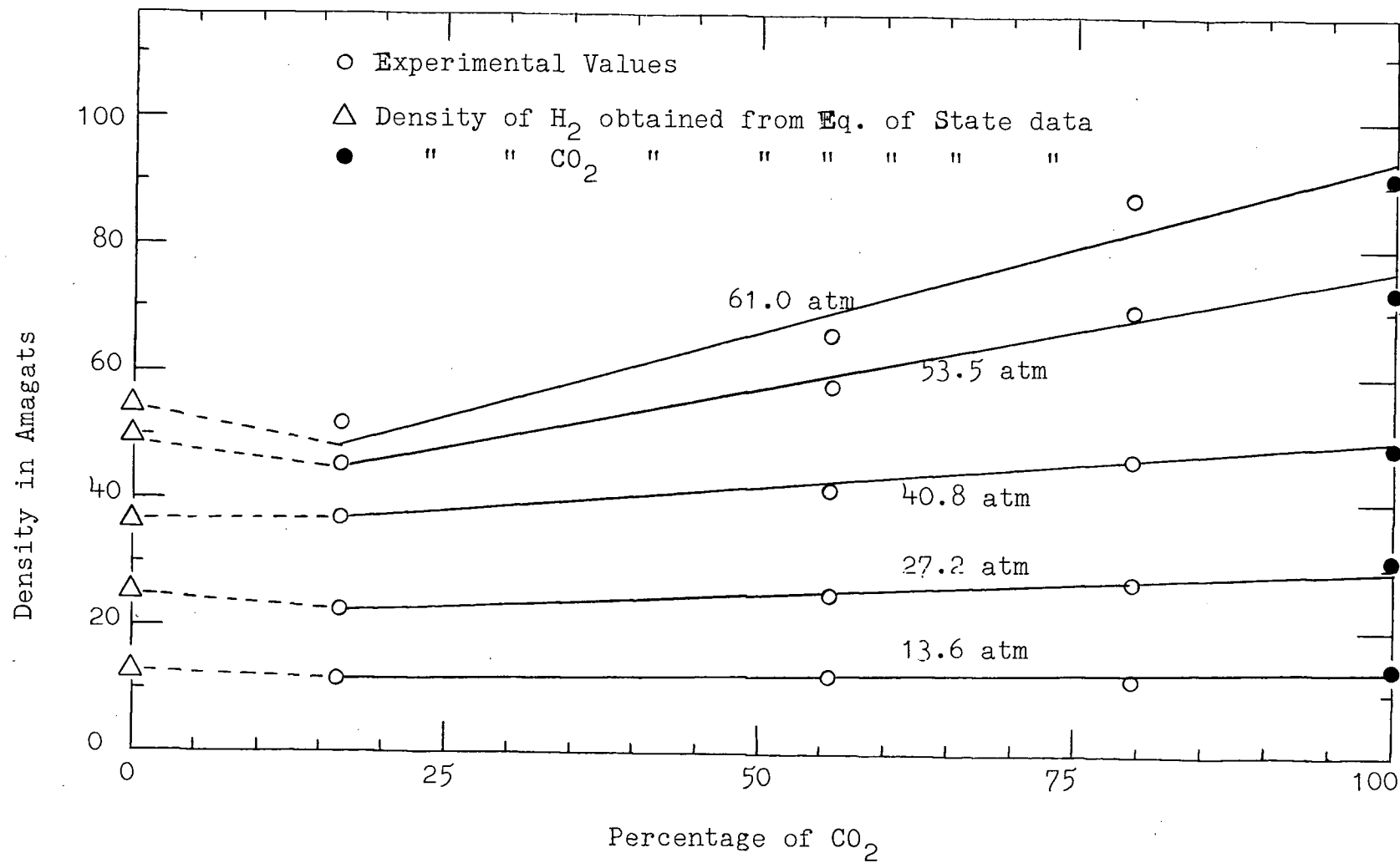


FIG. 4. Density of H₂-CO₂ mixture as a function of composition.

at about 60 atmospheres and was less than that at lower temperatures.

The signal strength versus pressure is shown in fig. 5 for 55% CO₂ and 79.4% CO₂ at room temperature, whereas fig. 6 shows the similar plot at 400°K for 55% CO₂, 45% H₂ mixture.

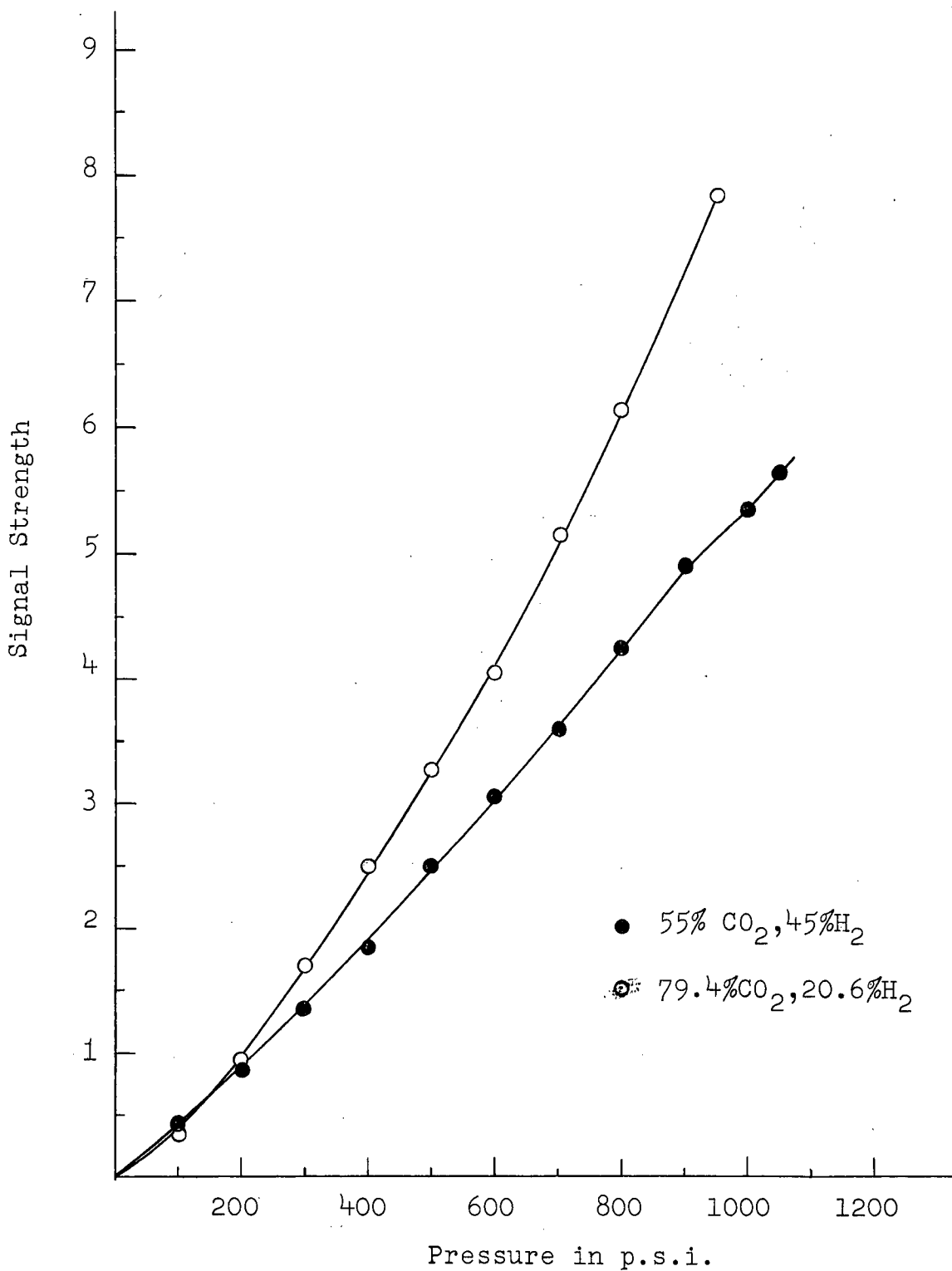


FIG. 5. SIGNAL STRENGTH vs. PRESSURE FOR H₂ - CO₂ MIXTURE AT 293°K.

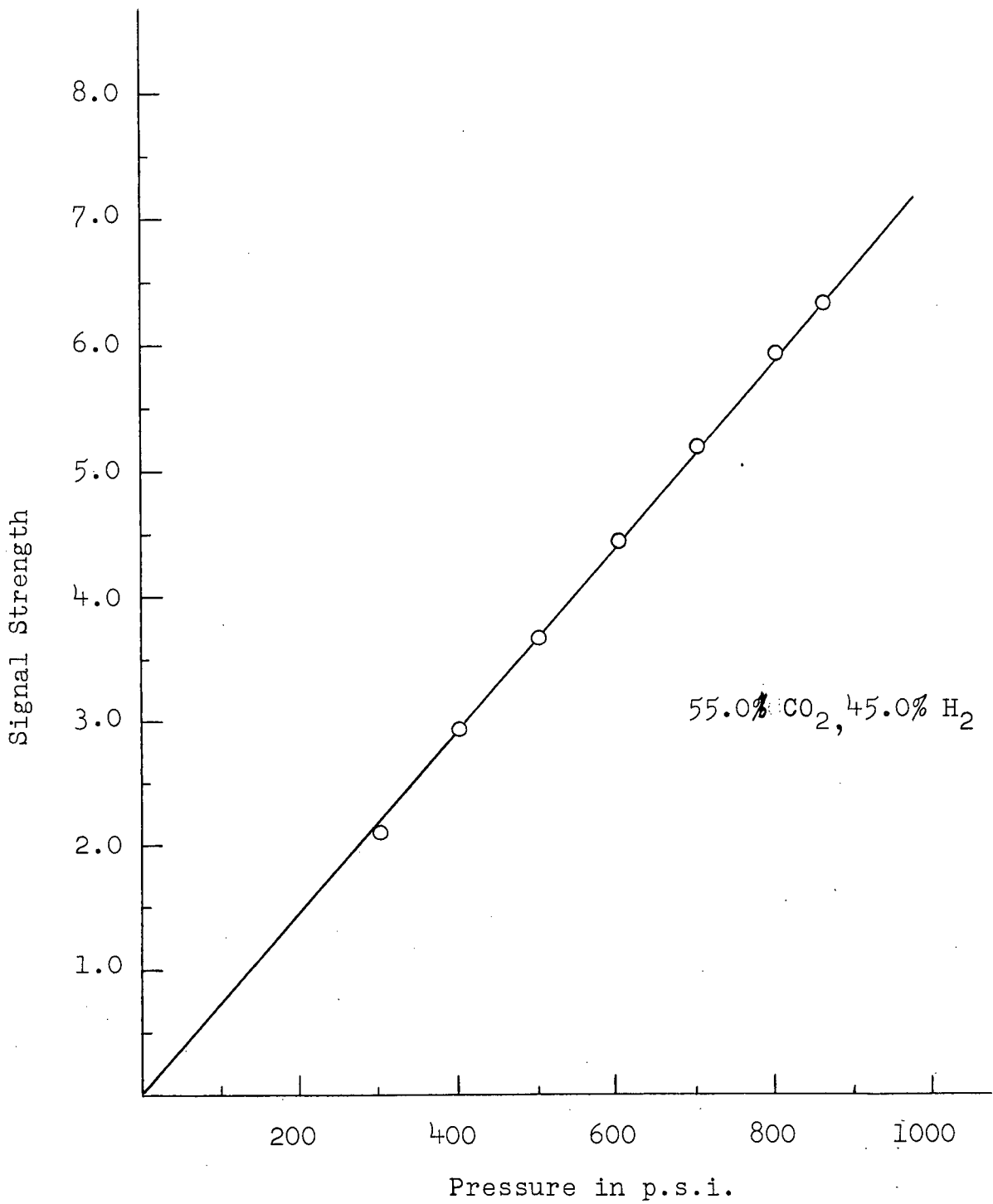


FIG. 6. SIGNAL STRENGTH vs. PRESSURE FOR H₂ - CO₂ MIXTURE AT 400°K.

CHAPTER III

THEORY3.1. HYDROGEN

The internal degrees of freedom of a diatomic molecule such as H_2 are:

1. Electronic (orbital and spin)
2. Vibrational
3. Rotational states of the nuclei
4. Nuclear spin states.

Since the vibrational energy of the ^{first excited state of the} molecule is of the order of $6000^\circ K$ and since $\epsilon_{\text{electronic}} > \epsilon_{\text{vib}}$, the degrees of freedom corresponding to the electronic and vibrational states of the molecule can be considered to be frozen even up to $1000^\circ K$. As a result the H_2 molecule can be considered as a rigid rotator with an extra degree of freedom corresponding to the spin state of the molecule. Hence the state of a hydrogen molecule can be described by the rotational quantum numbers J, m_J and the proton spin quantum numbers I, m_I .

Since the protons are fermions, the total wave-function of H_2 must be antisymmetrical in the two atoms with respect to permutation of the two protons. The vibrational and electronic parts of the wave-function are symmetrical in the ground state which is the only state that is occupied. The rotational wave-function is symmetrical for even J and antisymmetrical for odd J . The spin wave-function is symmetric for $I=1$ and antisymmetric for $I=0$. In order to have the total wave-function to

be antisymmetric $I=0$ should be associated with even J and $I=1$ should be associated with odd J . These two modifications are called para- and ortho- hydrogen respectively.

For H_2 at thermal equilibrium the distribution of the molecules among the J states is given by Boltzmann's distribution function

$$P_J \propto g_J \exp(-E_J/k.T) \quad (3.1.1.)$$

where P_J is the fraction of the total number of molecules that are in J state, g_J is the degeneracy of the state and T is the temperature of the system

$$g_J = (2I+1)(2J+1) = (2J+1) \quad \text{For } J \text{ even i.e. } I=0$$

$$= 3(2J+1) \quad \text{For } J \text{ odd i.e. } I=1$$

and
$$E_J = \frac{J(J+1)}{2I_0} = J(J+1)k\Theta_R \quad (3.1.2.)$$

where

I_0 = Moment of Inertia of the molecule

k = Boltzmann's Constant

Θ_R = 85.3°K for H_2

The equilibrium ratio of ortho- to para- hydrogen is

$$r = \frac{\sum_{\text{odd}} 3(2J+1) \exp(-J(J+1)\Theta_R/T)}{\sum_{\text{even}} (2J+1) \exp(-J(J+1)\Theta_R/T)} \quad (3.1.3.)$$

At high temperatures where $\Theta_R \ll T$, $r \rightarrow 3$, and at low temperatures as $T \rightarrow 0$, $r \rightarrow 0$. At room temperature, since T is well above Θ_R the ratio is close to 3. As the temperature is lowered the above equation predicts that all the molecules will be converted to para- hydrogen. Since the transition from ortho- to para- involves changing total spin angular momentum in the molecule, the transition probability is very small and

the equilibrium with respect to ortho-para ratio cannot be achieved in a short time. Therefore, H_2 must be treated as a mixture of two separate gases. Para- H_2 with $I=0$ gives no N.M.R. signal whereas ortho- hydrogen behaves like a $I=1$ system. N molecules of H_2 at room temperature give a signal proportional to $\frac{3}{4} NI(I+1) = \frac{3}{2} N$.

The fractional distribution of the molecules among different J states is given in Table 1 for (i) 100% ortho- hydrogen and (ii) 100% para- hydrogen.

TEMP IN °K	100% ortho- H ₂				100% para- H ₂			
	J = 1	J = 3	J = 5	J = 7	J = 0	J = 2	J = 4	J = 6
77.5	1.0				0.993	0.007		
100.0	0.9995	0.0005			0.971	0.029		
200.0	0.965	0.035			0.72	0.28		
300.0	0.879	0.119	0.002		0.517	0.468	0.015	
400.0	0.778	0.214	0.008		0.397	0.562	0.05	
500.0	0.688	0.290	0.022		0.322	0.580	0.096	0.003
600.0	0.613	0.343	0.042	0.001	0.271	0.578	0.142	0.009
700.0	0.550	0.379	0.067	0.004	0.234	0.564	0.184	0.018
	$P_J = \frac{3(2J+1) \exp[-J(J+1)85.3/T]}{\sum_{J \text{ odd}} 3(2J+1) \exp[-J(J+1)85.3/T]}$				$P_J = \frac{(2J+1) \exp[-J(J+1)85.3/T]}{\sum_{J \text{ even}} (2J+1) \exp[-J(J+1)85.3/T]}$			

Table I. Fractional population of the rotational states for H₂.

3.2. Theory of Relaxation in H₂

The hamiltonian of the spin rotational and dipolar interaction of the H₂ molecule can be written as

$$k \mathcal{H} = \frac{\gamma H' k}{2} \sum_{m=-1}^1 L_{1m} S_{1,-m} + \left(\frac{6\pi}{5}\right)^{1/2} \gamma H'' \sum_{m=-2}^2 L_{2m} S_{2,-m} \quad (3.2.1.)$$

where L_{1m} and L_{2m} are random functions of the lattice operators and S_{1m} and S_{2m} are the operators acting on the nuclear spin variables.

$$\begin{aligned} L_{10} &= \sqrt{2} J_z & S_{10} &= \sqrt{2} I_z \\ L_{1\pm 1} &= J_{\pm} & S_{1\pm 1} &= I_{\pm} \\ L_{20} &= Y_{20} & S_{20} &= \left(\frac{2}{3}\right)^{1/2} [3I_z^2 - I(I+1)] \\ L_{2\pm 1} &= Y_{2\pm 1} & S_{2\pm 1} &= I_z I_{\pm} + I_{\pm} I_z \\ L_{2\pm 2} &= Y_{2\pm 2} & S_{2\pm 2} &= I_{\pm}^2 \end{aligned} \quad (3.2.2.)$$

In a gas where there are frequent collisions, the rotational angular momentum vector \vec{J} undergoes changes due to the anisotropic intermolecular forces acting on the molecule during the collision. This causes the magnetic fields at the sites of the nuclei to fluctuate thereby producing nuclear spin transitions which bring the spin system to equilibrium. Thus the molecular collisions establish equilibrium among the J levels very rapidly whereas the nuclear spins are relaxed slowly through a weak coupling to J as shown in fig. 7.

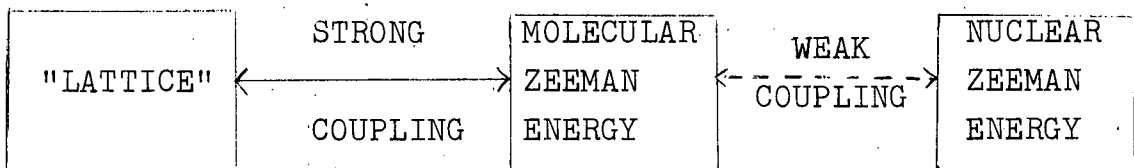


FIG. 7. Nature of Coupling between Nuclear Spins and the "lattice".

The "Lattice" here refers to all degrees of freedom that are available to a molecule except the one corresponding to the nuclear spins. It remains at constant temperature T even after exchanging energy with the nuclear spin system because of its large thermal capacity.

From the general theory of relaxation it can be shown that (Abragam¹)

$$\frac{1}{T_1} = \frac{\nu^2 H'^2}{2} J_{11}(\omega_I) + \frac{16\pi}{5} \nu^2 H''^2 I(I+1) \left\{ J_{21}(\omega_I) + 4 J_{22}(2\omega_I) \right\} \quad (3.2.3.)$$

where

H' = 27 gauss is the spin rotational coupling constant

H'' = 34 gauss is the dipolar coupling constant.

$I = \frac{1}{2}$ in the case of hydrogen

$$J_{lm}(\omega_I) = \int_{-\infty}^{\infty} e^{-i\omega_I t} G_{lm}(t) dt \quad (3.2.4.)$$

where

$$G_{lm}(t) = \frac{1}{2} \left[\overline{L_{lm}(0) L_{lm}^{\dagger}(t)} + \overline{L_{lm}^{\dagger}(0) L_{lm}(t)} \right] \quad (3.2.5.)$$

The bar represents the ensemble average. In Schwinger's model³ all the molecules were assumed to be in the lowest rotational state ($J=1$) and the molecule was allowed to make transitions between the three m_J states. It was further assumed in his model that all the correlation functions decay with the same time constant

$$\overline{L_{lm}(0) L_{lm}^{\dagger}(t)} = \overline{L_{lm}(0) L_{lm}^{\dagger}(0)} e^{-t/\tau_c} \quad (3.2.6.)$$

Needler and Opechowski⁴ (1961) suggested that more accurate expression for correlation function would be

$$\overline{L_{lm}(0) L_{lm}^{\dagger}(t)} = \overline{L_{lm}(0) L_{lm}^{\dagger}(0)} e^{-im\omega_J t} e^{-t/\tau_c} \quad (3.2.7.)$$

Johnson and Waugh⁵ (1962) pointed out that if the frequency of effective collisions is much larger than ω_J and if only $J=1$ state is populated, then $G_{l_m}(t)$ can be characterised by two correlation times only, one for L_{1m} ($m = -1, 0, +1$) and the other for L_{2m} ($m = \pm 2, \pm 1, 0$).

The expression for $\frac{1}{T_1}$ can then be written as

$$\frac{1}{T_1} = \frac{2}{3} \gamma^2 H^2 J(J+1) \frac{\tau_1}{1 + (\omega_I - \omega_J)^2 \tau_1^2} + \frac{6}{5} \frac{\gamma^2 H^2 J(J+1)}{(2J-1)(2J+3)} \left[\frac{\tau_2}{1 + (\omega_I - \omega_J)^2 \tau_2^2} + 4 \frac{\tau_2}{1 + 4(\omega_I - \omega_J)^2 \tau_2^2} \right] \quad (3.2.8.)$$

providing that all the molecules are in their lowest rotational state $(J, 1)$. This assumption starts to break down seriously at room temperature where the population of $J=3$ state is about 12%. Bloom (private communication) has proposed to evaluate the correlation functions taking into account the transitions between different J states which will be described in detail in the following sections.

3.2.1. Correlation Functions of Intra-molecular Interactions.

From equations (3.2.3.), (3.2.4.) and (3.2.5.) and the discussion that followed, it is clear that the correlation functions $G_{l_0}(t)$ have to be evaluated in order to obtain an explicit expression for T_1 . In the following discussion the treatment of Bloom and Oppenheim⁹ is followed closely. The operator L_{10} has non-zero matrix elements only for the case $J=J_0$, where J_0 and J are the initial and final rotational states of the molecule, whereas the operator L_{20} has non-zero matrix elements for the cases $J=J_0$ and $J=J_0 \pm 2$. The latter

oscillates for free molecule at an angular frequency $(E_{J_0+2} - E_{J_0})/k$ which is always greater than 10^{14} sec^{-1} for ortho- H_2 . Needler and Opechowski⁴ have shown that the contribution from the non-diagonal terms is negligible compared with the contribution from the diagonal terms as long as the collision frequencies are smaller than 10^{13} sec^{-1} . As the collision frequency in H_2 gas does not exceed 10^{12} sec^{-1} even at several hundred atmospheres at room temperature, the matrix elements between different J states can be neglected.

Therefore, the important non-zero matrix elements of L_{ℓ_0} are given by

$$\langle JM | L_{\ell_0} | JM \rangle = [f_{\ell}(J)]^{1/2} C(J, \ell, J; M, 0) \quad (3.2.9.)$$

where $C(J, \ell, J, M, 0)$ is a Clebsch-Gordon coefficient as defined by Rose¹⁹

and

$$f_1(J) = 2J(J+1) \quad (3.2.10.)$$

$$f_2(J) = \frac{5}{4\pi} \frac{J(J+1)}{(2J-1)(2J+3)} \quad (3.2.11)$$

The correlation function of $L_{\ell_0}(t)$ may be written as

$$G_{\ell_0}(t) = \sum_{J_0 M_0} P_{J_0 M_0} \langle J_0 M_0 | L_{\ell_0} | J_0 M_0 \rangle \sum_{J, M} W(J, M, t / J_0 M_0, 0) \langle JM | L_{\ell_0} | JM \rangle \quad (3.2.12)$$

$$= \sum_{J_0 M_0} P_{J_0 M_0} [f_{\ell}(J_0)]^{1/2} C(J_0, \ell, J_0, M_0, 0) \sum_{J, M} W(J, M, t / J_0, M_0, 0) \times [f_{\ell}(J)]^{1/2} C(J, \ell, J, M, 0) \quad (3.2.13)$$

where $W(J, M, t / J_0, M_0, 0)$ is the probability that the molecule is in the rotational state J, M at time t given that it is in

the state J_0, M_0 at $t=0$, and

$$P_{J_0, M_0} = \frac{1}{2J_0+1} P_{J_0} = \frac{\exp[-E_{J_0}/kT]}{\sum_J (2J+1) \exp[-E_J/kT]} \quad (3.2.14)$$

is the probability that a molecule is in the state J_0, M_0 of energy E_{J_0} for a system at temperature T . $W(J, M, t/J_0, M_0, 0)$ satisfies the master equation

$$\dot{W}(J, M, t/J_0, M_0, 0) = \sum_{J', M'} A(J, M; J', M') W(J', M', t/J_0, M_0, 0) \quad (3.2.15)$$

where $A(J, M, J', M')$ is the transition probability per unit time for the transition $J', M' \rightarrow JM$

For $J = J'$, $M = M'$

$$A(J, M; J, M) = -\sum_{J' \neq J} \sum_M A(J, M; J', M) - \sum_{M \neq M'} A(J, M; J, M') \quad (3.2.16)$$

Defining the tensor polarisation of order l in the state J for molecules initially in the state J_0, M_0 as

$$m_{JJ_0, M_0}^l(t) = \sum_M C(J, l, J, M, 0) W(J, M, t/J_0, M_0, 0) \quad (3.2.17)$$

and using equation (3.2.15), it may be seen that the following differential equation is satisfied

$$\dot{m}_{JJ_0, M_0}^l(t) = \sum_{J', M'} W(J', M', t/J_0, M_0, 0) \sum_M C(J, l, J, M, 0) A(J, M; J', M') \quad (3.2.18)$$

Weak Collision Approximation.

It is assumed that the anisotropic intermolecular interactions are "weak" so that first order perturbation theory may be used to calculate the transition probability $A(J, M; J', M')$.

If each term in the anisotropic interaction hamiltonian can be expressed as a product of a "lattice" operator and a rotational operator $Y_{\lambda\mu}(\Omega)$, where $Y_{\lambda\mu}(\Omega)$ is a spherical harmonic of order λ

the matrix element between states J, M and J', M' is given by

$$\langle JM | Y_{\lambda\mu} | J'M' \rangle = \delta_{M, M'+\mu} \left[\frac{(2J'+1)(2\lambda+1)}{4\pi(2J+1)} \right]^{1/2} C(J'\lambda J; M\mu) C(J'\lambda J; 00) \quad (3.2.19)$$

Since the transition probability is proportional to the square of the matrix element between the initial and final states, the contribution of this term to the transition probability is

$$A_{\lambda}(JM, J'M') = Q_{\lambda}(J, J') \left[C(J'\lambda J; M', M-M') \right]^2 \quad (3.2.20)$$

$Q_{\lambda}(J, J')$ contains all the information about the anisotropic intermolecular interactions and will be evaluated later.

Using equation (3.2.20) and equations (6.23a) and (6.23b) of Rose, it can be shown that

$$\sum_M C(J\ell J; M, 0) A_{\lambda}(JM, J'M') = C(J'\ell J'; M'0) B_{\ell\lambda}(J, J') \quad (3.2.21)$$

where

$$B_{\ell\lambda}(J, J') = \frac{2J+1}{2J'+1} Q_{\lambda}(J, J') (-1)^{\lambda+\ell-J-J'} \left[\frac{(2J+1)(2J'+1)}{4\pi} \right]^{1/2} W(JJ'JJ'; \lambda, \ell) - \delta_{JJ'} \sum_{J''} \frac{2J''+1}{2J'+1} Q_{\lambda}(J'', J') \quad (3.2.22)$$

where $W(JJ'JJ'; \lambda, \ell)$ is a Racah coefficient.

Using equations (3.2.18), (3.2.21) and (3.2.22), it can be shown that the tensor polarisation satisfies the following equation

$$\dot{m}_{JJ_0 M_0}^{\ell}(t) = \sum_{J'} B_{\ell}(J, J') m_{J' J_0}^{\ell}(t) \quad (3.2.23)$$

where $B_{\ell}(J, J') = \sum_{\lambda} B_{\ell\lambda}(J, J')$ (3.2.24)

From equation (3.2.17) the initial conditions are obtained as

$$m_{J_0 M_0}^{\ell}(0) = C(J_0 \ell J_0; M_0 0) \delta_{JJ_0} \quad (3.2.25)$$

and the solutions to the equation (3.2.23) are given by

$$m_{J_0 M_0}^{\ell}(t) = \sum_{\alpha} a_{J_0 M_0}^{\ell\alpha} e^{-\Lambda_{\ell\alpha} t} \quad (3.2.26)$$

The number of terms in the sum is equal to the number of

equations (3.2.15) used in solving equation (3.2.23) which is the same as the number of rotational states that are significantly populated. From the initial conditions it follows that

$$a_{J_0 M_0}^{l\alpha} = b_{J_0}^{l\alpha} C(J_0 l J_0; M_0, 0) \quad (3.2.27)$$

where $b_{J_0}^{l\alpha}$ are independent of time.

The correlation function $G_{l_0}(t)$ defined by equation (3.2.13) can now be written using equations (3.2.17), (3.2.26) and (3.2.27) as below.

$$G_{l_0}(t) = \sum_{J_0} [f_l(J_0)]^{1/2} \sum_{M_0} P_{J_0 M_0} [C(J_0 l J_0, M_0, 0)]^2 \sum_{\alpha} e^{-\Lambda_{l\alpha} t} \sum_J [f_l(J)]^{1/2} b_{J_0}^{l\alpha} \quad (3.2.28)$$

since
$$\frac{1}{2J_0+1} \sum_{M_0} [C(J_0 l J_0; M_0, 0)]^2 = \frac{1}{2l+1} \quad (3.2.29)$$

and
$$P_{J_0 M_0} = \frac{1}{2J_0+1} P_{J_0} \quad (3.2.30)$$

equation (3.2.28) can be written as

$$G_{l_0}(t) = \frac{1}{2l+1} \sum_{J_0} P_{J_0} f_l(J_0) \sum_{\alpha} C_{J_0}^{l\alpha} e^{-\Lambda_{l\alpha} t} \quad (3.2.31)$$

where

$$C_{J_0}^{l\alpha} = \left[\frac{1}{f_l(J_0)} \right]^{1/2} \sum_J [f_l(J)]^{1/2} b_{J_0}^{l\alpha} \quad (3.2.32)$$

It may be noted that the correlation function can always be written as a sum of exponential functions of time in the weak collision approximation. The Fourier transform of the correlation function is given by

$$\begin{aligned} J_{l_0}(\omega) &= \int_{-\infty}^{\infty} e^{-i\omega t} G_{l_0} dt \\ &= \frac{2}{(2l+1)} \sum_{J_0} P_{J_0} f_l(J_0) \sum_{\alpha} \frac{C_{J_0}^{l\alpha} \Lambda_{l\alpha}}{\Lambda_{l\alpha}^2 + \omega^2} \end{aligned} \quad (3.2.33)$$

since it follows from equation (3.2.7) that

$$J_{lm}(\omega) = J_{l_0}(\omega - m\omega_J) \quad (3.2.34)$$

the expression for $\frac{1}{T_1}$ can be written as, using equation (3.2.3)

$$\frac{1}{T_1} = \frac{\gamma^2 H'^2}{2} \frac{2}{3} \sum_{J_0} P_{J_0} f_1(J_0) \sum_{\alpha} \frac{C_{J_0}^{\alpha} \Lambda_{1\alpha}}{\Lambda_{1\alpha}^2 + \omega^2} + \frac{12\pi}{5} \gamma^2 H''^2 \frac{2}{5} \sum_{J_0} P_{J_0} f_2(J_0) \sum_{\alpha} \frac{C_{J_0}^{2\alpha} \Lambda_{2\alpha}}{\Lambda_{2\alpha}^2 + \omega^2} \quad (3.2.35)$$

From the above expression, it may be seen that

$$\frac{1}{T_1} = \sum_{J_0} P_{J_0} \left(\frac{1}{T_1} \right)_{J_0}$$

where $\left(\frac{1}{T_1} \right)_{J_0}$ is the relaxation rate for an ensemble of molecules which are all initially in the state J_0 .

3.3. Application of the Theory to some Special Cases:

3.3.1. Infrequent Transitions between States of Different J.

When the transitions between different J states occur much less frequently than the transitions between different M states within a J manifold, it can be shown from equations (3.2.20), (3.2.22) and (3.2.24) that

$$B_{\ell}(J, J') = B_{\ell}(JJ) \delta_{JJ'} \quad (3.3.1.)$$

and the index α can be replaced by J_0

From equations (3.2.23), (3.2.26), (3.2.27) and (3.3.1.), it may be shown that

$$C_{J_0}^{\ell\alpha} = \left[\frac{1}{f_{\ell}(J_0)} \right]^{1/2} \sum_J [f_{\ell}(J)]^{1/2} \delta_{JJ_0} = 1 \quad (3.3.2.)$$

and
$$\Lambda_{\ell J_0} = - B_{\ell}(J_0, J_0) \quad (3.3.3.)$$

Therefore

$$J_{\ell 0}(\omega) = \frac{2}{2\ell+1} \sum_{J_0} P_{J_0} f_{\ell}(J_0) \frac{\Lambda_{\ell J_0}}{\Lambda_{\ell J_0}^2 + \omega^2} \quad (3.3.4.)$$

$$= \frac{2}{2\ell+1} \sum_{J_0} P_{J_0} f_{\ell}(J_0) \frac{\tau_{\ell}^{J_0}}{1 + \omega^2 \tau_{\ell}^{J_0 2}} \quad (3.3.5.)$$

where $\frac{1}{\tau_{\ell}^{J_0}} = -B_{\ell}(J_0, J_0)$

At low temperatures in H_2 , $P_{J_0} = \delta_{J_0, 1}$ and equation (3.3.5.) is the same result as originally derived by Schwinger. Equation (3.3.5.) was also derived by Bloom and Oppenheim ⁷ as a generalisation of Schwinger's result for the case in which transitions between different rotational states are negligible.

3.3.2. Two-level System.

In this case it will be assumed that only two of the rotational states are appreciably populated so that only two of the equations (3.2.23) need to be considered to evaluate T_1 with reasonable accuracy. For H_2 this situation can be achieved below $450^\circ K$ since at this temperature the population of $J=5$ state is only about 1.38%.

The equations to be solved for the two-level system are

$$\begin{aligned} \dot{m}_{J_1, J_0, M_0}^{\ell} &= B_{\ell}(J_1, J_1) m_{J_1, J_0, M_0}^{\ell} + B_{\ell}(J_1, J_2) m_{J_2, J_0, M_0}^{\ell} \\ \dot{m}_{J_2, J_0, M_0}^{\ell} &= B_{\ell}(J_2, J_1) m_{J_1, J_0, M_0}^{\ell} + B_{\ell}(J_2, J_2) m_{J_2, J_0, M_0}^{\ell} \end{aligned} \quad (3.3.6.)$$

where J_0 can take the values of J_1 and J_2 .

Solving these two equations the rate constants $\Lambda_{\ell\alpha}$ and the coefficients $C_{J_0}^{\ell\alpha}$ can be obtained where $\alpha = 1, 2$ and $J_0 = J_1, J_2$.

$$\Lambda_{\ell i} = -\frac{1}{2} \left[B_{\ell}(J_1, J_1) + B_{\ell}(J_2, J_2) + (-1)^{i+1} \left\{ \left[B_{\ell}(J_1, J_1) - B_{\ell}(J_2, J_2) \right]^2 + 4 B_{\ell}(J_1, J_2) B_{\ell}(J_2, J_1) \right\}^{1/2} \right] \quad (3.3.7.)$$

$$C_{J_1}^{e1} = \frac{\Lambda_{e2} + B_e(J_1, J_1)}{\Lambda_{e2} - \Lambda_{e1}} + \left[\frac{f_e(J_2)}{f_e(J_1)} \right]^{1/2} \frac{B_e(J_2, J_1)}{\Lambda_{e2} - \Lambda_{e1}} \quad (3.3.8.)$$

$$C_{J_1}^{e2} = - \frac{\Lambda_{e1} + B_e(J_1, J_1)}{\Lambda_{e2} - \Lambda_{e1}} - \left[\frac{f_e(J_2)}{f_e(J_1)} \right]^{1/2} \frac{B_e(J_2, J_1)}{\Lambda_{e2} - \Lambda_{e1}}$$

and $C_{J_2}^{e2}$ and $C_{J_2}^{e1}$ are obtained from $C_{J_1}^{e1}$ and $C_{J_1}^{e2}$ respectively, by permuting 1 and 2.

By substituting equations (3.3.7.) and (3.3.8.) into equation (3.2.33), $J_{e0}(\omega)$ can be expressed in terms of $B(J, J')$.

In the short correlation time limit i.e. $\Lambda_{e\alpha} \gg \omega$ for a two-level system

$$\sum_{\alpha} \frac{C_{J_0}^{e\alpha} \Lambda_{e\alpha}}{\Lambda_{e\alpha}^2 + \omega^2} = \frac{C_{J_0}^{e1}}{\Lambda_{e1}} + \frac{C_{J_0}^{e2}}{\Lambda_{e2}} \quad (3.3.9.)$$

Using equation (3.3.8.) the above expression can be written as

$$\frac{C_{J_1}^{e1}}{\Lambda_{e1}} + \frac{C_{J_2}^{e2}}{\Lambda_{e2}} = \frac{-B_e(J_2, J_2) + \left[\frac{f_e(J_2)}{f_e(J_1)} \right]^{1/2} B_e(J_2, J_1)}{\Lambda_{e1} \Lambda_{e2}} \quad (3.3.10)$$

and by symmetry

$$\frac{C_{J_2}^{e1}}{\Lambda_{e1}} + \frac{C_{J_1}^{e2}}{\Lambda_{e2}} = \frac{-B_e(J_1, J_1) + \left[\frac{f_e(J_1)}{f_e(J_2)} \right]^{1/2} B_e(J_1, J_2)}{\Lambda_{e1} \Lambda_{e2}} \quad (3.3.11)$$

Substituting into equation (3.2.33.), $J_e(0)$ can be expressed as

$$J_e(0) = \frac{2}{2\ell+1} \frac{1}{\Lambda_{e1} \Lambda_{e2}} \left[P_{J_1} f_e(J_1) (-B_e(J_2, J_2)) + P_{J_2} f_e(J_2) (-B_e(J_1, J_1)) \right. \\ \left. + \left\{ f_e(J_1) f_e(J_2) \right\}^{1/2} \left\{ P_{J_1} B_e(J_2, J_1) + P_{J_2} B_e(J_1, J_2) \right\} \right] \quad (3.3.12)$$

In the limit of no changes in J

$$B_e(J_1, J_2) = B_e(J_2, J_1) = 0$$

Therefore

$$\Lambda_{\ell_1} = -B_{\ell}(J_1, J_1) = \frac{1}{\tau_{\ell}^{J_1}}$$

$$\Lambda_{\ell_2} = -B_{\ell}(J_2, J_2) = \frac{1}{\tau_{\ell}^{J_2}}$$

and equation (3.3.12) reduces to

$$J_{\ell}^{(0)} = \frac{2}{2\ell+1} \left[P_{J_1} f_{\ell}(J_1) \tau_{\ell}^{J_1} + P_{J_2} f_{\ell}(J_2) \tau_{\ell}^{J_2} \right] \quad (3.3.13)$$

Equation (3.3.13) was first derived by Johnson and Waugh⁵ for the special case described above.

3.4. Evaluation of $B_{\ell}(J, J')$ in terms of Intermolecular Anisotropic Interactions.

The anisotropic intermolecular potential between two molecules, labelled 1 and 2 respectively, is assumed to consist of two terms

$$\mathcal{H}_R = \mathcal{H}_R^{(1)} + \mathcal{H}_R^{(2)} \quad (3.4.1.)$$

where

$$\mathcal{H}_R^{(1)} = b^{(1)}(r) P_2(\cos \theta'_1) \quad (3.4.2.)$$

and

$$\mathcal{H}_R^{(2)} = b^{(2)}(r) \sum_{q=-2}^2 a_{2q} Y_{2q}(\Omega'_1) Y_{2q}^*(\Omega'_2) \quad (3.4.3.)$$

$b^{(1)}(r)$ and $b^{(2)}(r)$ are functions of the separation of the centres of mass of 1 and 2, $P_2(\cos \theta'_1)$ is the Legendre polynomial of order 2 of the angle θ'_1 , which the molecular axis of molecule 1 makes with \vec{r} , $Y_{2q}(\Omega'_1)$ and $Y_{2q}(\Omega'_2)$ are second order spherical harmonics and Ω'_1 and Ω'_2 are the orientations of the symmetry axes of molecules 1 and 2, respectively, with respect to \vec{r} . The a_{2q} are constants.

$\mathcal{H}_R^{(1)}$ is the most general potential if molecule 1 is an ortho- H_2 molecule restricted to $J=1$ state and molecule 2 has no rotational degrees of freedom such as He or para- H_2 res-

stricted to its ground state ($J=0$). $\mathcal{H}_R^{(2)}$ depends on the orientations of both the molecules and is the most general form if both 1 and 2 molecules are ortho- H_2 in the ground rotational state (i.e. $J=1$) and if there are no transitions between different rotational states. These conditions are realised at sufficiently low temperatures for H_2 when the population of $J=3$ state is negligible. The number of terms that are required to specify the most general form of \mathcal{H}_R at higher temperatures depends on the state of largest J which contributes appreciably to the relaxation rate. However, as the additional terms will only increase the number of parameters and complicate the analysis too much to obtain any information on the intermolecular potentials, it will be assumed that $\mathcal{H}_R^{(1)}$ and $\mathcal{H}_R^{(2)}$ are given by the equations (3.4.2.) and (3.4.3.) respectively. It will further be assumed that there is no interference between the contributions from $\mathcal{H}_R^{(1)}$ and $\mathcal{H}_R^{(2)}$ to $Q_2(J, J')$ and hence $Q_2(J, J')$ may be written as

$$Q_2(J, J') = Q_2^{(1)}(J, J') + Q_2^{(2)}(J, J') \quad (3.4.4.)$$

In order to obtain the $Q_2(J, J')$ it is necessary to evaluate the transition probability per unit time $A(JM, J'M')$ of molecule 1. $A(JM, J'M')$ is obtained after averaging over the equilibrium ensemble of molecule 2, the averages being taken over all position, momentum and angular momentum states of molecule 2.

The transition probability per unit time of a molecule between the states J, M and J', M' is given by ¹

$$A(JM, J'M') = \frac{1}{\hbar^2} \int_{-\infty}^{\infty} e^{-i\omega_{JJ'} t} \overline{\langle J'M' | \mathcal{H}_R^{(1)}(t) | JM \rangle \langle JM | \mathcal{H}_R^{(1)}(0) | J'M' \rangle} dt \quad (3.4.5.)$$

providing that the anisotropic interaction between the molecules is quite small so that perturbation theory can be used, and that the energy difference between the initial and final rotational states $\hbar\omega_{JJ'}$ is much smaller than kT . The bar represents an ensemble average, the average being taken over all the relative positions and momenta of molecules 1 and 2.

Transforming $\mathcal{H}_R^{(1)}$ to laboratory reference frame

$$P_2(\cos \theta') = \frac{4\pi}{5} \sum_{\mu=-2}^2 Y_{2\mu}(\Omega_1) Y_{2\mu}^*(\Omega) \quad (3.4.6.)$$

where Ω_1 and Ω are the orientations of molecule 1 and vector \vec{R} respectively, in the space fixed coordinate system in which the z-axis is along \vec{H}_0 .

Substituting equation (3.4.6.) into (3.4.5.) and using (3.2.20)

$$Q_2^{(1)}(J, J') = \frac{4\pi}{5} \left(\frac{2J'+1}{2J+1} \right) [C(J' 2 J; 00)]^2 j^{(1)}(\omega_{JJ'}) \quad (3.4.7.)$$

where

$$j^{(1)}(\omega_{JJ'}) = \frac{1}{\hbar^2} \int_{-\infty}^{\infty} e^{-i\omega_{JJ'} t} k^{(1)}(t) dt \quad (3.4.8.)$$

and;

$$k^{(1)}(t) = \overline{b^{(1)}(r(t)) Y_{2,-\mu}(\Omega(t)) b^{(1)*}(r(0)) Y_{2\mu}^*(\Omega(0))} \quad (3.4.9.)$$

is the correlation function of $b^{(1)}(r) Y_{2,-\mu}(\Omega)$ which is independent of μ for a gas. The correlation time $k^{(1)}(t)$ decays in a time of the order of average time of a single collision

τ_{coll} between a pair of molecules in a dilute gas.

$$\tau_{coll} \approx \frac{a}{(3kT/\mu)^{1/2}} = \frac{a}{V_0} \quad (3.4.10)$$

where a is the approximate range of the intermolecular interactions, μ is the reduced mass of molecules 1 and 2 and V_0 is the r.m.s. value of their relative velocity.

Since

$$\begin{aligned} j^{(1)}(\omega_{JJ'}) &\approx j^{(1)}(0) && \text{if } \omega_{JJ'} \tau_{coll} \ll 1 \\ j^{(1)}(\omega_{JJ'}) &\ll j^{(1)}(0) && \text{if } \omega_{JJ'} \tau_{coll} \gg 1 \end{aligned} \quad (3.4.11)$$

it can be concluded that very little energy is exchanged between rotational and translational degrees of freedom if

$$\omega_{JJ'} \tau_{coll} \ll 1$$

The only non-zero terms for $Q_2^{(1)}(JJ')$ correspond to $J'=J$ and $J'=J \pm 2$. For H_2 molecule

$$Q_2^{(1)}(J, J \pm 2) \ll Q_2(J, J) \quad (3.4.12)$$

since, at $700^\circ K$ $\omega_{31} \tau_{coll} \approx 8$

The correlation functions given by equation (3.4.9.)

were calculated by Bloom and Oppenheim⁶ using the "constant acceleration approximation". Using the results of their theory⁶

(P. 866) $j^{(1)}(0)$ can be written as

$$j^{(1)}(0) = \rho a^4 (2\pi\beta\mu)^{1/2} I^{(1)}(2) \quad (3.4.13)$$

where ρ is the number density of molecules of type 2 and

$$I^2(\rho) = \int_0^\infty dy \left[\int_0^\infty [g(x)]^{1/2} x^{3/2} \mathcal{L}^{(q)}(ax) J_{p+\frac{1}{2}}(xy) dx \right]^2 \quad (3.4.14)$$

where a is the characteristic length for the spherically symmetric intermolecular potential between molecules 1 and 2,

$x = r/a$; $g(x)$ is the radial distribution function for

the pair of molecules under consideration, $J_{p+\frac{1}{2}}$ is the Bessel function of $p+\frac{1}{2}$ and μ is the reduced mass.

Substituting (3.4.13) in (3.4.7.), $Q_2^{(1)}(J,J)$ can be written as

$$Q_2^{(1)}(J,J) = \left(\frac{4\pi}{5r^2}\right) \rho a^4 (2\pi\beta\mu)^{1/2} I^{(1)}(2) \left[\frac{J(J+1)}{(2J-1)(2J+3)} \right] \quad (3.4.15)$$

Evaluating the Racah coefficients in equation (3.2.22)

$B_2^{(1)}(J,J)$ is obtained as

$$B_1^{(1)}(J,J) = -\frac{3}{J(J+1)} Q_2^{(1)}(J,J) \quad (3.4.16)$$

$$B_2^{(1)}(J,J) = B_1(J) \frac{3(4J^2+4J-7)}{(2J-1)(2J+3)} \quad (3.4.17)$$

for $\lambda = 2$

The contribution of $\mathcal{H}_R^{(2)}$ to the $B_2(J,J)$ will now be evaluated. It is assumed that the dominant interaction is the quadrupole-quadrupole interaction for which the values of a_q in equation (3.4.3.) are

$$a_0 = 6, a_1 = a_{-1} = -4, a_2 = a_{-2} = 1 \quad \text{and} \\ b^{(2)}(r) = (4\pi Q_1 Q_2) / r^5 \quad (3.4.18)$$

Making the transformation to the laboratory reference frame

$$\mathcal{H}_R^{(2)} = \left(\frac{56\pi}{45}\right)^{1/2} b^{(2)}(r) \sum_{m, m', \mu} (-1)^m C(2, 2, 4; m, m', \mu) \\ \times Y_{2m}(\Omega_1) Y_{2m'}(\Omega_2) Y_{4, -\mu}(\Omega) \quad (3.4.19)$$

$\mathcal{H}_R^{(2)}$ produces transitions of molecule 1 from the state J', M' to the state J, M while molecule 2 undergoes a simultaneous transition from the state J''', M''' to state J''', M'' . Denoting the transition probability for this process by

$A((J^I M^I, J^I M^I)(J^{II} M^{II}, J^{III} M^{III}))$, $A(J^I M^I, J^I M^I)$ is obtained as

$$A^{(2)}(J^I M^I, J^I M^I) = \sum_{J^{II}} \sum_{J^{III}} \sum_{M^{II}} \sum_{M^{III}} A((J^I M^I, J^I M^I)(J^{II} M^{II}, J^{III} M^{III})) \quad (3.4.20)$$

where

$$A[(J^I M^I, J^I M^I)(J^{II} M^{II}, J^{III} M^{III})] = \sum_{m, m'} \left(\frac{56\pi}{45} \right) j^{(2)}(\omega_{JJ', J''J'''}) [C(224, m, m')]^2 \quad (3.4.21)$$

$$\times \frac{P_{J''''}}{2J''''+1} \left| \langle J^I M^I | Y_{2m}(\Omega_1) | J^I M^I \rangle \right|^2 \left| \langle J^{II} M^{II} | Y_{2m'}(\Omega_2) | J^{III} M^{III} \rangle \right|^2$$

and

$$\hbar \omega_{JJ', J''J'''} = (E_J - E_{J'}) + (E_{J''} - E_{J'''}) \quad (3.4.22)$$

$j^{(2)}(\omega)$ is the Fourier transform of $k^{(2)}(t)$ which is given by

$$k^{(2)}(t) = (N-1) \overline{G^{(2)}(r(0)) Y_{4-\mu}(\Omega(0)) G^{(2)}(r(t)) Y_{4-\mu}(\Omega(t))} \quad (3.4.23)$$

Using equation (3.2.19) to obtain the matrix elements in equation (3.4.21) and summing over m, m', M^{II} and M^{III} and defining $Q_2^{(2)}(JJ')$ by equation (3.2.20), $Q_2^{(2)}(J, J')$ is obtained as

$$Q_2^{(2)}(J, J') = \frac{7}{10\pi} [C(J, 2, J', 00)]^2 \sum_{J'' J'''} P_{J''''} [C(J'' J''', 00)]^2 j^{(2)}(\omega_{JJ', J''J'''}) \quad (3.4.24)$$

$k^{(2)}(t)$ also decays in a time of the order of τ_{coll}

Therefore,

$$j^{(2)}(\omega) \approx j^{(2)}(0) \quad \text{if} \quad \omega \tau_{coll} \ll 1 \quad (3.4.25)$$

$$j^{(2)}(\omega) \ll j^{(2)}(0) \quad \text{if} \quad \omega \tau_{coll} \gg 1$$

$Q_2^{(2)}(JJ')$ is non-zero for $J' = J$ and $J' = J \pm 2$ and $J'' = J''$ and $J'' = J'' \pm 2$. Up to the order of 500°K only $J=1$ and 3 states for ortho- H_2 and $J=0, 2$ and 4 states for para- H_2 need to be considered. The following transitions $(J', J'' \leftrightarrow J, J''')$ give appreciable contribution to $Q_2^{(2)}(J, J')$. For ortho-ortho collisions $\omega_{JJ', J''J'''} = 0$ for $(1, 3 \leftrightarrow 3, 1)$ transitions and for all other transitions $\omega_{JJ', J''J'''} \tau_{coll} \gg 1/2$ at room temperature.

For ortho-para collisions $\omega_{JJ'J''J'''} = 0$ only for $(J, J' \leftrightarrow J, J'')$. For the transitions $(1, 2 \leftrightarrow 3, 0)$ and $(1, 4 \leftrightarrow 3, 2)$ $\omega_{JJ'J''J'''} \tau_{coll} \approx 4.7$ at room temperature. According to Van Kranendonk's²⁰ calculation of $j(\omega)$ versus ω for a quadrupole-quadrupole interaction, $j(\omega)$ is large for $\omega \tau_{coll} \leq 5$ and rapidly decreases for higher values of ω . Therefore, the above-mentioned transitions have to be taken into account for ortho-para interactions.

Using equations (3.4.20) and (3.4.21) the ratio of the transition rates $(J' \rightarrow J)$ and $(J \rightarrow J')$ for molecule 1 is obtained as

$$\frac{A(JM, J'M')}{A(J'M', JM)} = \begin{cases} e^{-\beta h \omega_{JJ'}} & \text{for } (JJ' \leftrightarrow JJ'') \\ e^{-\beta h \omega_{JJ''J'''}} & \text{for } (J'J'' \leftrightarrow JJ'') \end{cases} \quad (3.4.26)$$

Since the Boltzmann factor is lost in the latter case, Oppenheim suggested a prescription to treat these collisions which was discussed in more detail in a separate paper by Bloom and Oppenheim⁹. The prescription is to multiply the upward transitions and downward transitions of molecule 1 by

ϵ_1 and ϵ_2 respectively where

$$\epsilon_1 = \frac{1}{2} (1 + e^{-\beta h \omega_{JJ'J''J'''}}) \quad (3.4.27)$$

and

$$\epsilon_2 = \frac{1}{2} (1 + e^{+\beta h \omega_{JJ'J''J'''}}) \quad (3.4.28)$$

The transitions $(1, 3 \leftrightarrow 3, 1)$ and $(J, J'' \leftrightarrow J, J'')$ will be referred to as resonant transitions caused by resonant collisions while the transitions of the type $(1, 2 \leftrightarrow 3, 0)$ and $(1, 4 \leftrightarrow 3, 2)$ will be called as quasi-resonant transitions caused by quasi-resonant collisions in the rest of this thesis.

All the other transitions for which $k \omega_{JJ'J''J'''} \neq 0$ are
termed as non-resonant transitions.

CHAPTER IV

EXPERIMENTAL RESULTS AND DISCUSSION4.1. GENERAL REMARKS

The spin-lattice relaxation time T_1 was measured in normal H_2 and its mixtures with He and CO_2 as a function of density and temperature from $293^\circ K$ up to $700^\circ K$. The densities used were sufficiently high to be away from T_1 minimum and yet low enough for the three body collisions to be negligible. Under these conditions the theory predicts that T_1 is proportional to the density. The highest pressures used in the experiments were of the order of 2000 p.s.i. The experiment at any temperature was started with the highest pressure available and T_1 was measured at different pressures reducing the pressure in convenient steps. The lowest pressure reached at any temperature was determined by signal to noise considerations. At room temperature this was about 100 p.s.i. (≈ 7 amagats) whereas at $738^\circ K$ it was about 600 p.s.i. (≈ 15 amagats).

4.2. HYDROGEN4.2.1. Results.

Typical plots of T_1 versus density are shown in figures 8a and 8b for normal H_2 at room temperature and at $738^\circ K$ respectively. The most probable value of T_1 at any pressure and temperature was obtained by fitting the straight line through the data $\log[A(\infty) - A(t)]$ versus t by eye and the error on this value was obtained by drawing the straight line through the

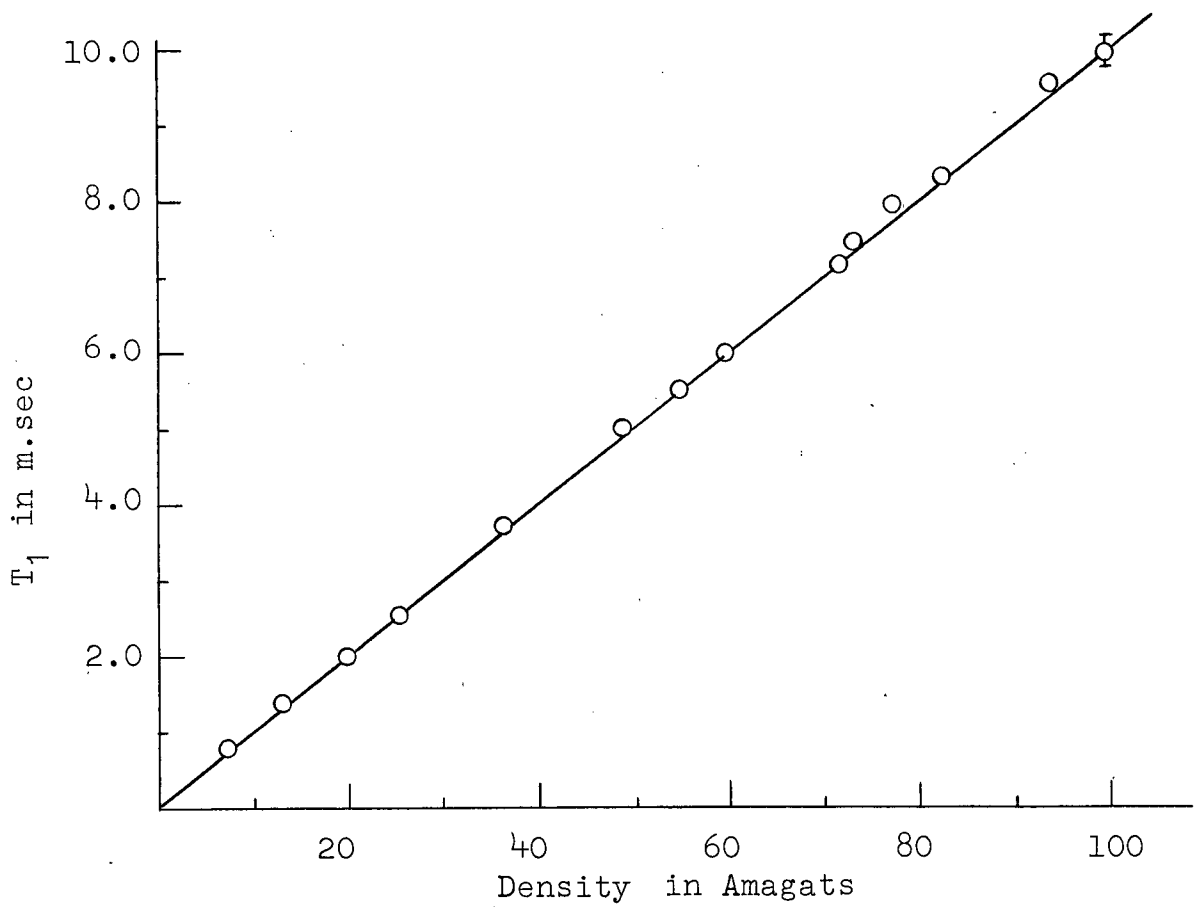


FIG. 8a. T_1 vs. Density at 293°K in normal H_2

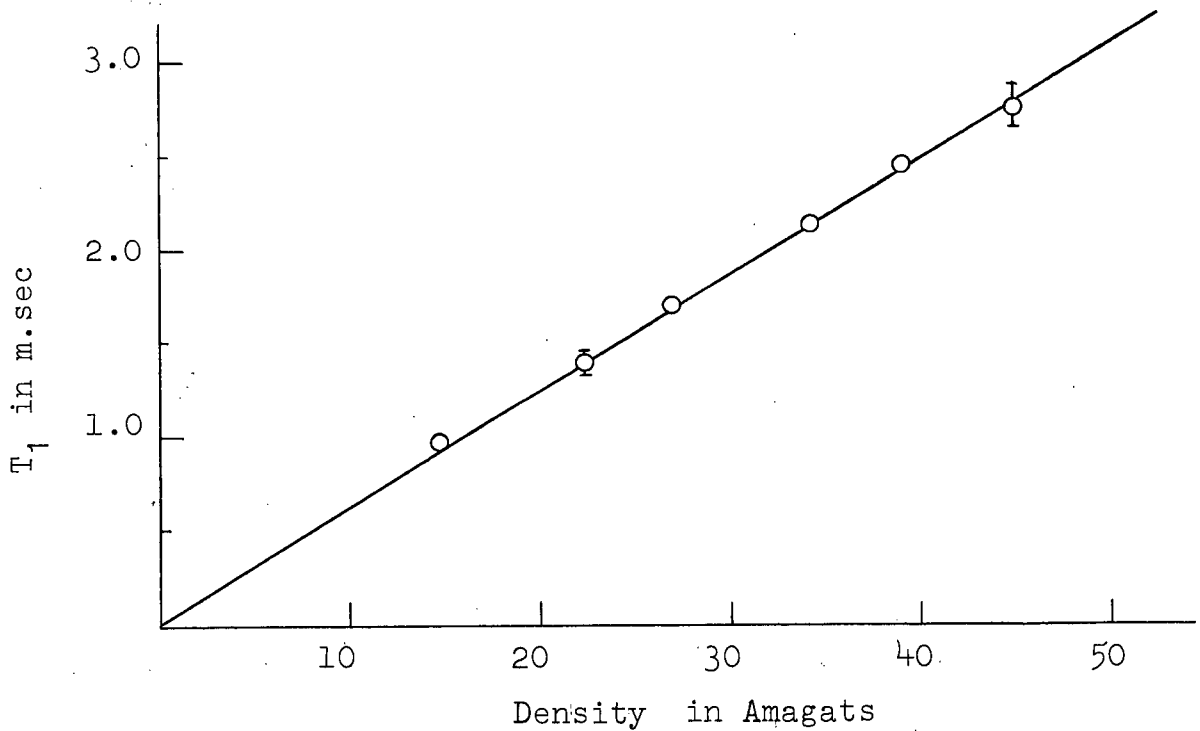


FIG. 8b. T_1 vs. Density at 738°K in normal H_2

extreme points. However, a least squares fit was carried out in a few selected cases on an I.B.M. 7040 computer and the slope thus obtained agreed with that of the best fit by eye within 5%. The solid line in figures 8a and 8b represents the least squares fit and the errors represented as $\pm \delta$ correspond to the condition that there is a 5% probability that the correct experimental values be outside the limits given by the error $\pm \delta$.

Knowing the temperature and pressure, the number density of the gas was obtained from the tables given by Wooley et al.¹⁴ As these tables were given only up to 600°K, Wooley has suggested (private communication) that the estimate of density at higher temperatures as a function of pressure can be obtained to a good approximation from the following equation

$$PV/RT = \exp [B\rho + C\rho^2]$$

where

$$B = 0.0055478 T^{-1/4} - 0.03688 T^{-3/4} - 0.22004 T^{-5/4}$$

and

$$C = 0.004788 T^{-3/2} - 0.04053 T^{-2}$$

The computations were carried out on an I.B.M. 7040 computer and the density was obtained as a function of pressure in the temperature range 500°K - 1200°K.

In figure 9 T_1/ρ is plotted as function of temperature from 293°K up to 738°K along with the data available below room temperature from previous work.

The data at room temperature from the present work may be compared with the previous work of Williams²¹ (1962), Johnson and Waugh⁵ (1962), Lipsicas²² (1962), Armstrong²³ (1966) and Riehl²⁴ (1966). Lipsicas obtained the value of T_1/ρ as 0.125 m.sec/Amagat which is 25% higher than the value

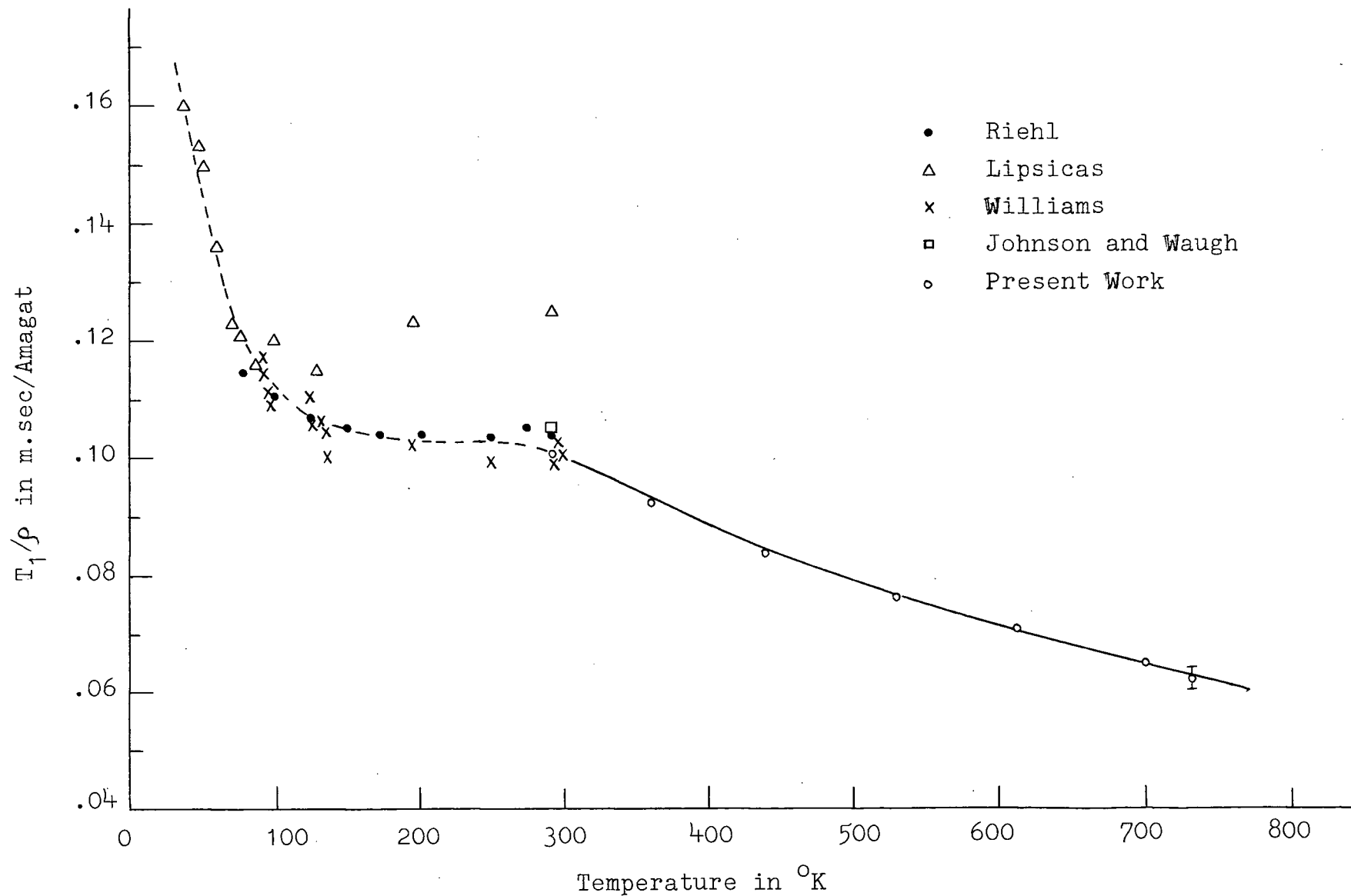


FIG. 9. T_1/ρ as a function of temperature in normal H_2 .

obtained in the present work. The value obtained in the present work is 0.100 m.sec/Amagat and agrees, within experimental errors, with that of Williams (0.100 m,sec/Amagat), Johnson and Waugh (0.105 m.sec/Amagat), Armstrong (0.106 m.sec/Amagat) and Riehl (0.105 m.sec/Amagat). Lipsicas' data differs significantly from Williams' and Riehl's between 120°K and 293°K also, though it agrees very well with their data below 100°K. On examination of Lipsicas' data as presented in his thesis it appears that the discrepancy is due to the high densities that were used in his measurements. Presumably, the effect of three body collisions increased the apparent value of T_1/ρ . In fact, Armstrong analysed the dependence of T_1 on ρ for high densities assuming that T_1 is given by

$$T_1 = A\rho + B\rho^2$$

and his work indicates that the contribution from ρ^2 term to T_1 is about 10% if ρ is of the order of 100 amagats.

Though the absolute values differ, the general trend of the curve is the same in all the cases. T_1/ρ decreases very sharply with increase of temperature from low temperatures up to 150°K and remains constant between 150°K and 293°K. As the temperature is increased above room temperature T_1/ρ decreases gradually to a value of 0.602 m.sec/Amagat at 738°K.

4.2.2. Interpretation.

In this section, the theory discussed in the previous chapter will be used to extract information on the intermolecular anisotropic interactions from the experimental data of temperature dependence of T_1/ρ in H_2 , assuming that the

isotropic part of the intermolecular potential is given by a Lennard-Jones potential. The discussion will be confined to a two level system even though the fractional population of the $J=5$ state is 0.03 at 500°K and 0.07 at 700°K and this assumption is not strictly valid at these temperatures.

In order to interpret the results it is necessary to write down the expression for $\frac{1}{T_1}$ explicitly. From equations (3.2.22), (3.3.12) and (3.2.3.)¹ it may be seen that $\frac{1}{T_1}$ is essentially a function of $Q_{\lambda}(JJ')$ and the Racah coefficients.

Using the equations (3.4.15) and (3.4.24) $Q_2^{(1)}(JJ)$ and $Q_2^{(2)}(JJ)$ can be written as follows:

$$Q_2^{(1)}(JJ) = \frac{4\pi}{5} \frac{J(J+1)}{(2J-1)(2J+3)} (\eta_0)^{H_2-H_2} \quad (4.2.1.)$$

$$Q_2^{(2)}(JJ) = \frac{7C}{25\pi} \frac{J(J+1)}{(2J-1)(2J+3)} (\eta_1)^{H_2-H_2} \quad (4.2.2.)$$

where

$$(\eta_0)^{H_2-H_2} = \frac{j^{(1)}(0)}{h^2} = \frac{\rho_{H_2} a^4 (2\pi\beta M)^{1/2} I^{(1)}(2)}{h^2} \quad (4.2.3.)$$

$$(\eta_1)^{H_2-H_2} = \frac{j^{(2)}(0)}{h^2} = \frac{\rho_{H_2} a^4 (2\pi\beta M)^{1/2} I^{(2)}(4)}{h^2} \quad (4.2.4.)$$

and

$$C = \frac{5}{2} \left\langle \frac{J(J+1)}{(2J-1)(2J+3)} \right\rangle \quad (4.2.5.)$$

where $\langle \rangle$ represents the ensemble average.

While evaluating the $Q_2^{(2)}(JJ')$ it is assumed that only those collisions in which total rotational angular momentum is conserved are important. As the molecule 2 could either be an ortho- or para- H_2 molecule, $Q_2^{(2)}(JJ')$ is a function of the rotational angular momentum quantum numbers of both ortho- and para- H_2 . The treatment of these two types of collisions was

given in Section 3.4. of Chapter III. Treating the resonant and quasi-resonant collisions as described in the previous chapter and assuming that non-resonant collisions do not contribute significantly to $Q_2^{(2)}(J, J')$, $Q_2^{(2)}(J+2, J)$ and $Q_2^{(2)}(J-2, J)$ are given by

$$Q_2^{(2)}(J+2, J) = \frac{63}{40\pi} \frac{(2J+1)}{(2J+5)} \Delta(J) \left\{ \frac{(2J+1)}{(2J+5)} \Delta(J) P_{J+2}(\eta_1)^{H_2-H_2} F + \sum_{J''} \left(\frac{2J''+1}{2J''+5} \right) \Delta(J'') \right. \\ \left. \times P_{J''+2}^{(1-F)} \epsilon_1(\eta_1)^{H_2-H_2} \right\} \quad (4.2.6.)$$

$$Q_2^{(2)}(J-2, J) = \frac{63}{40\pi} \Delta(J-2) \left\{ \Delta(J-2) P_{J-2} F(\eta_1)^{H_2-H_2} \right. \\ \left. + \sum_{J''} P_{J''-2} \Delta(J''-2) (1-F) \epsilon_2(\eta_1)^{H_2-H_2} \right\} \quad (4.2.7.)$$

where

$$\Delta(J) = \frac{(J+1)(J+2)}{(2J+1)(2J+3)} \quad (4.2.8.)$$

$$F = \frac{\rho_0}{\rho_{H_2}} = 0.75 \text{ for normal } H_2 \quad (4.2.9.)$$

and ϵ_1 and ϵ_2 are given by equations (3.4.27) and (3.4.28).

Substituting equations (4.2.1.), (4.2.2.), (4.2.6.) and (4.2.7.) into equation (3.2.22), using the relation given by equation (3.4.4.) and evaluating the Racah coefficients,

$B_{l_2}(J, J')$ are obtained as follows:

$$B_1(1,1) = -(x+S_1) \rho(\eta_1)^{H_2-H_2} \quad ; \quad B_1(1,3) = \left(\frac{2}{3}\right)^{1/2} S_3 \rho(\eta_1)^{H_2-H_2} \quad (4.2.10)$$

$$B_1(3,3) = -(x/9+S_2) \rho(\eta_1)^{H_2-H_2} \quad ; \quad B_1(3,1) = \left(\frac{2}{3}\right)^{1/2} S_4 \rho(\eta_1)^{H_2-H_2}$$

$$B_2(1,1) = -\left(\frac{3}{5}x+S_1\right) \rho(\eta_1)^{H_2-H_2} \quad ; \quad B_2(1,3) = \left(\frac{6}{25}\right)^{1/2} S_3 \rho(\eta_1)^{H_2-H_2} \quad (4.2.11)$$

$$B_2(3,3) = -\left(\frac{41}{135}x+S_2\right) \rho(\eta_1)^{H_2-H_2} \quad ; \quad B_2(3,1) = \left(\frac{6}{25}\right)^{1/2} S_4 \rho(\eta_1)^{H_2-H_2}$$

where

$$X = \left(\frac{12\pi}{25} \left(\frac{\eta_0'}{\eta_1'} \right)^{H_2-H_2} + \frac{21C}{125\pi} \right) \quad (4.2.12)$$

$\eta' = \eta/\rho$ where ρ is the density in ideal amagats and

$$S_1 = \frac{27}{250} \frac{F}{\pi} P_3 + \left(\frac{1-F}{\pi} \right) \left[\frac{21}{250} \epsilon_1 P_2 + \frac{3}{25} \epsilon_2 P_4 \right]$$

$$S_2 = \frac{27}{250} \frac{F}{\pi} P_1 + \left(\frac{1-F}{\pi}\right) \left[\frac{9}{50} \epsilon_2 P_0 + \left(\frac{1}{15} \epsilon_1 + \frac{81}{875} \epsilon_2\right) P_2 + \frac{2}{21} \epsilon_2 P_4 \right]$$

$$S_3 = \frac{27}{250} \frac{1}{\pi} \left[F P_1 + (1-F) \left(\frac{5}{3} \epsilon_2 P_0 + \frac{6}{7} \epsilon_1 P_2 \right) \right] \quad (4.2.13)$$

$$S_4 = \frac{27}{250} \frac{1}{\pi} \left[F P_3 + (1-F) \left(\frac{7}{9} \epsilon_1 P_2 + \frac{10}{9} \epsilon_2 P_4 \right) \right]$$

Substituting equations (4.2.10) and (4.2.11) in the equation (3.3.12) to obtain $J_1(0)$ and $J_2(0)$ and using equation (3.2.3.) ρ/T_1 is obtained as

$$\begin{aligned} \rho/T_1 = & \frac{2}{3} \frac{\gamma^2 H'^2 \left[\left(\frac{2P_1}{9} + 12P_3 \right) X + \left\{ 2P_1(S_2 + 2S_4) + 4P_3(3S_1 + S_3) \right\} \right]}{\eta'_1 \left[\frac{1}{9} X^2 + \left(\frac{1}{9} S_1 + S_2 \right) X + \left(S_1 S_2 - \frac{2}{3} S_3 S_4 \right) \right]} \quad (4.2.14) \\ & + 6 \frac{\gamma^2 H''^2 \left[\frac{2}{675} (41P_1 + 54P_3) X + \left\{ \frac{2}{5} P_1 (S_2 + \frac{2}{5} S_4) + \frac{4}{5} P_3 \left(\frac{1}{3} S_1 + \frac{1}{5} S_3 \right) \right\} \right]}{\eta'_1 \left[\frac{41}{225} X^2 + \left(\frac{3}{5} S_2 + \frac{41}{135} S_1 \right) X + \left(S_1 S_2 - \frac{6}{25} S_3 S_4 \right) \right]} \end{aligned}$$

It may be noted from the above expression that ρ/T_1 is a function of $(\eta'_0/\eta'_1)^{H_2-H_2}$, $(\eta'_1)^{H_2-H_2}$ and F .

In view of the general theory now available it was felt necessary to reinterpret the data available below room temperature from other work. These data had been interpreted previously neglecting the transitions between states of different J , a restriction which has been removed by the new theory. The data of T_1/ρ obtained by Lipsicas and Hartland²⁵ as a function of ortho- H_2 and Riehl's²⁴ and Williams'²¹ data of T_1/ρ in normal H_2 will be used to obtain $(\eta'_0)^{H_2-H_2}$ and $(\eta'_1)^{H_2-H_2}$ below room temperature.

The value of T_1/ρ due to ortho-para collisions alone corresponds to the condition that $F=0$ and that due to ortho-ortho collisions alone is obtained by equating F to 1. From

equation (4.2.14) it can be seen that $(\tau_1/\rho)_{OP}/(\tau_1/\rho)_{OO}$ depends only on $(\eta'_0/\eta'_1)^{H_2-H_2}$. $(\tau_1/\rho)_{OP}/(\tau_1/\rho)_{OO}$ was calculated for different values of (η'_0/η'_1) on an I.B.M. 7040 computer and fig. 10. shows the theoretical plots of $(\tau_1/\rho)_{OP}/(\tau_1/\rho)_{OO}$ as a function of $(\eta'_0/\eta'_1)^{H_2-H_2}$ at temperatures 77.8°K, 100°K, 200°K and 300°K. Using these theoretical curves, the value of $(\eta'_0/\eta'_1)^{H_2-H_2}$ corresponding to the experimental value of $(\tau_1/\rho)_{OP}/(\tau_1/\rho)_{OO}$ was obtained at different temperatures. Substituting these values of $(\eta'_0/\eta'_1)^{H_2-H_2}$ into equation (4.2.14) and using the experimental values of τ_1/ρ for normal H_2 , $(\eta'_1)^{H_2-H_2}$ was obtained at different temperatures.

Defining $(k_1)^{H_2-H_2}$ as

$$(k_1)^{H_2-H_2} = \frac{0.134}{k^2} I^{(2)}(4) \quad (4.2.15)$$

$(\eta'_1)^{H_2-H_2}$ can be expressed, using the equation (4.2.4) as

$$(\eta'_1)^{H_2-H_2} = \rho_1 a^4 (2\pi \beta M)^{1/2} \frac{(k_1)^{H_2-H_2}}{0.134} \quad (4.2.16)$$

where $\rho_1 = 2.69 \times 10^{19} \text{ cm.}^{-3}$, an "Ideal Amagat".

Fig. 11 shows $(k_1)^{H_2-H_2}$ as a function of temperature when the quasi-resonant collisions are included and also when they are not included. It can be seen from the figure and the following discussion that the quasi-resonant terms probably contribute significantly even at 200°K though the population of J=3 state is only 3% at this temperature.

If the isotropic part of the intermolecular potential is assumed to be given by a Lennard-Jones potential for reasons discussed by Bloom, Oppenheim et al in their paper⁸, the temperature dependence of k_1 is determined by the radial dependence of the anisotropic part of the intermolecular potential.

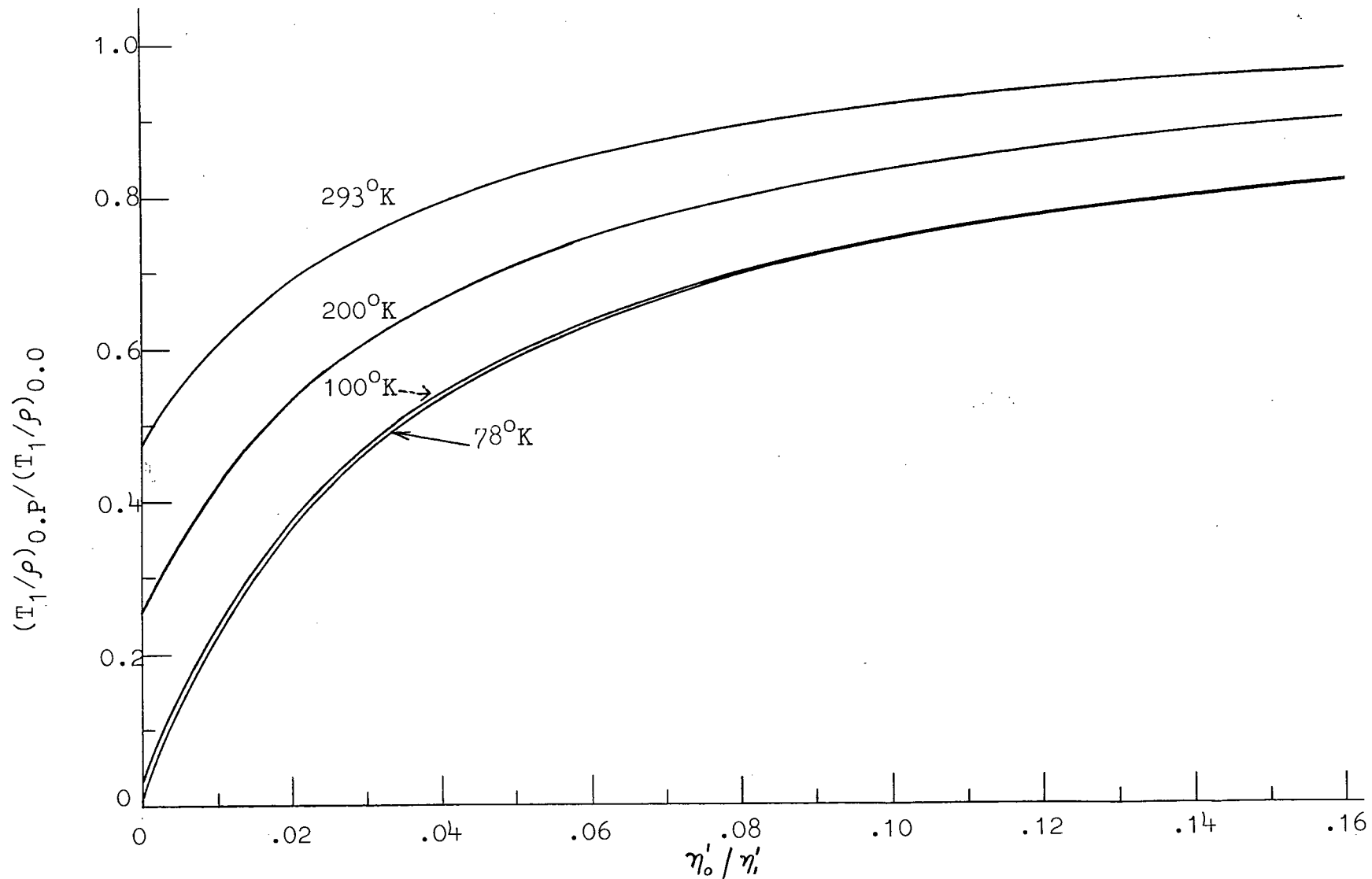


FIG. 10. Theoretical plots of $(T_1/\rho)_{0.P} / (T_1/\rho)_{0.0}$ as a function of η'_0 / η'_i as obtained from Eq.(4.2.14).

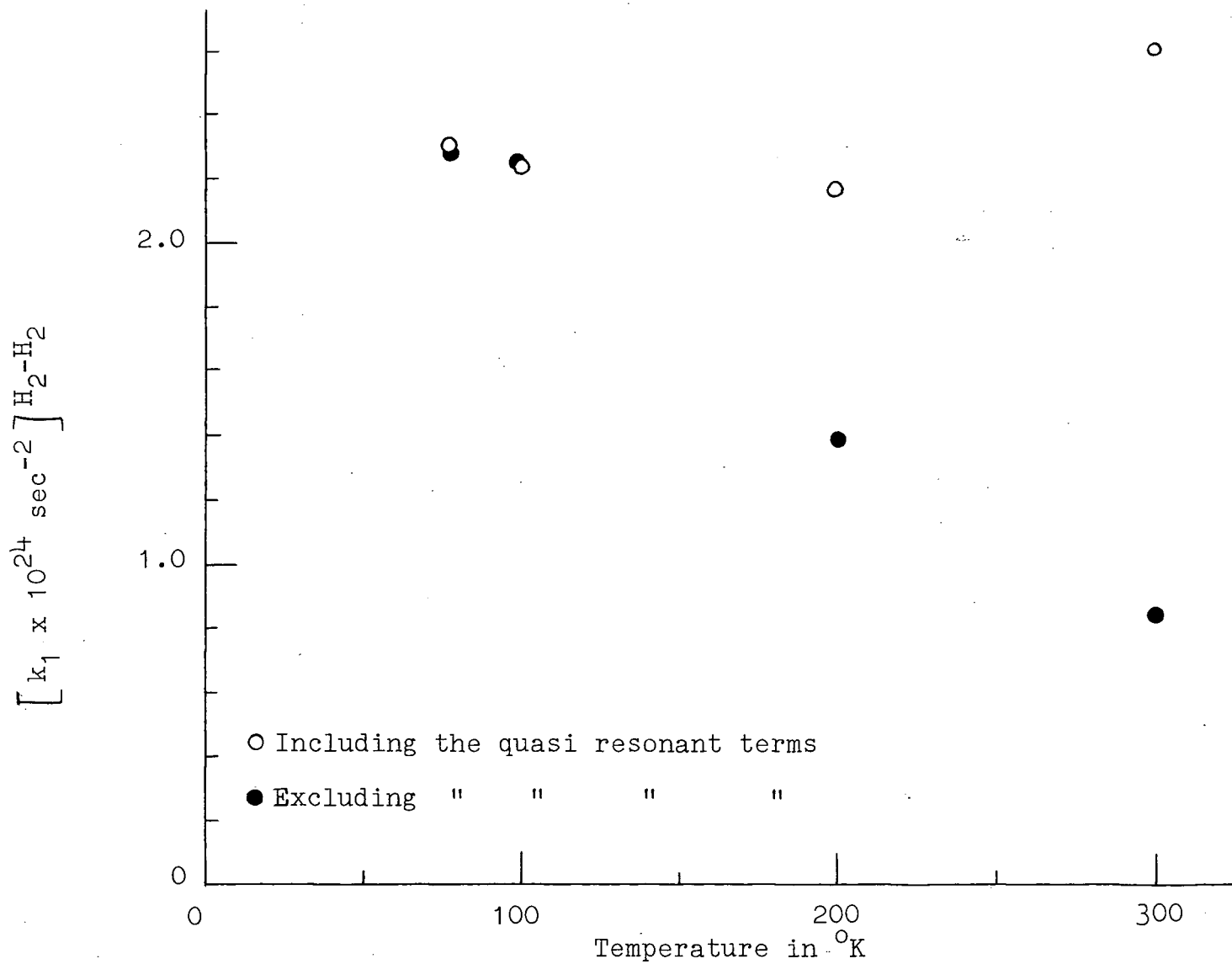


FIG. 11. Temperature dependence of $(k_1)_{H_2-H_2}$ as obtained from Eq.(4.2.14) and the experimental values of $(T_1/\rho)_{0.P}/(T_1/\rho)_{0.0}$ and (T_1/ρ) for normal H₂.

Assuming that the anisotropic potential is given by a simple power law

$$V^{(q)}(ax) = \frac{k \omega_n^{(q)}}{x^n} \quad (4.2.17)$$

$(k_1)^{H_2-H_2}$ can be expressed as

$$(k_1)^{H_2-H_2} = 0.134 (\omega_n^{(2)})^2 I(4, n) \quad (4.2.18)$$

Using the values of the integrals $I(p, n)$ given by Bloom, Oppenheim et al⁸, the theoretical values of $(k_1)^{H_2-H_2}$ can be computed at different temperatures by normalising the theoretical value to the experimental value at 200°K, to obtain $\omega_n^{(2)}$. Fig. 12 shows $[k_1(\tau)/k(200)]^{H_2-H_2}$ as a function of temperature along with the theoretical plots for different values of n . Fig. 12 also shows the experimental values of $[k_1(\tau)/k_1(200)]^{H_2-H_2}$ when the quasi-resonant terms are not included. It can be seen from the figure that $n=5$ gives a reasonable fit in the high temperature region which is consistent with quadrupole-quadrupole interaction. The disagreement in the low temperature region is believed to be due to the fact that the quantum effects are not taken into account adequately in the theory.

The quadrupole moment of the H_2 molecule can be obtained by comparing the experimental value at 200°K with the theoretical value. The value obtained in the present work is $(0.57 \pm 0.03) \times 10^{-26}$ e.s.u. as compared to the theoretical value of 0.65×10^{-26} e.s.u.

Having established that η'_1 is given by quadrupole-quadrupole interaction, the values of η'_1 at different temperatures were obtained from the following equation

$$\left[\frac{\eta'_1(\tau)}{\eta'_1(200)} \right]^{H_2-H_2} = \left(\frac{200}{\tau} \right)^{1/2} \frac{I(4, 5)_T}{I(4, 5)_{200^\circ K}} \quad (4.2.19)$$

○ Including the quasi resonant terms

● Excluding " " " "

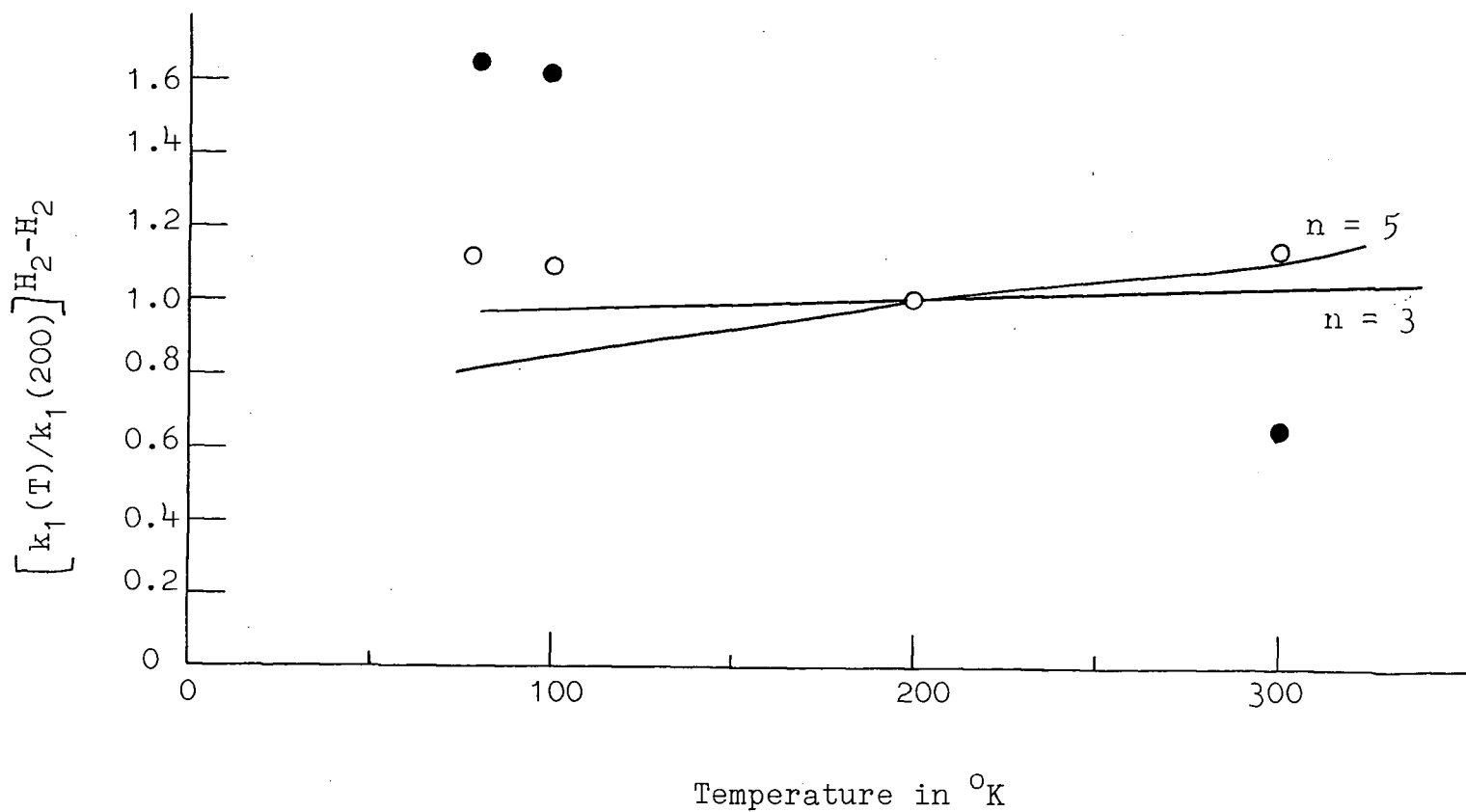


FIG. 12. Comparison of experimental values of $[k_1(T)/k_1(200)]^{H_2-H_2}$ with the theoretical values using Eq.(4.2.18).

The contribution from quadrupole-quadrupole interaction alone to τ_1/ρ is obtained from equation (4.2.14) by putting $\eta'_0 = 0$ which is shown in fig. 13 along with the experimental values of τ_1/ρ . It can be seen from the figure that the contribution from quadrupole-quadrupole interaction is quite significant throughout the temperature range.

Evaluation of $(\eta'_0)^{H_2-H_2}$

Equation (4.2.14) can be written as a polynomial of order 4 in X where X is defined by equation (4.2.12) and the solutions of this polynomial are found by Bairstowe's method on an I.B.M. 7040 computer at the University of British Columbia computation centre. All the four roots were real and only one of them was positive. Choosing the positive root, $(\eta'_0)^{H_2-H_2}$ can be evaluated knowing $(\eta'_1)^{H_2-H_2}$ and C.

Defining

$$(k_0)^{H_2-H_2} = \frac{6\pi}{5k^2} I^{(1)}(2) \quad (4.2.20)$$

$(\eta'_0)^{H_2-H_2}$ can be expressed as

$$(\eta'_0)^{H_2-H_2} = \rho_1 a^4 (2\pi\beta\mu)^{1/2} \frac{5}{6\pi} (k_0)^{H_2-H_2} \quad (4.2.21)$$

Fig. 14 shows k_0 as a function of temperature. The error bars represent $\pm 5\%$ error on the value of τ_1/ρ . A $\pm 10\%$ error on the value of $(\eta'_1)^{H_2-H_2}$ introduced the same error in the value of $(k_0)^{H_2-H_2}$ as shown by the error bars in the figure.

If a simple power law is assumed to describe the anisotropic potential, $(k_0)^{H_2-H_2}$ is given by

$$(k_0)^{H_2-H_2} = \frac{6\pi}{5} (\omega_n^{(1)})^2 I(2, n) \quad (4.2.22)$$

Using the numerical values of the integrals $I(2, n)$, $\omega_n^{(1)}$ can be obtained by equating the experimental value of k_0 to

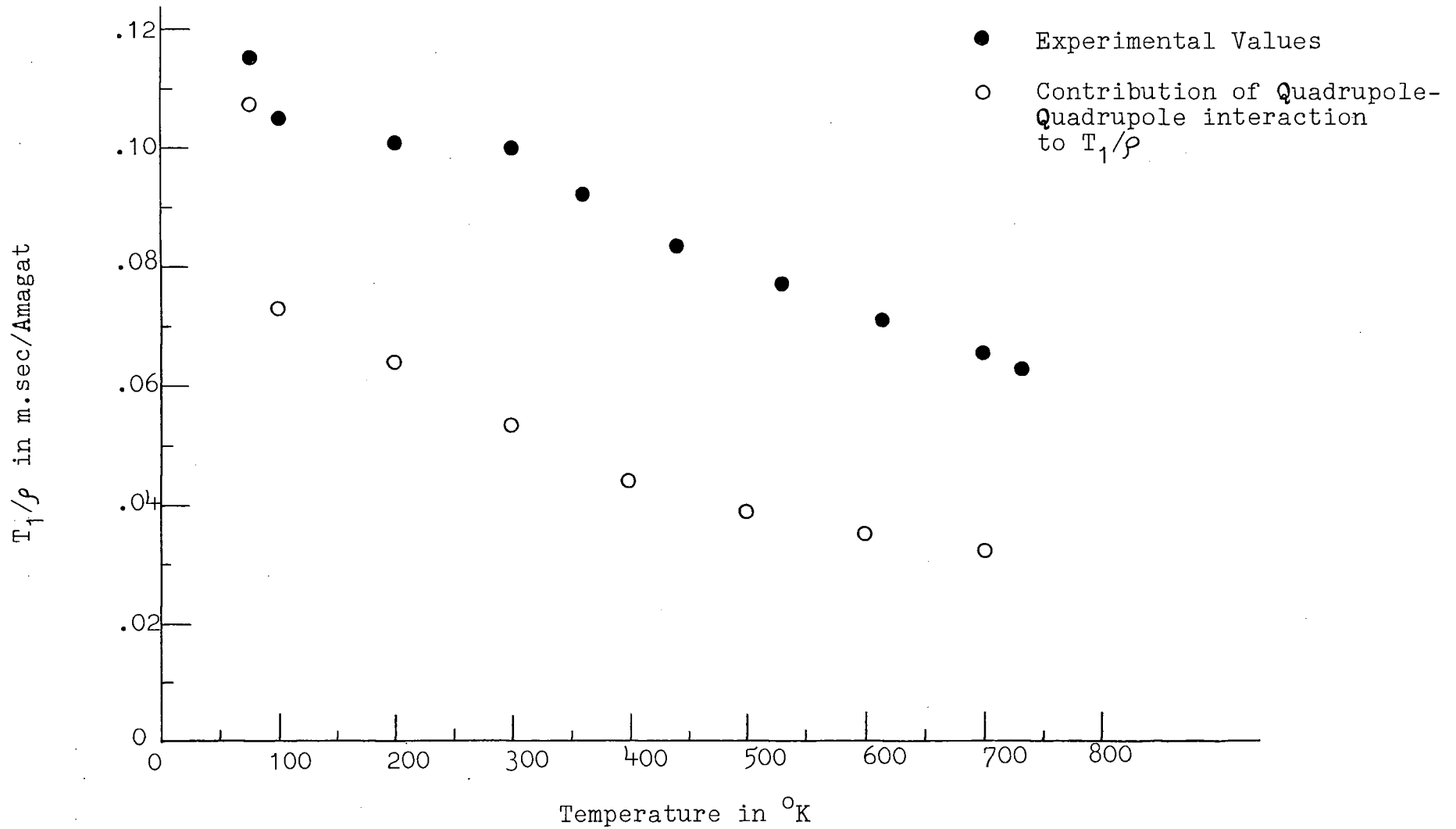


FIG. 13. Comparison of the experimental values of T_1/ρ with the computed values using Eq.(4.2.14) and assuming that only quadrupole-quadrupole interaction is important.

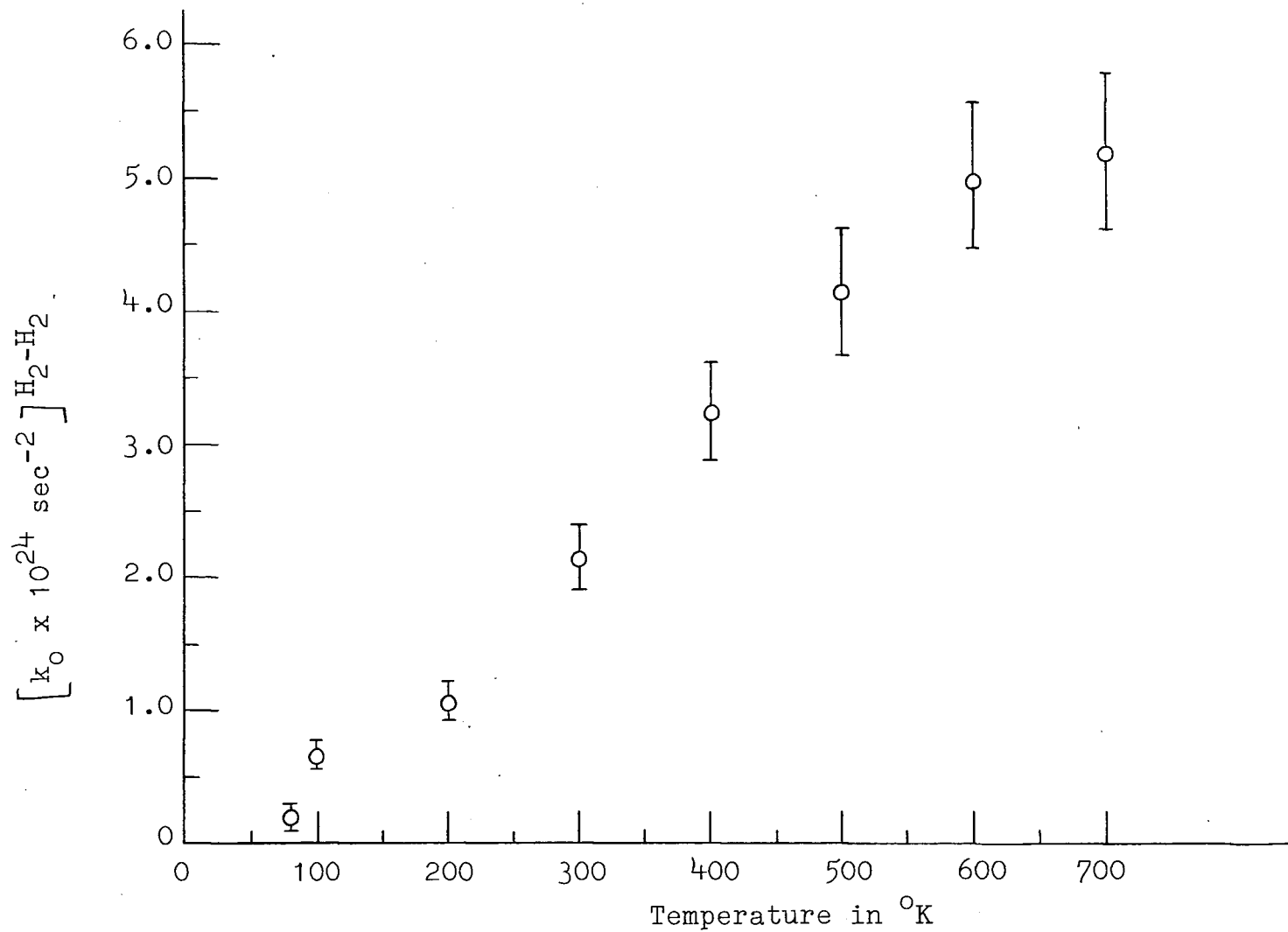


FIG. 14. Temperature dependence of $(k_0)_{\text{H}_2\text{-H}_2}$ as obtained from Eq.(4.2.14) and the experimental values of (T_1/ρ) in normal H_2 .

the theoretical value at 200°K for any n. Thus $[k_0(\tau)/k_0(200)]^{H_2-H_2}$ can be obtained as a function of temperature for different values of n. Fig. 15 shows the experimental values of $[k_0(\tau)/k_0(200)]^{H_2-H_2}$ along with the theoretical plots for different values of n. When a simple power law is assumed to express $b^{(n)}(ax)$ the experimental values are best fitted for n=15. However, the theoretical studies ⁸ of the form of the intermolecular potential between H₂ molecules which depends on the orientation of one of the molecules alone indicate that the simple form can better be represented in terms of an attractive part proportional to $1/r^6$ and a repulsive part proportional to $1/r^{n'}$. In this case $b^{(n)}(ax)$ is given by

$$b^{(n)}(ax) = \frac{k\omega_{n'}^{(n)}}{x^{n'}} + \frac{k\omega_6^{(n)}}{x^6} \quad (4.2.23)$$

The value of $\omega_6^{(n)}$ was computed theoretically ⁸ and is given to be $\omega_6^{(n)} = -1.85 \times 10^{12} \text{ sec}^{-1}$. K_0 is then given by

$$(k_0)^{H_2-H_2} = \frac{6\pi}{5} \left\{ (\omega_{n'}^{(n)})^2 I(2, n') + (\omega_6^{(n)})^2 I(2, 6) + 2\omega_{n'}^{(n)}\omega_6^{(n)} I(2, 6, n') \right\} \quad (4.2.24)$$

$\omega_{n'}^{(n)}$ is evaluated by equating this expression to the experimental value of k_0 at 200°K and using the tables III and IV given by Bloom, Oppenheim et al ⁸ to evaluate $I(2; n, n')$. $(k_0)^{H_2-H_2}$ at any other temperature is obtained from equation (4.2.24) using the values of $I(2; n, n')$ corresponding to that particular temperature. $[k_0(\tau)/k_0(200)]^{H_2-H_2}$ as a function of temperature is shown in fig. 15 for different values of n' . It can be seen from the figure that the agreement between the experimental and theoretical values is best for $n'=13$. As the values of the integrals for $I(2, 12)$ and $I(2, 6, 12)$ are not provided in the

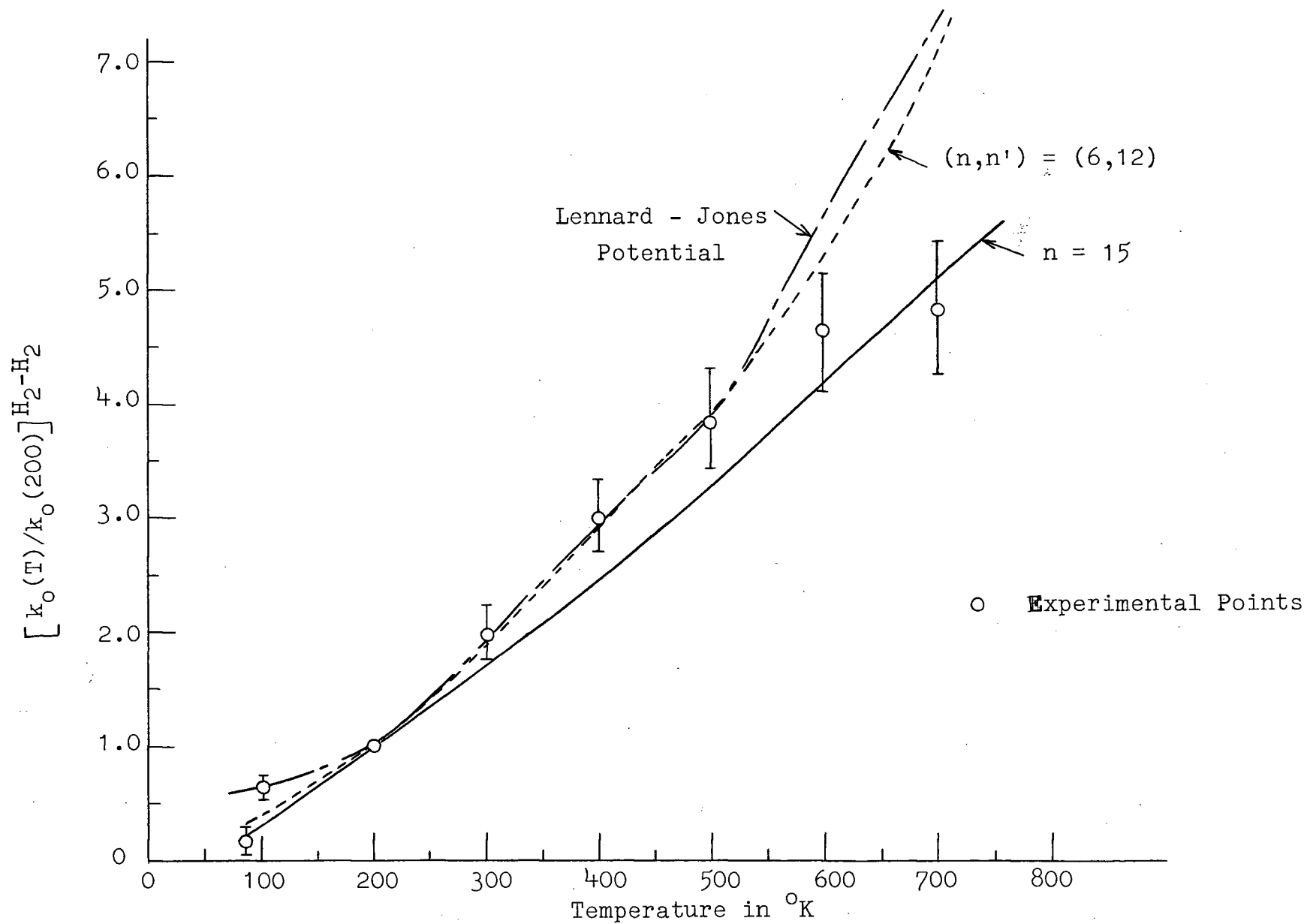


FIG. 15. Comparison of experimental values of $[k_o(T)/k_o(200)]_{H_2-H_2}$ with the theoretical values using Eqs.(4.2.22) and (4.2.24)

tables, the theoretical curve for $n'=12$ was obtained using the interpolated values of $I(2,12)$ and $I(2,6,12)$ and the plot thus obtained was found to be almost identical with that of $n'=13$. The departure of the experimental values from the theoretical values above 500°K is probably due to the fact that the analysis was carried out on the assumption that $J=5$ state can be neglected. At 500°K the population of $J=5$ state is about 2% and at 700°K it is about 6.7% and the effect of $J=5$ state has to be taken into account. Based on the analysis of two-level system $\mathcal{H}_R^{(1)}$ for H_2 can be represented by

$$\mathcal{H}_R^{(1)} = 1.95 \times 10^{-15} \text{ erg} \left\{ 1.61 \left(\frac{a}{r} \right)^{12} - \left(\frac{a}{r} \right)^6 \right\} P_2(\cos \theta') \quad (4.2.25)$$

and the intermolecular potential $V(r)$ can be written for an ortho-para pair as

$$V(r) = 4\epsilon \left[\left(\frac{a}{r} \right)^{12} - \left(\frac{a}{r} \right)^6 \right] + 1.95 \times 10^{-15} \left[1.61 \left(\frac{a}{r} \right)^{12} - \left(\frac{a}{r} \right)^6 \right] P_2(\cos \theta') \quad (4.2.26)$$

ergs

where equations (4.2.23) and (3.4.2.) were used and the isotropic part of the intermolecular potential was given by Lennard-Jones potential. If it is assumed that the anisotropic part is also given by Lennard-Jones potential, the theoretical values agree very well with the experimental values up to 500°K and the value obtained for $\omega_6^{(1)}$ is $\omega_6^{(1)} = -3.3 \times 10^{12} \text{ sec}^{-1}$. The intermolecular potential can be written for this case as

$$V(r) = 4\epsilon \left[\left(\frac{a}{r} \right)^{12} - \left(\frac{a}{r} \right)^6 \right] \left[1 + 0.173 P_2(\cos \theta') \right] \quad (4.2.27)$$

The values of the integrals $I(p,n)$ and $I(p,n,n')$ were given only up to $\beta\epsilon = 0.09$ in the tables referred to in the preceding paragraphs which corresponds to approximately 400°K for

H₂. However, it was found that $\log I(p, n)$ vs. $\log (\beta E)$ as well as $\log I(p, n, n')$ vs $\log (\beta E)$ are linear and the values of the integrals at higher temperatures were obtained from the extrapolated values of these plots. The actual computation of these integrals was carried out by Lipsicas (private communication) extending the range of βE down to 0.01. These values agree with the extrapolated values. The actual values are presented in Table II for $0.03 \leq \beta E \leq 0.09$.

n	p	$\beta\epsilon$					
		0.03	0.04	0.05	0.06	0.08	0.09
5	2	0.1394	0.1276	0.1190	0.1123	0.1027	0.0991
	4	0.0914	0.0836	0.0799	0.0753	0.0672	0.0648
7	2	0.1646	0.1424	0.1267	0.1149	0.0986	0.0926
	4	0.1125	0.0972	0.0863	0.0783	0.0671	0.063
9	2	0.2516	0.2067	0.1762	0.1541	0.1244	0.1139
	4	0.1763	0.1446	0.1231	0.1076	0.0867	0.0793
15	2	1.8029	1.3151	1.0131	0.8116	0.5626	0.4813
	4	1.3098	0.9534	0.7332	0.5867	0.4061	0.3473
17	2	3.957	2.8028	2.1054	1.6489	1.0964	0.920
	4	2.896	2.0455	1.5336	1.1996	0.7965	0.668
19	2	9.0533	6.2486	4.5916	3.5246	2.2569	1.8586
	4	6.6630	4.5851	3.3617	2.5773	1.6477	1.3565
21	2	21.4131	14.448	10.415	7.8542	4.859	3.9322
	4	15.833	10.65	7.6580	5.7678	3.5622	2.8814

Table II. Values of $I(p,n)$ for dilute H_2 gas including the first quantum correction for a Lennard-Jones isotropic potential.

4.3. H₂ and He Mixture.

4.3.1. Results.

The proton spin relaxation time was measured in H₂ and He mixtures as a function of density and composition from room temperature up to 700°K. The data were taken at room temperature for five concentrations of the mixture but the temperature dependence was studied for only two mixtures, one with 32.2% He and the other with 77.0% He. Typical plots of T_1 vs. ρ are shown in fig. 16a for 32.2% He and 77.0% He mixtures at room temperature whereas fig. 16b shows the plot for 77.0% He mixture at 700°K, which represents the worst signal to noise conditions. The solid line in both cases represents the least square fit for the data.

Fig. 17 shows T_1/ρ as a function of percentage of He present in the mixture at different temperatures. Within experimental errors and judging from the data available, the dependence of T_1/ρ on the concentration of He was found to be linear at higher temperatures but all the data at room temperature cannot be fitted by a straight line. However, when a straight line is drawn through the data as shown in fig. 17, it is difficult to say whether the deviation of the data from the linear fit is significant or not. If it is significant the extrapolation of T_1/ρ to 100% He is perhaps not justified. The theoretical investigation gave more insight to this problem which will be discussed in the following section.

Assuming that the extrapolation is valid, the values of T_1/ρ for 100% He are given in Table III for different temp-

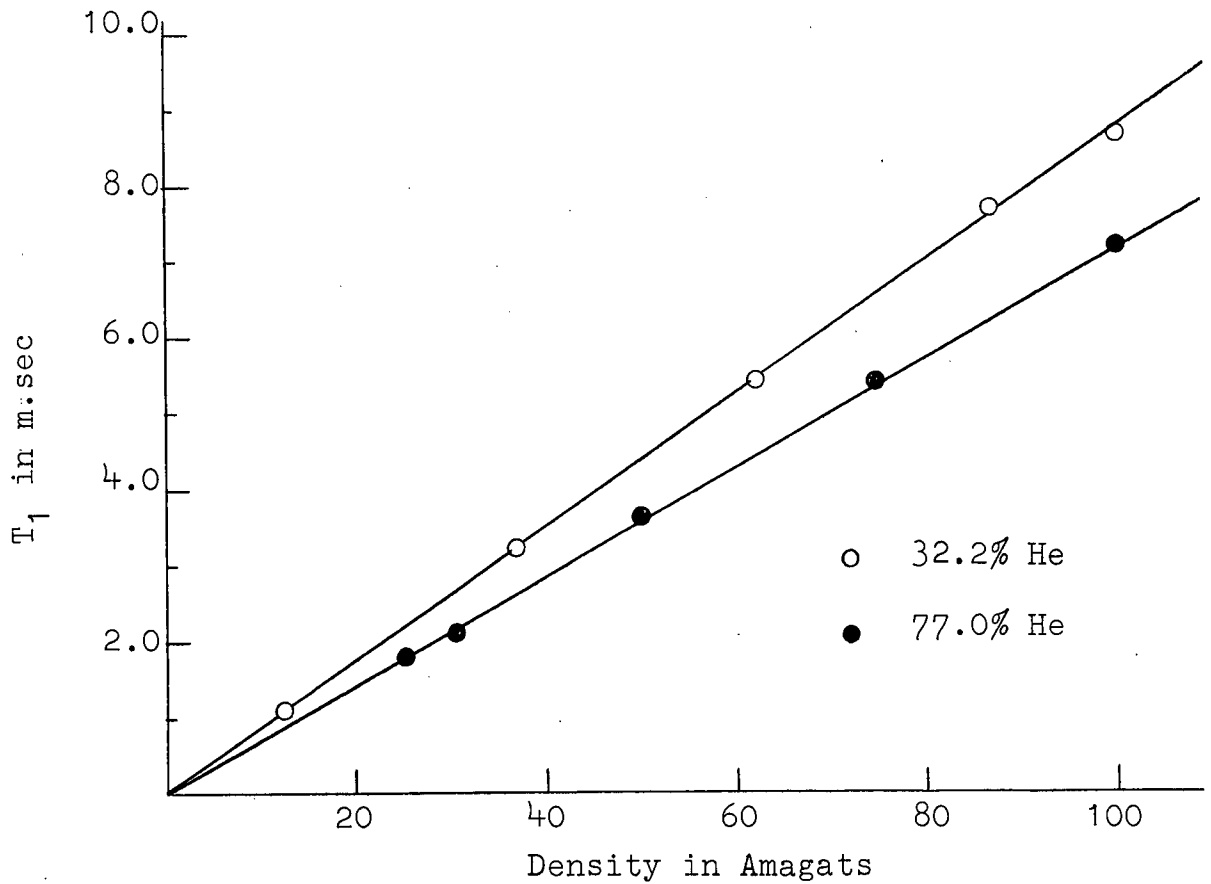


FIG. 16a. T_1 versus Density at 293°K in H_2 -He mixture.

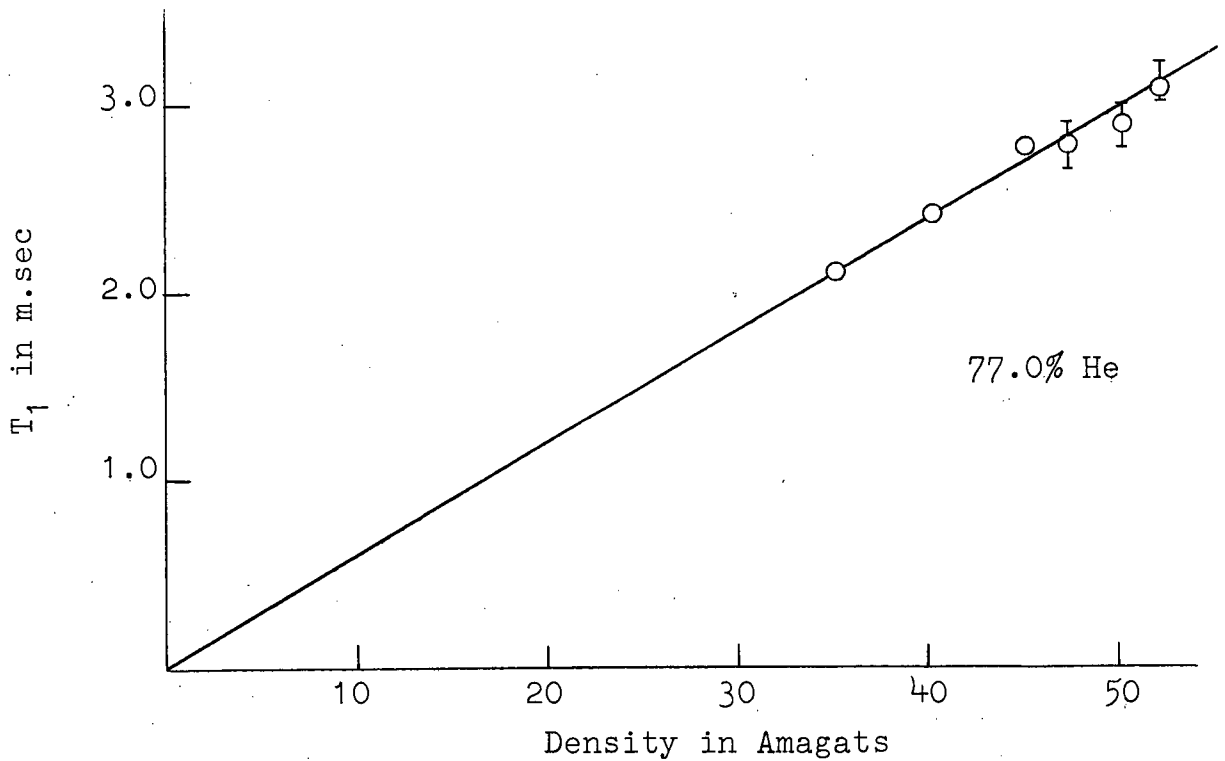


FIG. 16b. T_1 versus Density at 738°K in H_2 -He mixture.

eratures.

TEMP.	$(T_1/\rho)_{\text{H}_2\text{-He}}$ (m.sec/Amagat)
293°K	0.0645
400°K	0.0635
500°K	0.0615
600°K	0.06
700°K	0.059
750°K	0.058

Table III. $(T_1/\rho)_{\text{H}_2\text{-He}}$ obtained from extrapolating the experimental data to 100% He.

TABLE III. (continued)

4.3.2. Interpretation.

If ρ_{H_2} and ρ_{He} represent the number of H_2 and He molecules per unit volume respectively, then the density of the combined system is given by

$$\rho_T = \rho_{H_2} + \rho_{He} \quad (4.3.1.)$$

and if ρ_o and ρ_p are the densities of ortho- and para- H_2 respectively, then

$$\rho_{H_2} = \rho_o + \rho_p \quad (4.3.2.)$$

The fractional densities for the mixture can be defined as

$$\tilde{\rho}_{He} = \frac{\rho_{He}}{\rho_T} ; \quad \tilde{\rho}_{H_2} = \frac{\rho_{H_2}}{\rho_T} ; \quad \tilde{\rho}_o = \frac{\rho_o}{\rho_T} \quad (4.3.3.)$$

and for normal H_2 $\tilde{\rho}_o = (3/4) \tilde{\rho}_{H_2}$

For this mixture there are three types of interactions that have to be considered: (i) the interaction between ortho-ortho molecules, (ii) the interaction between ortho-para molecules, (iii) the interaction between ortho- He atoms. The first two types of interactions were discussed in the previous section and the interaction between ortho- H_2 and He molecules will be discussed below.

H_2 - He Interaction:-

This interaction depends on the orientation of molecule 1 alone and hence can be represented by the hamiltonian $\mathcal{H}_R^{(1)}$. As discussed in the previous chapter, because of the large energy difference between rotational states, the transitions produced by this interaction are those with no change in the rotational angular momentum of the molecule, i.e. $\Delta J = 0$. Thus this contributes only to $Q_2^{(1)}(J, J)$. Using equation

(3.4.15) this can be written as

$$Q_2^{(1)}(J,J)_{H_2-He} = \left(\frac{4\pi}{5}\right) \frac{J(J+1)}{(2J-1)(2J+3)} \rho \tilde{\rho}_{He} (\eta'_0)^{H_2-He} \quad (4.3.4.)$$

where

$$(\eta'_0)^{H_2-He} = \rho_1 \frac{a^4 (2\pi\beta\mu)^{1/2}}{\hbar^2} I^{(1)}(2) \quad (4.3.5.)$$

$$= \frac{5}{6\pi} \rho_1 a^4 (2\pi\beta\mu)^{1/2} (k_0)^{H_2-He} \quad (4.3.6.)$$

a , μ and $I^{(1)}(2)$ are evaluated using appropriate parameters for the $H_2 - He$ interactions ²⁶ and $(\eta'_0)^{H_2-He}$ is defined as

$$(\eta'_0)^{H_2-He} = (\eta_0)^{H_2-He} / \rho$$

where ρ is the density in ideal amagats.

Using equations (3.4.15), (3.4.16) and (3.4.17), the contribution to $B_1^{(1)}(J,J)$ and $B_2^{(1)}(J,J)$ due to $H_2 - He$ interactions can be written as

$$\left[B_1^{(1)}(J,J) \right]^{H_2-He} = - \frac{12\pi}{5} \tilde{\rho}_{He} (\eta'_0)^{H_2-He} \rho \frac{1}{(2J-1)(2J+3)} \quad (4.3.7.)$$

$$\left[B_2^{(1)}(J,J) \right]^{H_2-He} = - \frac{12\pi}{5} \tilde{\rho}_{He} (\eta'_0)^{H_2-He} \rho \frac{3(4J^2+4J-7)}{(2J-1)^2(2J+3)^2} \quad (4.3.8.)$$

Evaluating equations (4.3.7.) and (4.3.8.) for $J=1$ and $J=3$ and adding to the contributions from $H_2 - H_2$ interactions, $B_1(1,1)$, $B_1(3,3)$, $B_2(1,1)$ and $B_2(3,3)$ for the mixture can still be given by equations (4.2.10) and (4.2.11) if X is defined as

$$X = \left[\frac{12\pi}{25} \tilde{\rho}_{H_2} \left(\frac{\eta'_0}{\eta'_1}\right)^{H_2-H_2} + \frac{21C}{125\pi} \tilde{\rho}_{H_2} \right] + \frac{12\pi}{25} \tilde{\rho}_{He} \frac{(\eta'_0)^{H_2-He}}{(\eta'_1)^{H_2-H_2}} \quad (4.3.9.)$$

Therefore ρ/T_1 for any concentration of He is given by equation (4.2.14) where X is defined by equation (4.3.9.).

Equation (4.2.14) was solved for X as described in the

previous section using the experimental value of τ_1/ρ for the mixture at any composition. Having obtained X, $(\eta'_0)^{H_2-He}$ can be obtained from equation (4.3.9.) where $(\eta'_1)^{H_2-H_2}$ and $(\eta'_2)^{H_2-H_2}$ are obtained from the analysis of H_2 results.

It may be noted here that when the extrapolated value of τ_1/ρ for 100% He is used the hydrogen parameters need not be used and therefore the error due to the uncertainties in hydrogen parameters can be eliminated. The value of $(\eta'_0)^{H_2-He}$ was obtained from the experimental values of τ_1/ρ for 32.2% He 77.0% He and 100% He from room temperature up to 700°K, while the values below room temperature were obtained from Riehl's data²⁴ for 60% and 100% He. $(k_0)^{H_2-He}$ is obtained from equation (4.3.6.) and is shown in fig. 18 as a function of temperature. The theoretical plots of τ_1/ρ as a function of percentage of He were obtained for these three slightly different values of $(\eta'_0)^{H_2-He}$ both at room temperature and at 700°K. Fig. 19 shows these plots along with the experimental data. As can be seen from the figure the theoretical plot in which $(\eta'_0)^{H_2-He}$ obtained from 77.0% He mixture was used gives best fit to the experimental results. Also the theoretical plots indicate that the dependence of τ_1/ρ on the concentration of He is not linear. The value of τ_1/ρ for 100% He predicted by the theory is about 15% smaller than the extrapolated value at room temperature and at 700°K the value is only about 3% or 4% smaller. At sufficiently low temperatures when all the molecules are in their lowest rotational state one would not expect this non-linear dependence of τ_1/ρ on the percentage of He as this is a manifestation of transitions between different J states. From the above con-

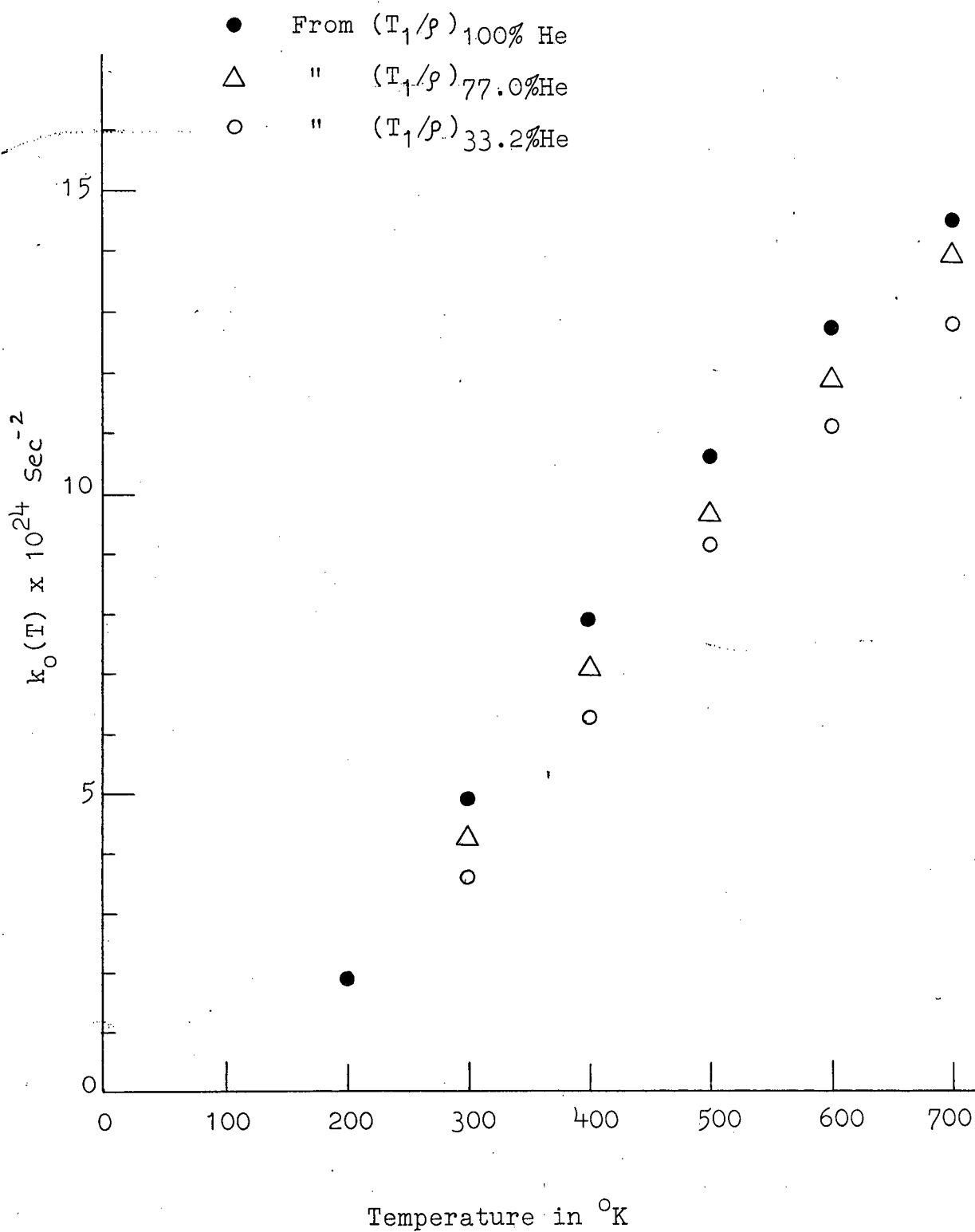


FIG. 18. Temperature dependence of $(k_0)_{\text{H}_2\text{-He}}$ as obtained from Eq.(4.2.14) and using the experimental values of (T_1/ρ) in $\text{H}_2\text{-He}$ mixture.

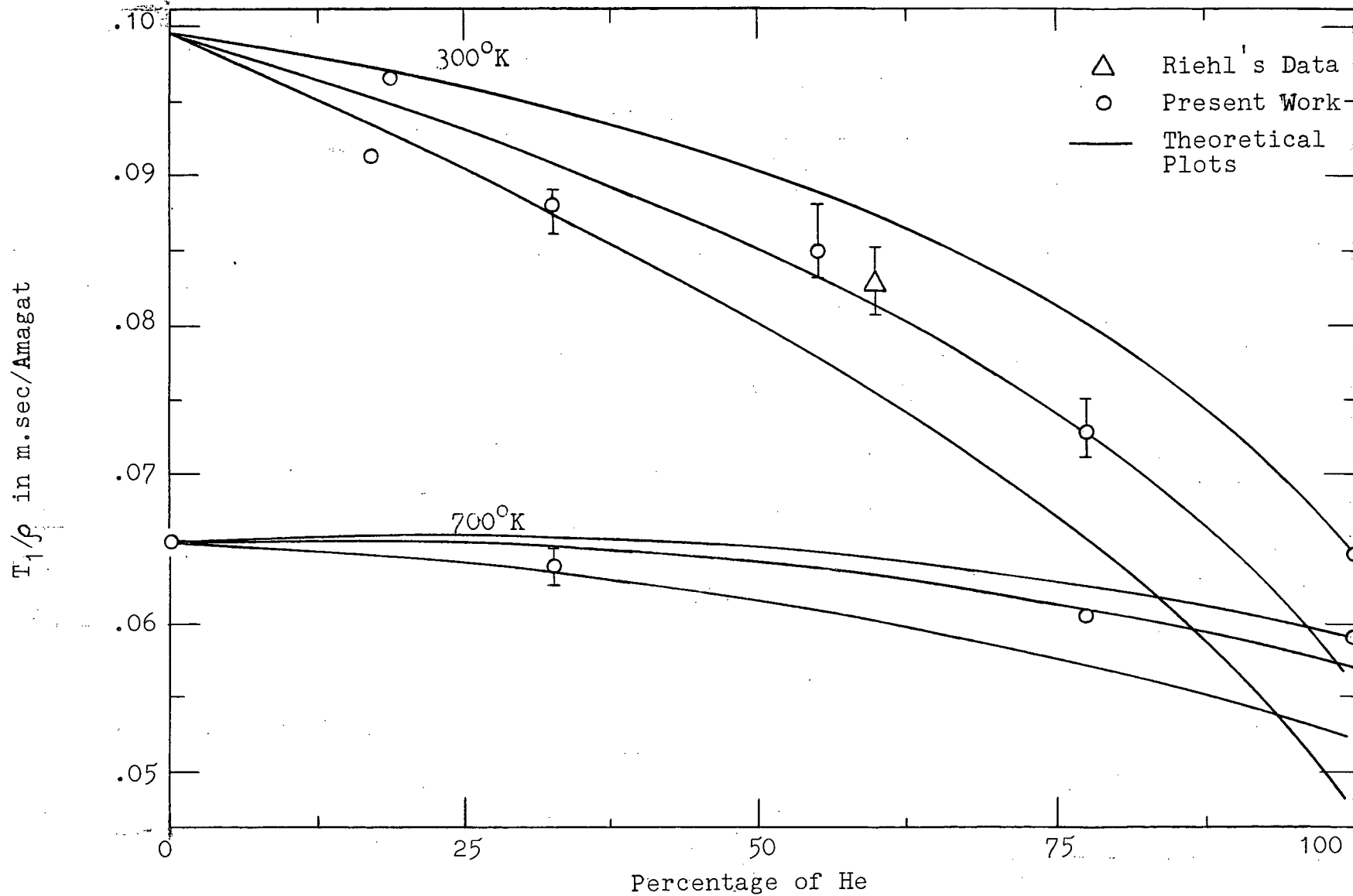


FIG. 19. Theoretical plots of T_1/ρ versus %He when Eq.(4.2.14) was normalised with the experimental values at 32.2% He, 77.0% He and 100% He.

siderations it can be said that the dependence of τ_1/ρ on the concentration of He is not linear above 150°K and the extent of non-linearity is smaller at higher temperatures. At lower concentrations of He, $H_2 - H_2$ collisions play an important role in relaxation mechanism and hence the value of $(\eta'_0)^{H_2-He}$ obtained from 32.2% He mixture includes the errors of H_2 parameters. Under these circumstances the value of $(\eta'_0)^{H_2-He}$ as obtained from 77.0% He mixture is perhaps a good compromise as is also indicated by fig. 19.

Fig. 20 shows the computed values of τ_1/ρ for 100% He using equations (4.3.9.) and (4.2.14) when normalised at 32.2% He and 77.0% He from room temperature up to 700°K, along with the experimental values as obtained from extrapolating the data to 100% He. Below room temperature equation (4.2.14) was normalised with Riehl's data for 60% He to compute the value of

τ_1/ρ for 100% He.

Fig. 21 shows $[k_0(\tau)/k_0(293)]^{H_2-He}$ as a function of temperature along with the various theoretical plots. The theoretical plots were obtained as described in the case of H_2 assuming that $b^{(n)}(ax)$ is given by

$$b^{(n)}(ax) = k \omega_n^{(n)} / x^n \quad (4.3.10)$$

and also by

$$b^{(n)}(ax) = \frac{k \omega_{n'}^{(n)}}{x^{n'}} + \frac{k \omega_6^{(n)}}{x^6} \quad (4.3.11)$$

where $\omega_6 = -\omega_{n'}$

The plots were shown for the case $n=19$ when $b^{(n)}(ax)$ is given by equation (4.3.10) and for $n'=13$ and 15 when $b^{(n)}(ax)$ is given by equation (4.3.11). It was seen in the case of H_2

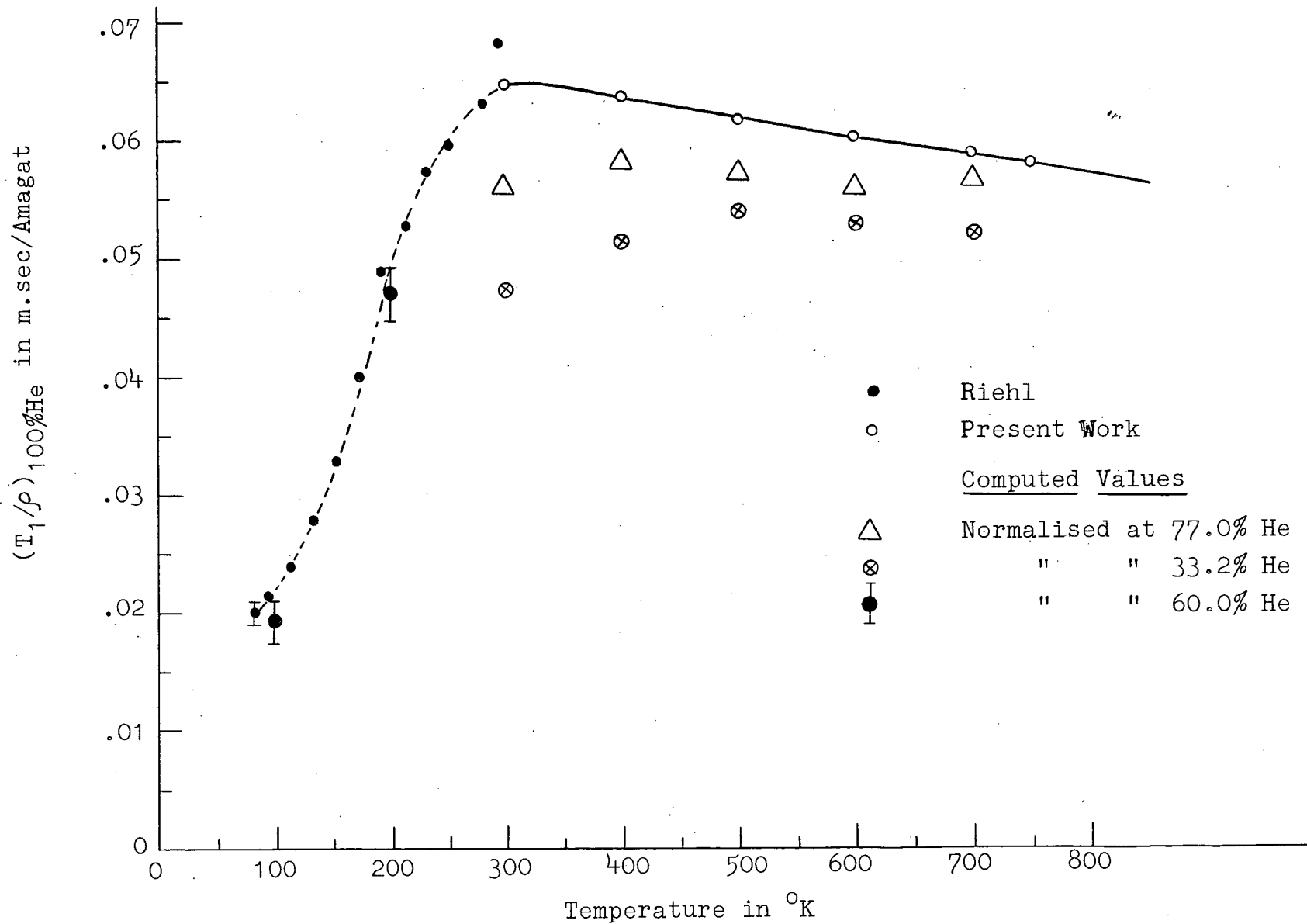


FIG. 20. Comparison of the extrapolated values of $(T_1/\rho)_{H_2-He}$ with the computed values using Eq.(4.2.14)

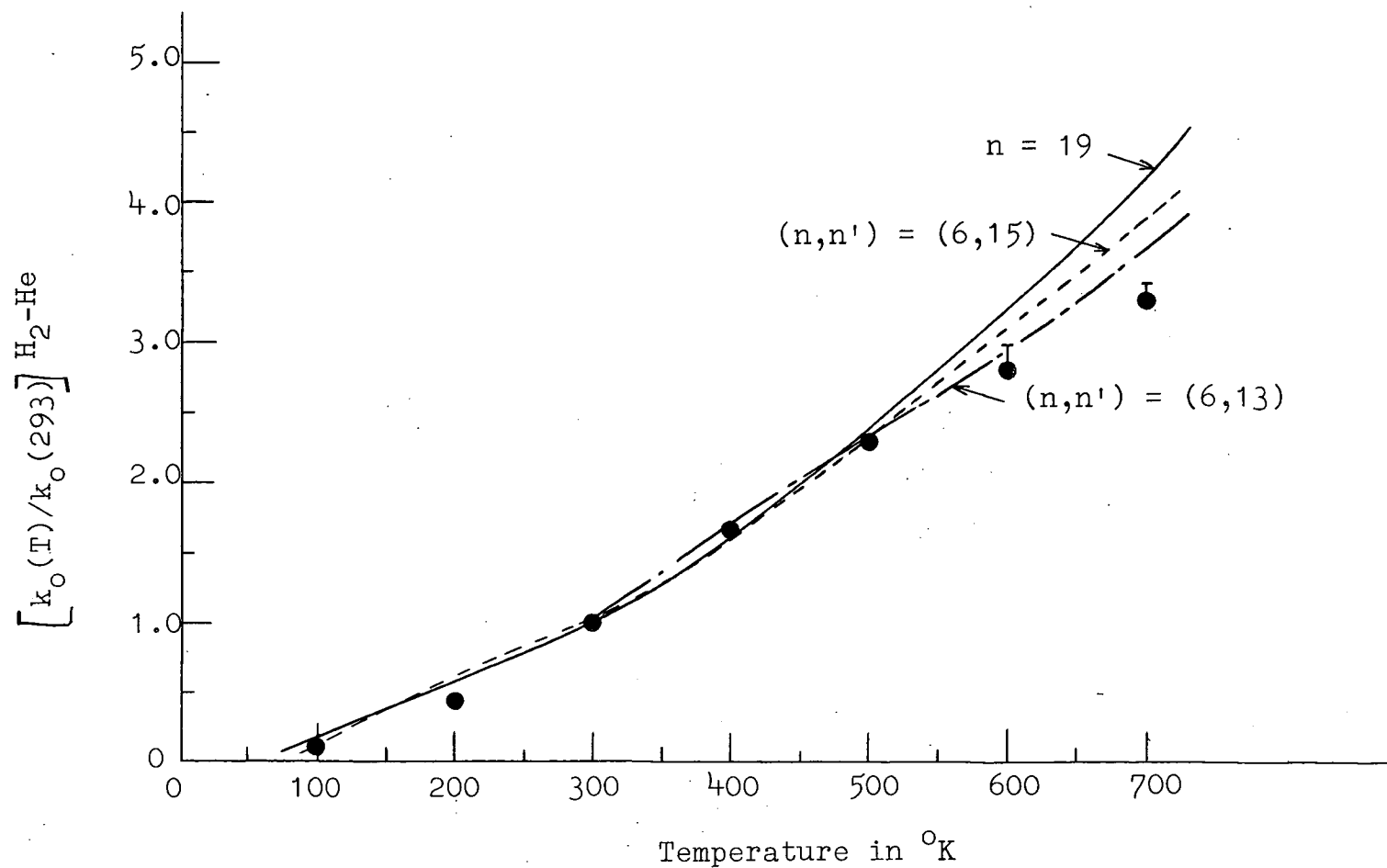


FIG. 21. Comparison of the experimental values of $[k_0(T)/k_0(293)]_{H_2-He}$ with the theoretical values using Eqs.(4.2.22) and (4.2.24)

that the theoretical curve obtained for the case $n'=12$ is almost identical with $n'=13$. It can be seen from the figure that the experimental data are adequately represented when

$$C''(ax) = \frac{\hbar \omega_{12}''}{x^{12}} - \frac{\hbar \omega_6''}{x^6} \quad (4.3.12)$$

and the intermolecular potential for $H_2 - He$ pair can be written as

$$V_0(r) = 4\epsilon \left[\left(\frac{a}{r}\right)^{12} - \left(\frac{a}{r}\right)^6 \right] \left[1 + 0.284 P_2(\cos \theta') \right] \quad (4.3.13)$$

Riehl has also obtained an expression for the intermolecular potential between H_2 and He molecules using scattering theory to evaluate the collision cross-sections. He assumed that the isotropic and anisotropic parts of the intermolecular potentials have the same dependence on r and that this dependence is given by $[A \exp(-kr) - B r^{-6}]$ where A, k and B are constants. He also computed the values of T_i/ρ using the Bloom-Oppenheim theory^{6,7,8} as well as scattering theory, assuming that the anisotropic part is given by

$$V_2(r) = 4\epsilon \delta \left[\left(\frac{a}{r}\right)^{15} - \left(\frac{a}{r}\right)^6 \right] \quad (4.3.14)$$

and the isotropic part is given by Lennard-Jones potential. For the best fit of his data below room temperature, he obtained $\delta = 0.28$ from scattering theory and $\delta = 0.14$ from Bloom-Oppenheim theory when the theoretical value was normalised to the experimental value at $100^\circ K$. This is perhaps due to the fact that the Bloom-Oppenheim theory does not take into account the quantum effects. It was found that when the theoretical value using the Bloom-Oppenheim theory was normalised to the experimental value at $300^\circ K$ or above, using the 77.0% He sample,

the value of ξ obtained was 0.173 instead of 0.14.

If Riehl's theory was fitted to the same data at 300°K, it appears that the value of ξ so obtained would be less than 0.28 by at least 10%. This may indicate that the quantum effects neglected in the Bloom-Oppenheim theory may not be as important above room temperature as at lower temperatures.

4.4. H₂ - CO₂ Mixture.

4.4.1. Results.

T_1 was measured in H₂ - CO₂ mixture for three concentrations of CO₂ at room temperature as a function of density. The temperature dependence of τ_1/ρ was studied for two of these mixtures where the total number density of the gas was determined as described in Chapter II.

Fig. 22 shows the dependence of T_1 on ρ at room temperature for 16.4% CO₂, 55.0% CO₂ and 77.5% CO₂. It can be seen from the figure that T_1 does not depend linearly on density for higher concentrations of CO₂. τ_1/ρ vs. ρ at room temperature is shown in fig. 23 and the extrapolated value of τ_1/ρ to $\rho = 0$ gives τ_1/ρ in dilute gas. The same procedure was used to obtain the value of τ_1/ρ in dilute gas at higher temperatures. Fig. 24 shows τ_1/ρ as a function of percentage of CO₂ from room temperature up to 500°K. Within experimental errors τ_1/ρ was found to depend linearly on the concentration of CO₂.

Above 550°K, the recovery of magnetisation was found to be a sum of two exponentials and the ratio of the time con-

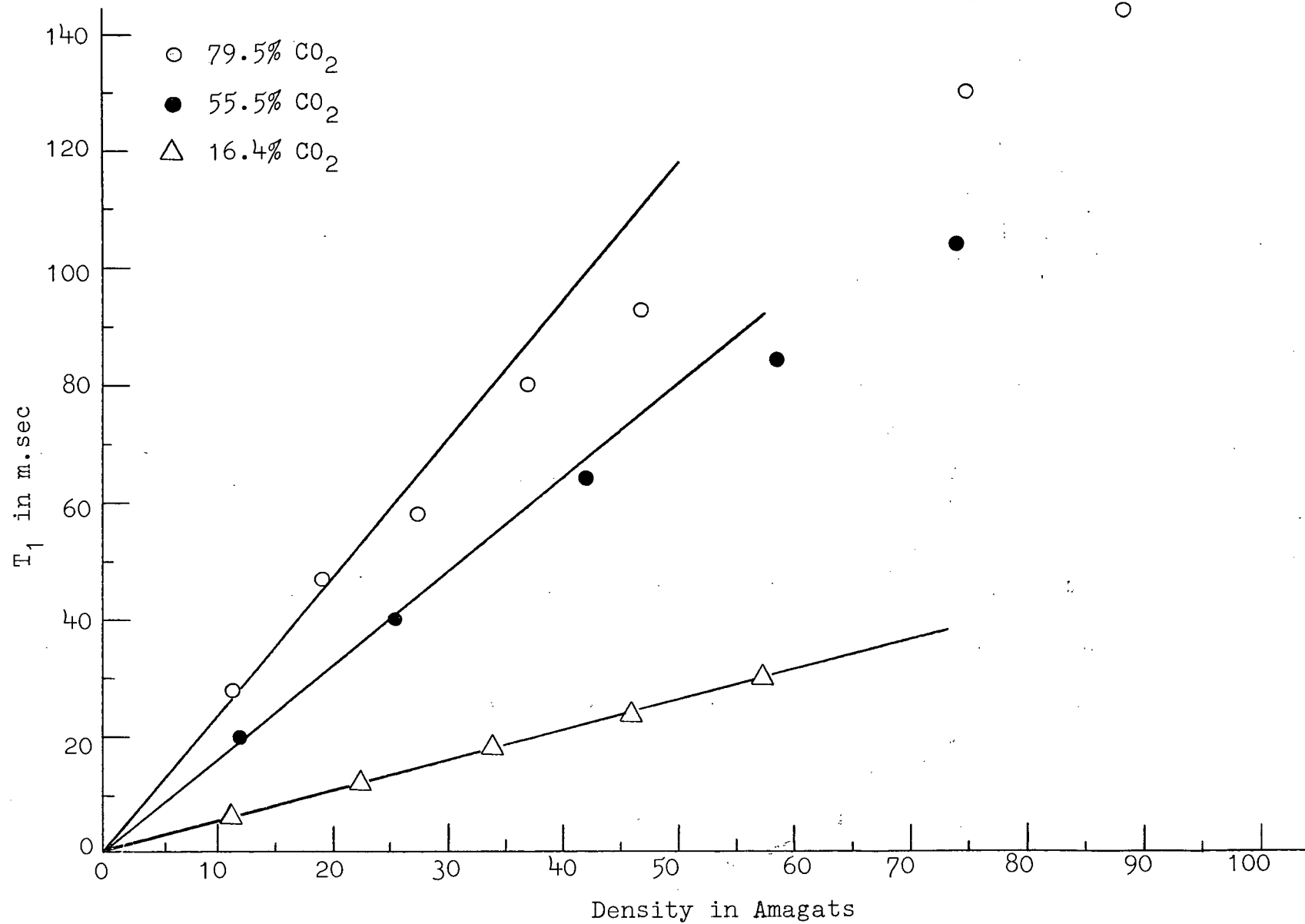


FIG.22. Dependence of T_1 on density at 293°K for H₂-CO₂ mixture.

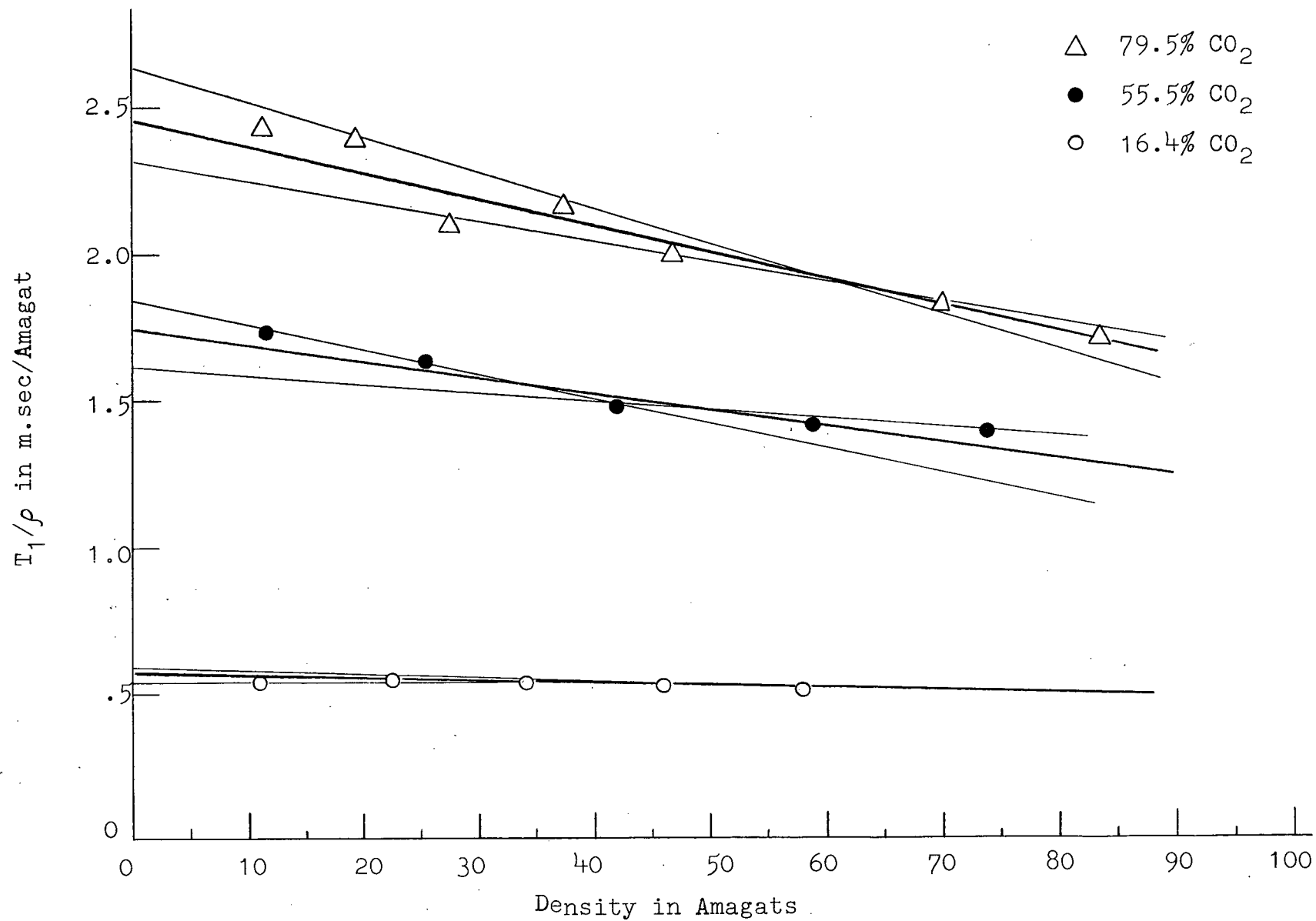


FIG. 23. Dependence of T_1/ρ on density at 293°K .

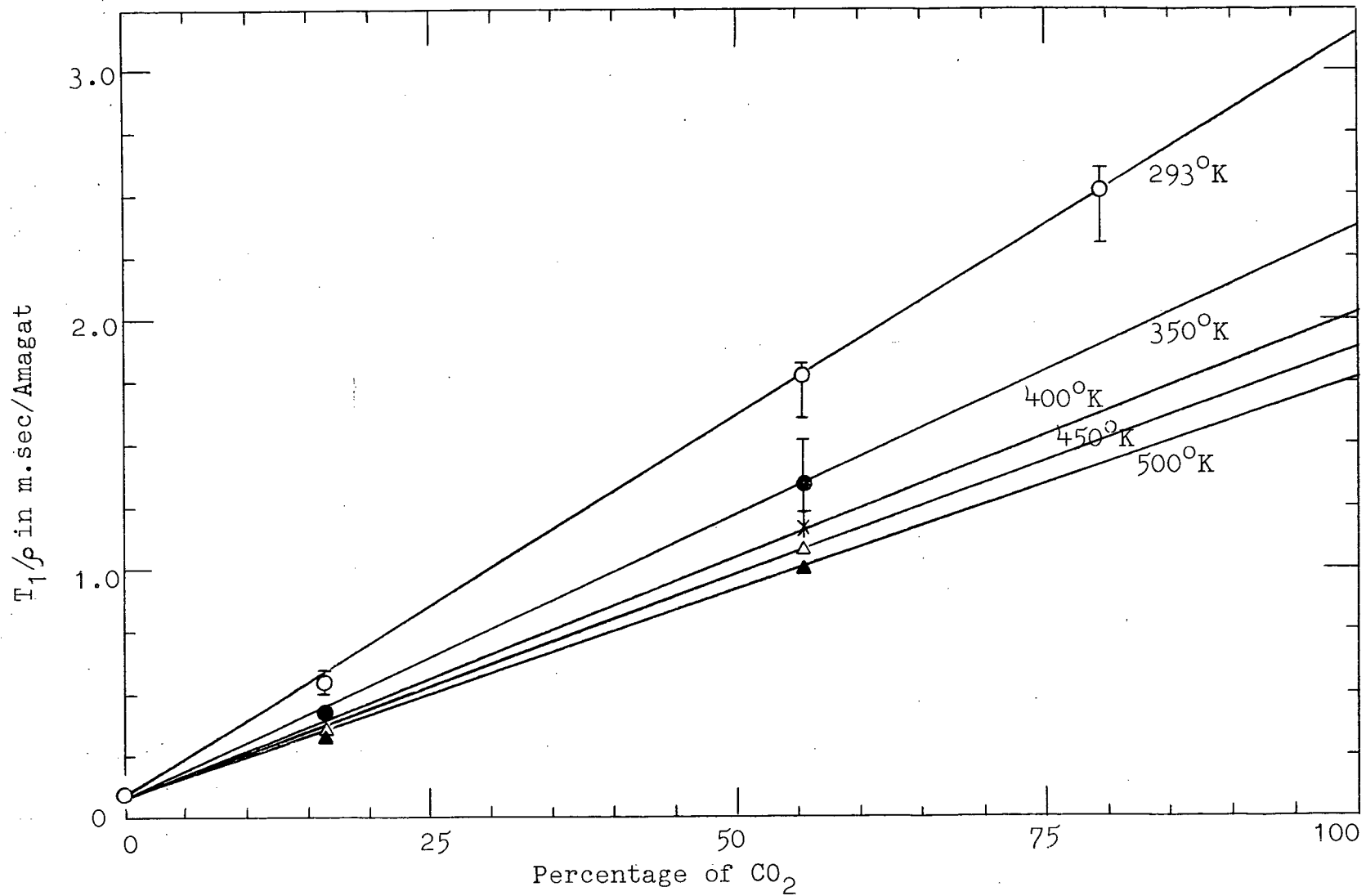


FIG. 24. Dependence of T_1/ρ on the percentage of CO_2 in $\text{H}_2\text{-CO}_2$ mixture.

stants was approximately 2.5 at 600°K. The reason for this was suspected to be H₂ and CO₂ reacting chemically to give rise to CO and H₂O and the two time constants could be due to the relaxation of protons in H₂ and H₂O. This reaction was studied by Graven and Long²⁷ from 800°C up to 1100°C in quartz vessels. According to their results the extent of reaction varied from 0.5% to 2.0%, depending on the reactant concentration, at 900°C and 0.53 second reaction time. The total pressure used by them was an atmosphere or less. In the present case the effect was noticeable for 55.0% CO₂ mixture even at 600°K. The pressures used were from 15 to 65 atmospheres. The material of the sample holder, Be-Cu, could be acting as a catalyst to the reaction and the high pressures involved could be the reason for the reaction to take place at much lower temperatures than anticipated. It may be noted that the effect could not be observed if the measurement was made within the first hour after the gas being introduced into the preheated sample holder and the effect was almost complete after 8 or 10 hours. Because of this complication the temperature dependence for H₂ - CO₂ mixtures was studied only up to 500°K.

The extrapolated value for 100% CO₂ gives the contribution due to H₂ - CO₂ collisions alone and $\log \left(\frac{\tau_1}{\rho} \right)_{100\% \text{ CO}_2}$ vs. $\log T^\circ \text{K}$ is shown in fig. 25. The deviation from linear dependence of $\log \left(\frac{\tau_1}{\rho} \right)_{100\% \text{ CO}_2}$ vs. $\log T$ at 450°K and 500°K is probably due to the effect of chemical reaction discussed above.

4.4.2. Interpretation.

The interaction between ortho- H₂ and CO₂ molecules can

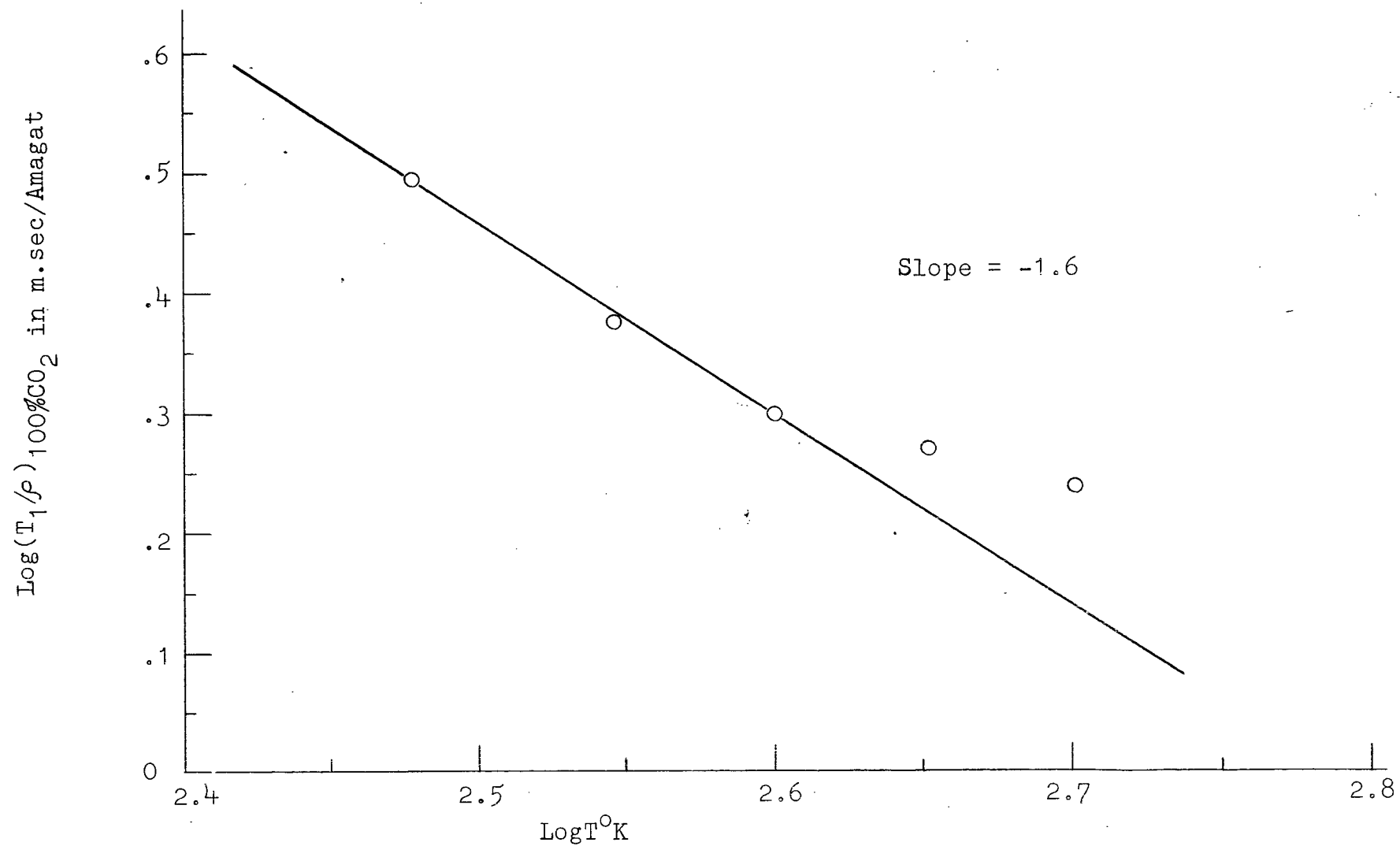


FIG. 25. Dependence of $\log(T_1/\rho)_{100\%CO_2}$ on $\log T^\circ K$ for H_2-CO_2 mixture.

be adequately described by quadrupole-quadrupole interaction since the molecules do not have a permanent dipole moment.

The hamiltonian for this interaction is given by

$$\mathcal{H}_R = \mathcal{H}_R^{(1)} + \mathcal{H}_R^{(2)} \quad (4.4.1.)$$

and

$$\mathcal{H}_R^{(2)} = 4\pi Q_0 Q_{CO_2} / r^5$$

where Q_0 is the quadrupole moment of ortho- H_2 molecule and Q_{CO_2} is the quadrupole moment of CO_2 molecule. It is assumed that this interaction cannot produce transitions between different J states of the ortho- molecule. Since the CO_2 molecule has a high moment of inertia compared with H_2 , many of its rotational states are populated. Collisions with H_2 molecules will produce transitions between different J states for CO_2 molecule. When these transitions are allowed the value of C for CO_2 becomes 5/2. The contributions to $B_1(J, J)$ and $B_2(J, J)$ due to $H_2 - CO_2$ interactions can be written as

$$B_1(J, J)_{H_2-CO_2} = \frac{12\pi}{5} \tilde{\beta}_{CO_2} \rho(\eta'_0)^{H_2-CO_2} \frac{1}{(2J-1)(2J+3)} + \frac{21}{25\pi} \frac{C_{CO_2} \tilde{\beta}_{CO_2} \rho}{(2J-1)(2J+3)} (\eta'_1)^{H_2-CO_2} \quad (4.4.2.)$$

$$B_2(J, J)_{H_2-CO_2} = B_1(J, J) \frac{3(4J^2 + 4J - 7)}{(2J-1)^2 (2J+3)^2} \quad (4.4.3.)$$

and X for $H_2 - CO_2$ mixture can be defined as

$$X = \left[\left(\frac{12\pi}{25} \left(\frac{\eta'_0}{\eta'_1} \right)^{H_2-H_2} \tilde{\beta}_{H_2} + \frac{21C}{125\pi} \tilde{\beta}_{H_2} \right) + \frac{\tilde{\beta}_{CO_2}}{(\eta'_1)^{H_2-H_2}} \left(\frac{12\pi}{25} (\eta'_0)^{H_2-CO_2} + \frac{21 C_{CO_2}}{125\pi} (\eta'_1)^{H_2-CO_2} \right) \right] \quad (4.4.4.)$$

where

$$(\eta'_0)^{H_2-CO_2} = \rho_1 a^4 (2\pi\beta\mu)^{1/2} \frac{5}{6\pi} (k_0)^{H_2-CO_2} \quad (4.4.5.)$$

$$(\eta'_1)^{H_2-CO_2} = \rho_1 a^4 (2\pi\beta\mu)^{1/2} \frac{1}{0.134} (k_1)^{H_2-CO_2} \quad (4.4.6.)$$

where a, μ are evaluated for $H_2 - CO_2$ interactions.

Evaluating equations (4.4.2.) and (4.4.3.) for $J=1$ and $J=3$ and adding to the contributions from $H_2 - H_2$ interactions

$B_{\ell}(J, J)$ and $B_{\ell}(J, J')$ for $H_2 - CO_2$ mixture are given by equations (4.2.10) and (4.2.11) where X is defined by equation (4.4.4.). ρ/T_1 for any composition of the mixture is given by equation (4.2.14) which can be solved for X on the computer as described in the previous sections.

From the value of X thus obtained X_{CO_2} can be obtained from equation (4.4.4.) knowing X_{H_2} . Using equations (4.4.5.) and (4.4.6.), $(k_0 + C k_1)^{H_2-CO_2}$ can be written as

$$(k_0 + C k_1)^{H_2-CO_2} = X_{CO_2} (\eta'_1)^{H_2-H_2} / 0.4 \rho_1 a^4 (2\pi\beta\mu)^{1/2} \tilde{\rho}_{CO_2} \quad (4.4.7.)$$

where $\rho_1 = \rho_T / \rho$; $C_{CO_2} = 5/2$

Fig. 26 represents $(k_0 + C k_1)^{H_2-CO_2}$ as a function of temperature. The theoretical plots of T_1/ρ vs. percentage of CO_2 are shown in fig. 27 for different values of X_{CO_2} as obtained from the analysis of the data in different mixtures at room temperature and at $500^\circ K$. The experimental data fits best the plots in which X_{CO_2} obtained from higher concentrations CO_2 were used. In this the theoretical plots also confirm the experimental observation that T_1/ρ is proportional to the concentration of CO_2 .

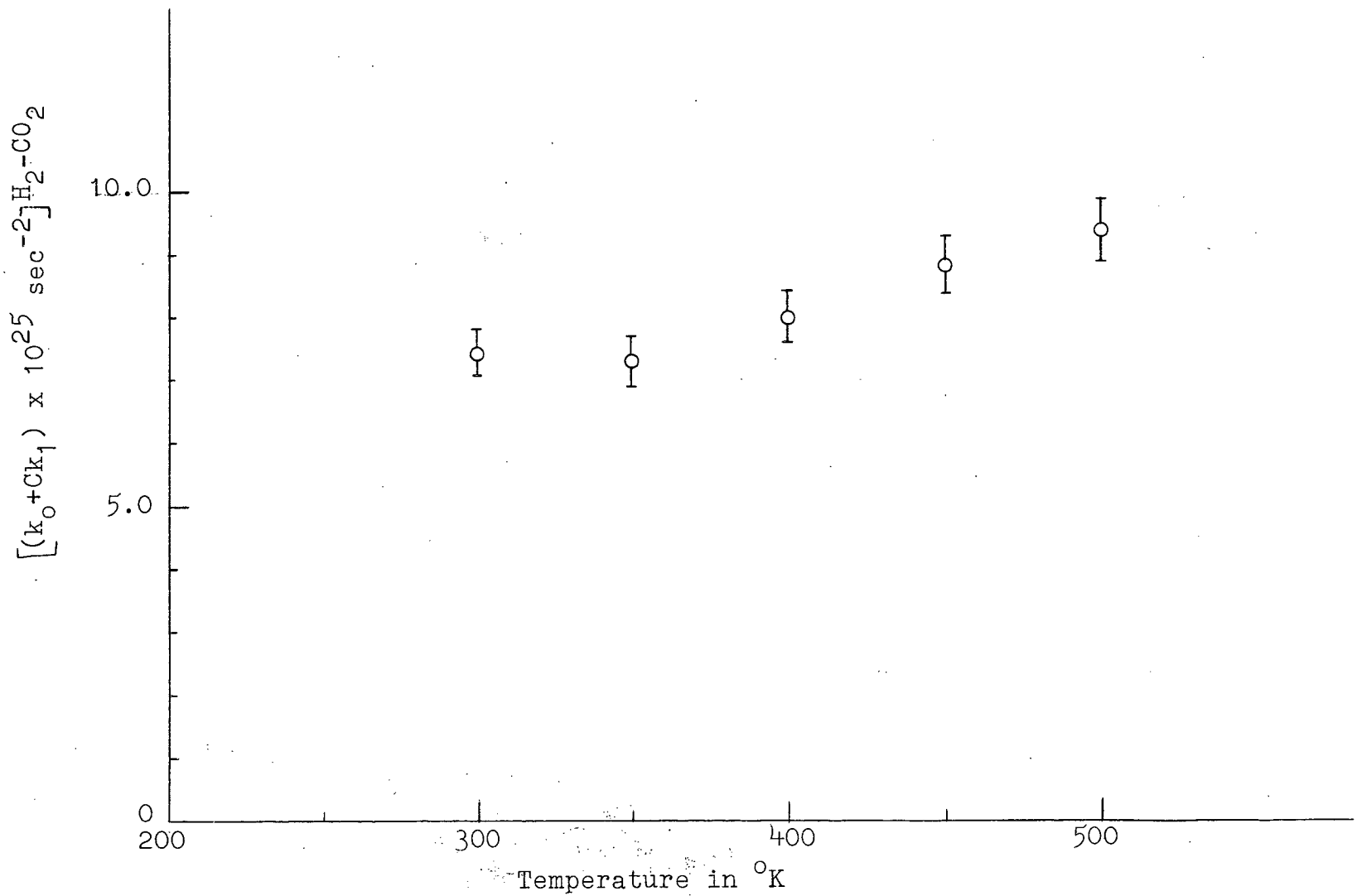


FIG. 26. Temperature dependence of $(k_0 + Ck_1)^{\text{H}_2\text{-CO}_2}$ as obtained from Eqs. (4.2.14) and (4.4.7) using the experimental values of T_1/ρ .

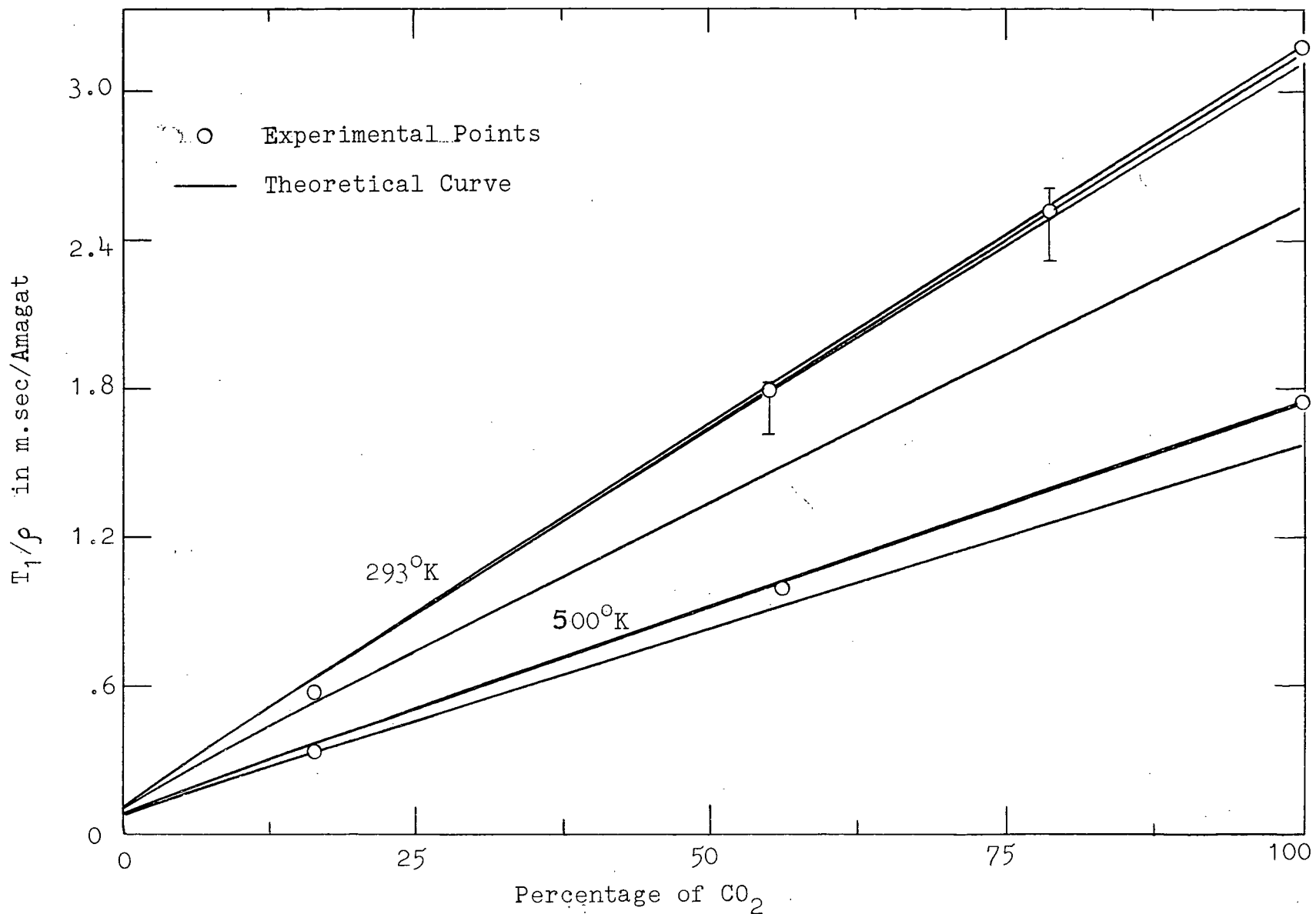


FIG. 27. Theoretical plots of T_1/ρ vs. % CO_2 in H_2 - CO_2 mixture when Eq. (4.2.14) was normalised with the experimental values at different concentrations of CO_2 .

The fact that $(k_0 + C k_1)^{H_2CO_2}$ does not vary very much with temperature indicates that the contributions from short range interactions to $k_0 \approx k_1$ are very small. Since the information is available only on $(k_0 + C k_1)$ and not on k_0 and k_1 separately, it is assumed that $C k_1 \gg k_0$ as a first approximation. The theoretical value of k_1 is obtained from equation (4.2.18) with $n=5$ and $\omega_6^{(2)}$ is obtained by normalising the theoretical and experimental values at $293^\circ K$. Fig. 28 shows the theoretical plots of $\left[k_1(\tau) / k_1(293^\circ K) \right]^{H_2CO_2}$ as a function of temperature along with the experimental values. The agreement between the theoretical and experimental plots indicate that the dominant contribution to the anisotropic interactions between H_2 and CO_2 molecules is quadrupole-quadrupole interaction. The quadrupole moment was obtained by normalising the theoretical and experimental values at $293^\circ K$ and the value obtained is $(4.83 \pm 0.3) \times 10^{-26}$ e.s.u. This value is comparable to the values obtained from other experiments.

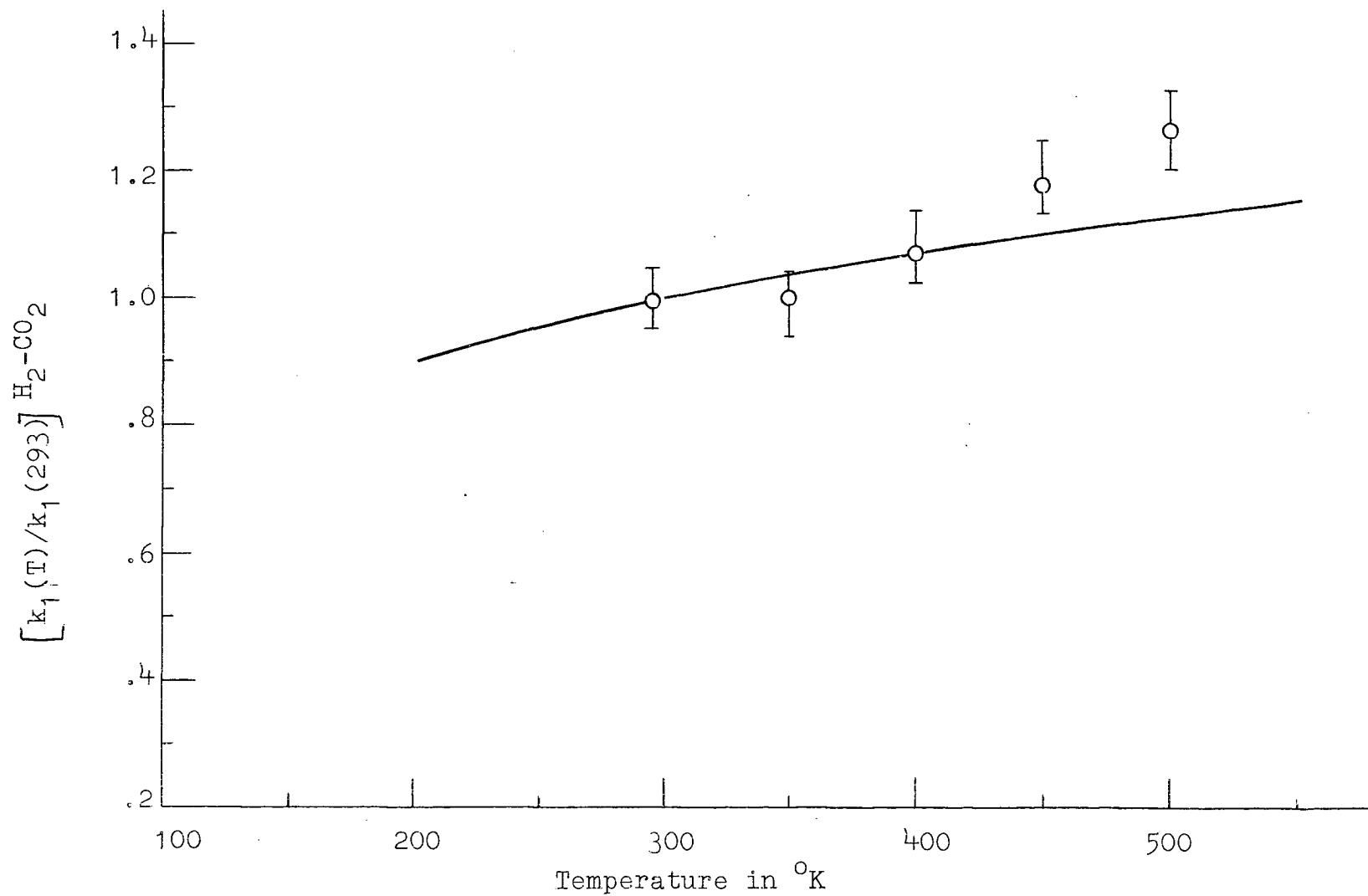


FIG. 28. Comparison of $[k_1(T)/k_1(293)]_{\text{H}_2\text{-CO}_2}$ with the computed values using Eq. (4.2.18).

CHAPTER V

EXPERIMENTAL RESULTS AND DISCUSSION (cont'd)5.1. METHANE5.1.1. Results

The proton spin-lattice relaxation time T_1 was measured in methane as a function of density from room temperature up to 700°K. Knowing the pressure, the density at any temperature was obtained from the compressibility tables given by "American Petroleum Institute".²⁸ Fig. 29a shows T_1 as a function of density up to 100 amagats at room temperature. It can be seen from the graph that the dependence of T_1 on density is linear in the low density region whereas it is non-linear at higher densities due to the effect of three body collisions. The value of τ_1/ρ in the dilute gas is obtained by plotting τ_1/ρ as a function of density and extrapolating it to zero density. Fig. 29b shows τ_1/ρ vs. ρ at room temperature. Figs. 30a and 30b show similar plots for CH_4 at 720°K and the same procedure is adopted at all other temperatures. The value of τ_1/ρ obtained at room temperature (20.2 m.sec/Amagat) is in agreement with the values obtained by Bridges²⁹ (21.0 \pm 5% m.sec/Amagat); Lipsicas, Bloom and Muller³⁰ (20.0 m.sec/Amagat) and Johnson and Waugh³¹ (23.0 m.sec/Amagat). Fig. 31 shows τ_1/ρ as a function of temperature along with the low temperature data available from other work whereas $\log(\tau_1/\rho)$ as a function of $\log T^\circ\text{K}$ is shown in fig. 32. The data can be

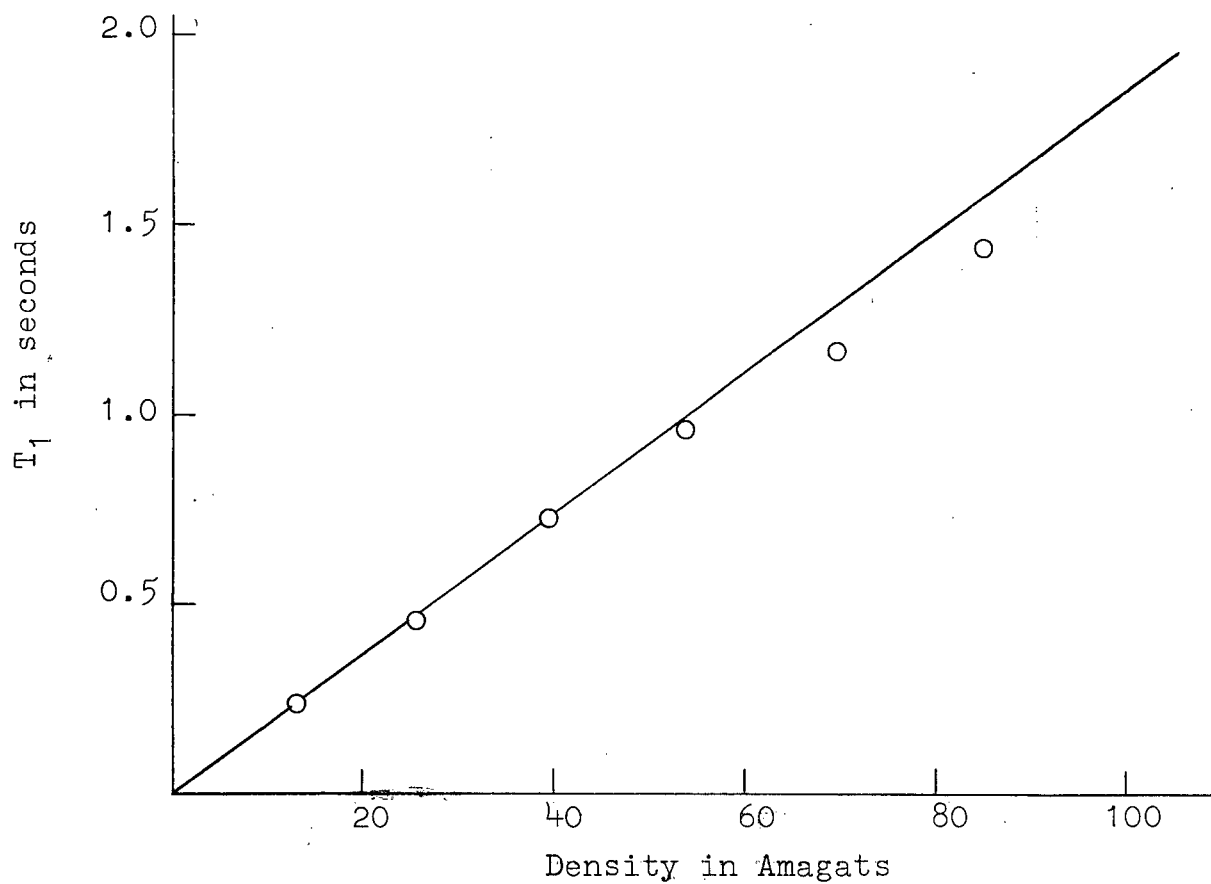


FIG. 29a. Dependence of T_1 on density at 293°K for CH_4 .

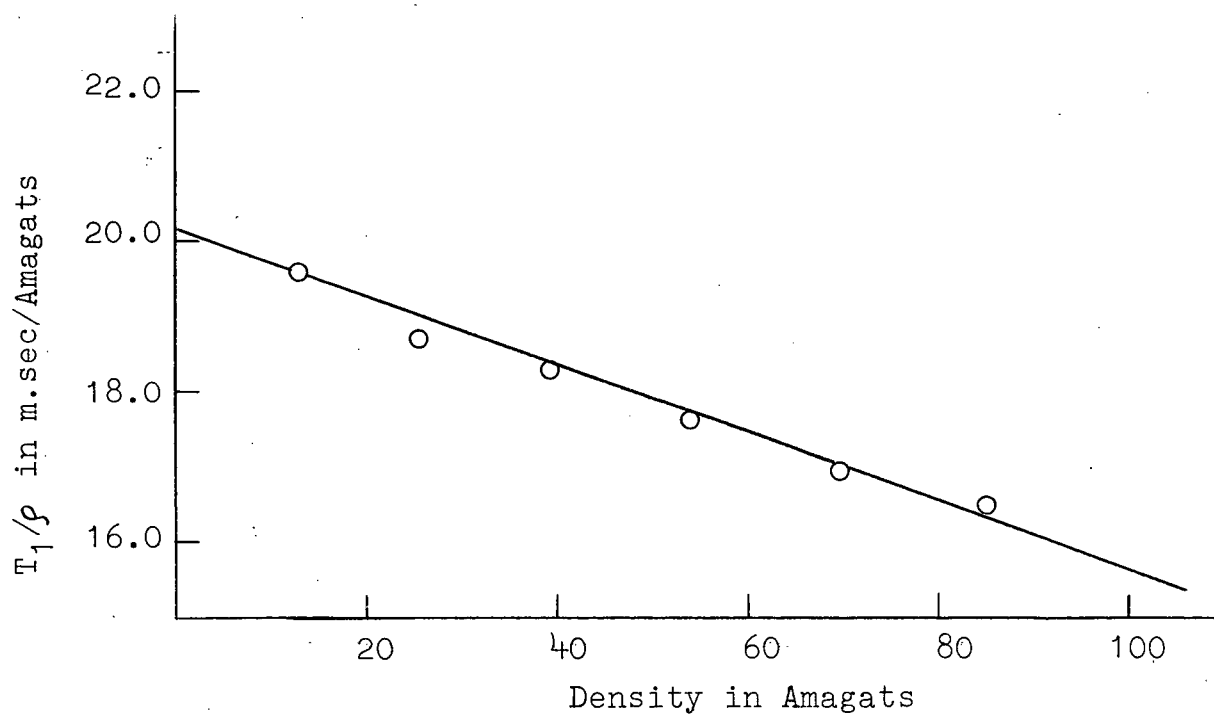


FIG. 29b. Dependence of T_1/ρ on density at 293°K for CH_4 .

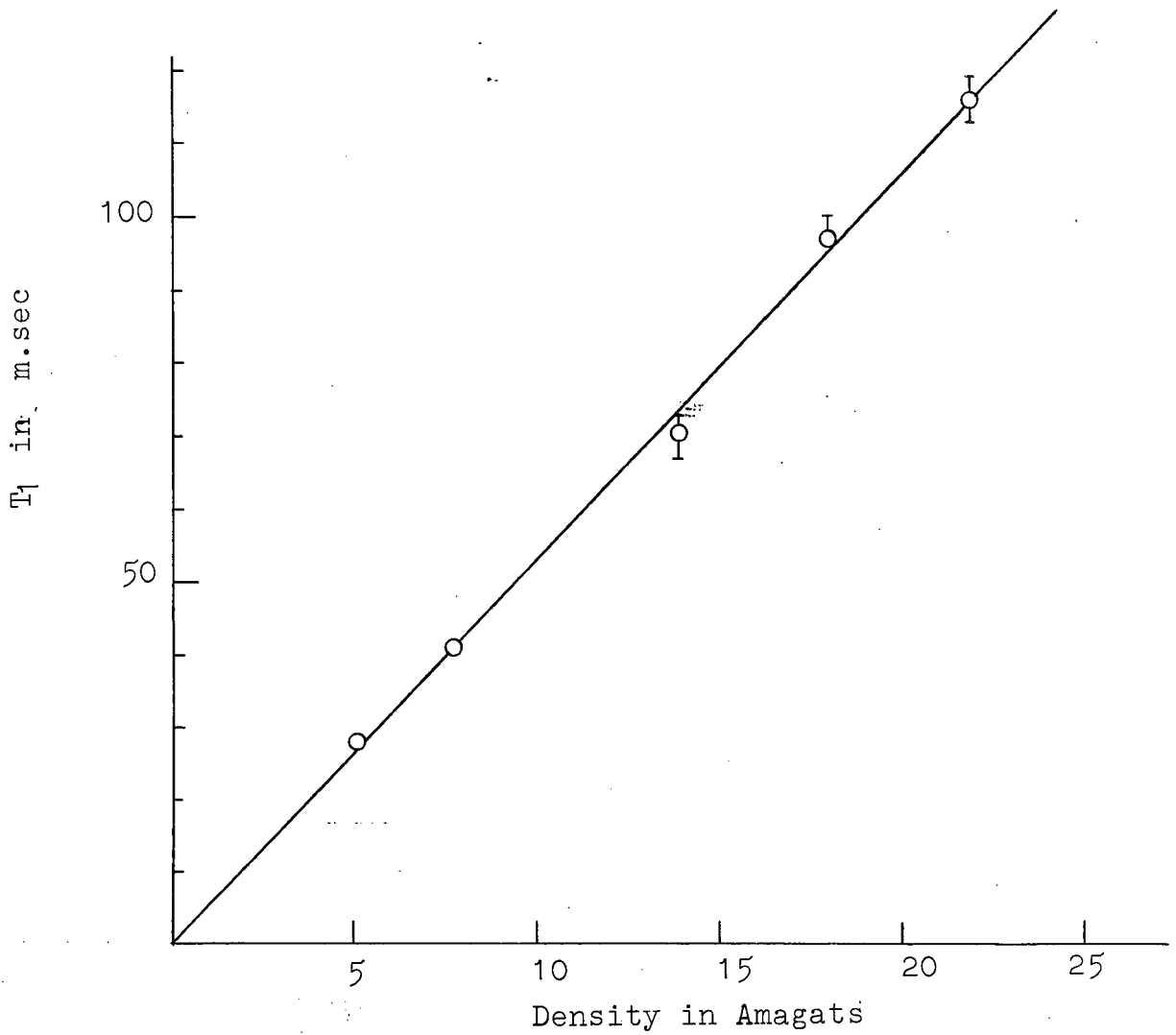


FIG. 30a. Dependence of T_1 on density at 720°K for CH_4 .

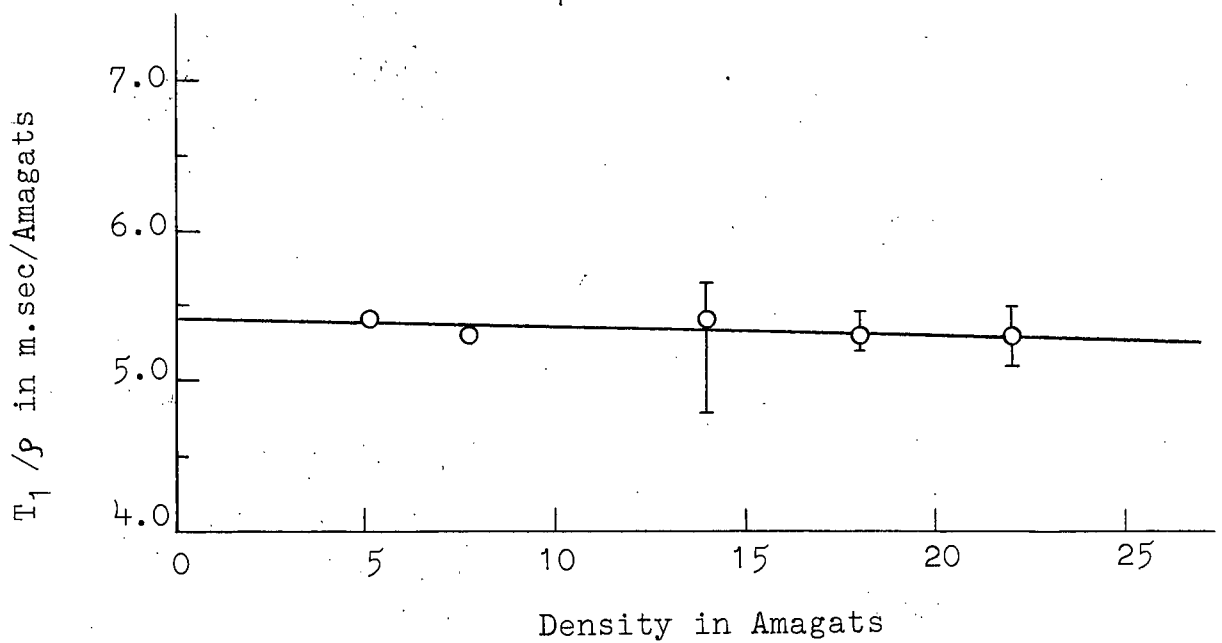


FIG. 30b. Dependence of T_1/ρ on density at 720°K for CH_4 .

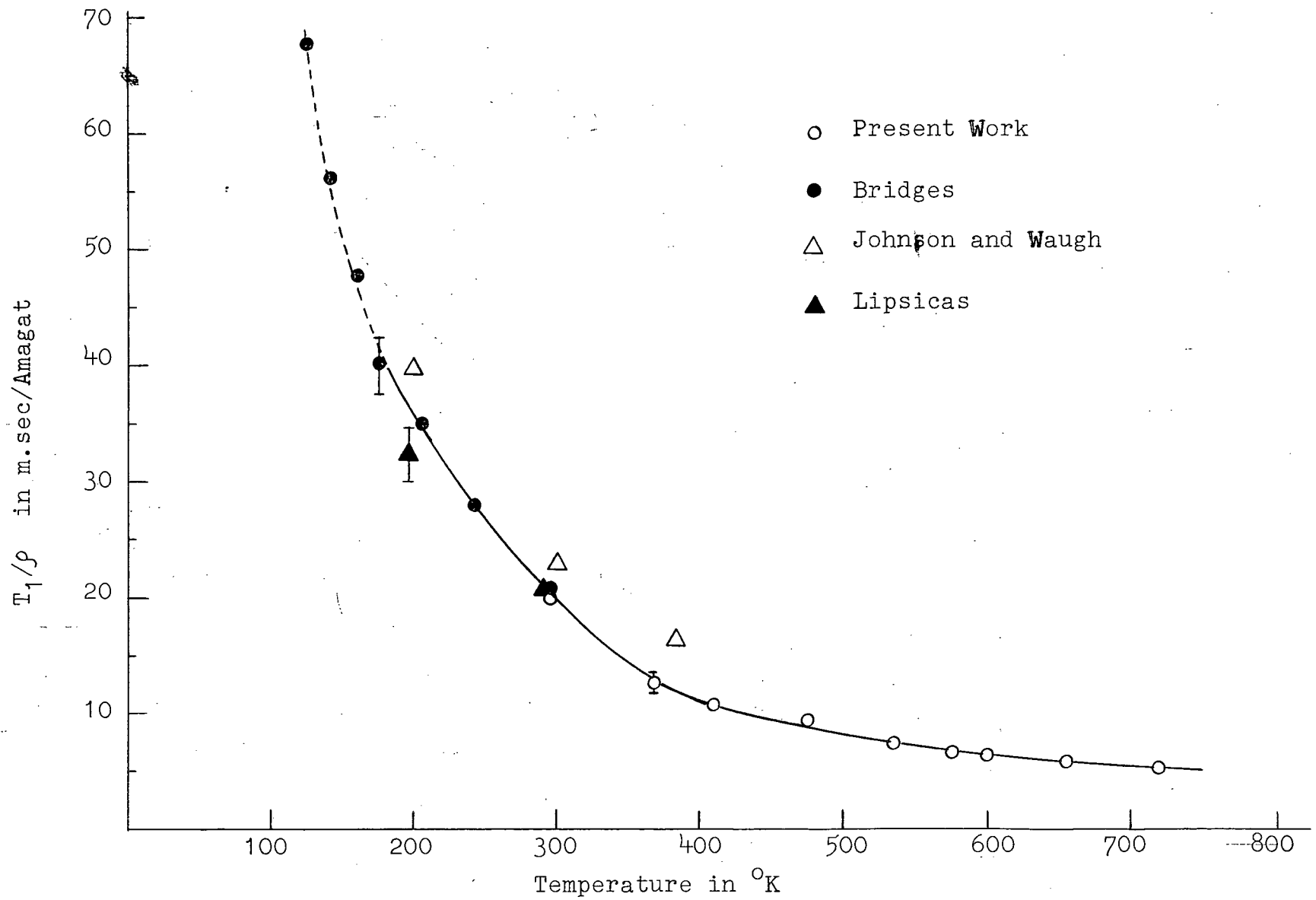


FIG. 31. Dependence of T_1/ρ on temperature for CH_4 .

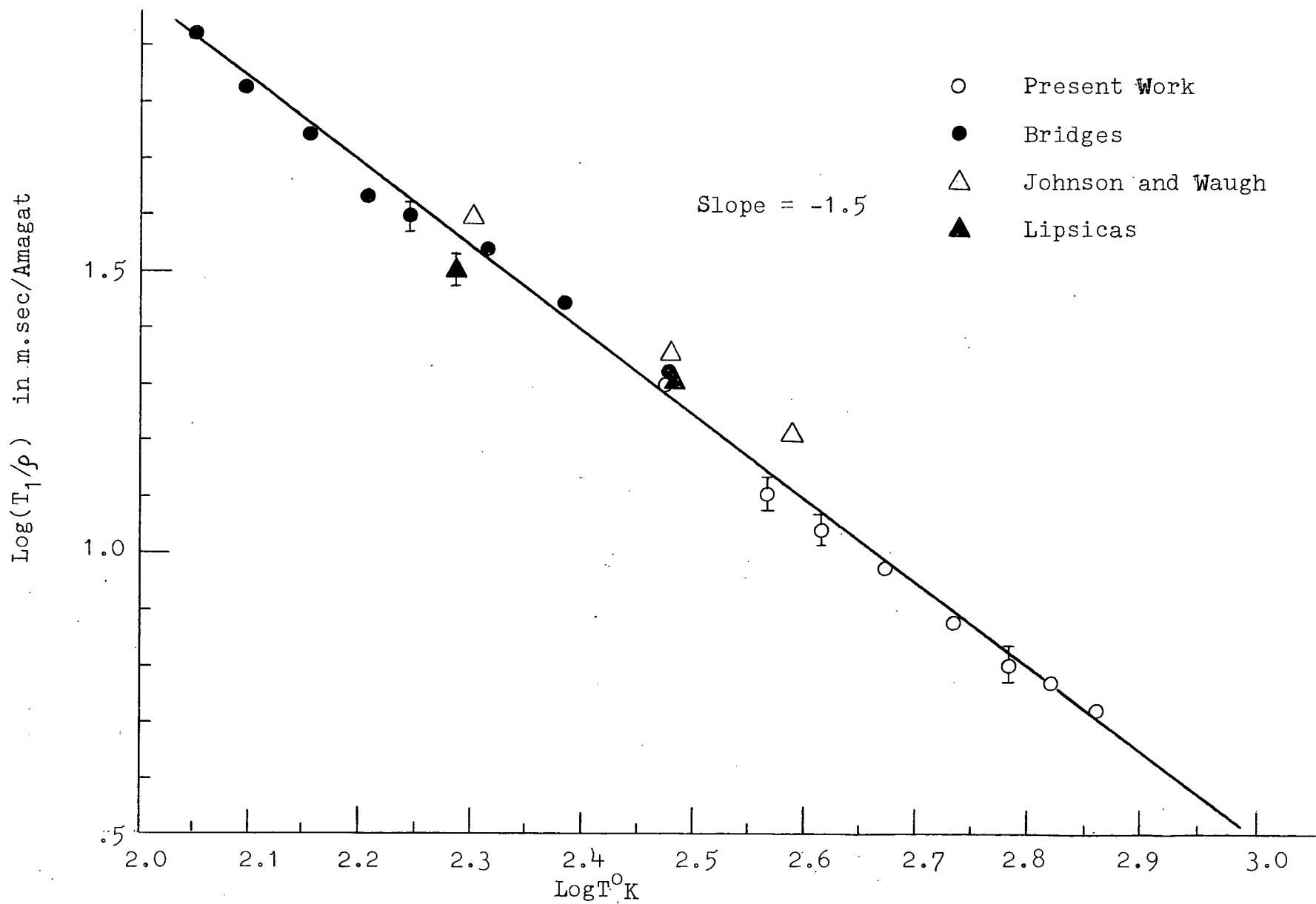


FIG. 32. $\text{Log}(T_1/\rho)$ as a function of $\text{log}T^\circ\text{K}$ for CH_4 .

fitted by a straight line with a slope equal to - 1.5 indicating that T_1/ρ is roughly proportional to $T^{-1.5}$. This is in agreement with the slopes obtained by Bridges²⁹ ($-1.45 \pm 5\%$), Johnson and Waugh³¹ (-1.42) and Trappeniers et al³² (-1.55 ± 0.03).

5.1.2. Interpretation.

Due to the high Moment of Inertia, the rotational states of the CH_4 molecule are closely spaced and hence quite a large number of rotational states are appreciably populated even at low temperatures. As a result, the theory developed in Chapter III cannot be directly applied to this system because of the large number of equations of (3.2.23) that have to be retained to give a correct representation of T_1 . Therefore, further approximations will be made to the general results obtained in Chapter III in order to get some information about anisotropic intermolecular interactions. Assuming that the intramolecular interactions that are responsible for the relaxation mechanism are given by spin-rotational interactions alone, the relaxation rate can be written in the short correlation time limit, using equation (3.2.35), as

$$\frac{1}{T_1} = \frac{2}{3} \gamma^2 H'^2 \sum_{J_0} P_{J_0} J_0 (J_0 + 1) \sum_{\alpha} \frac{C_{J_0}^{1\alpha}}{\Lambda_{1\alpha}} \quad (5.1.1.)$$

Assuming that $\Lambda_{1\alpha}$ is a slowly varying function of α

it can be replaced by its average value, $\langle \Lambda_{1\alpha} \rangle$ and can be taken outside the summation. Since $\sum_{\alpha} C_{J_0}^{1\alpha} = 1$ equation (5.1.1.) can be written as

$$\frac{1}{T_1} = \frac{2}{3} \gamma^2 H'^2 \overline{J_0 (J_0 + 1)} \frac{1}{\langle \Lambda_1 \rangle} \quad (5.1.2.)$$

where the bar represents the ensemble average.

Using the high temperature result

$$\overline{J(J+1)} \propto T \quad (5.1.3.)$$

the relaxation rate can be written as

$$\frac{1}{T_1} \propto \frac{T}{\langle \lambda_1 \rangle} \quad (5.1.4.)$$

If the transitions between different J states are infrequent compared with the transitions among different m_J levels of the same J-manifold, $1/\langle \lambda_1 \rangle$ can be identified with the correlation time τ_c of the spin-rotational interaction. Under such conditions

$$\frac{1}{T_1} \propto T \tau_c \quad (5.1.5.)$$

Since experimental results indicate that

$$\frac{1}{T_1} \propto T^{1.5} \quad (5.1.6.)$$

it can be concluded that

$$\tau_c \propto T^{0.5} \quad (5.1.7.)$$

Bloom and Oppenheim^{6,7} have evaluated τ_c for the case of diatomic molecules in terms of intermolecular anisotropic interactions using the "constant acceleration approximation" and they obtain for the case where no rotational transitions take place, a result of the form

$$\left(\frac{1}{\tau_c}\right)_J = \frac{\rho}{2k^2} \left(\frac{\pi\mu}{kT}\right)^{1/2} A(J) I^{(q)}(p) \quad (5.1.8.)$$

where $A(J)$ is a function of the rotational state J, $I^{(q)}(p)$ is defined by equation (3.4.14) and μ is the reduced mass.

The assumption that $\left(\frac{1}{\tau_c}\right)_J$ does not strongly depend on J is valid only if $A(J)$ does not strongly depend on J. The integrals

$I^{(q)}(p)$ are evaluated by Bloom, Oppenheim et al⁸ for the cases where the isotropic intermolecular potential is given by hard sphere potential and Lennard-Jones potential. For the

hard sphere model the integrals are independent of temperature and hence $\zeta_c \propto T^{0.5}$. Further this model predicts that $T_1/\rho \propto T^{1.5}$ for all systems like $\text{CH}_4 - \text{X}$. In fact, the $T^{1.5}$ behaviour is not observed for the case when X is He as can be seen from the following section. Therefore, the temperature dependence of T_1/ρ will be considered taking a more realistic form of the isotropic part of the intermolecular potentials namely the Lennard-Jones potential, and assuming that the anisotropic part is given by a simple power law

$$g^{(q)}(ax) = k \omega_n^{(q)} / x^n \quad (5.1.9.)$$

Then

$$1/T_1 \propto T^{3/2} / I(p, n) \quad (5.1.10)$$

where

$$I(p) / k^2 = \omega_n^{(p)2} I(p, n)$$

From the experimental values of T_1/ρ at different temperatures the temperature dependence of $[I(p, n)_T / I(p, n)_{293^\circ\text{K}}]_{\text{CH}_4-\text{CH}_4}$ is obtained from equation (5.1.10) and is shown in fig. 33 along with the theoretical plots of $[I(p, n)_T / I(p, n)_{293^\circ\text{K}}]_{\text{CH}_4-\text{CH}_4}$ vs. temperature as obtained from the tables given by Bloom, Oppenheim et al ⁸ for $n=3, 5$ and 7 . It may be worth mentioning here that the ratio of the integrals at different temperatures is independent of the parameter p . If the octopole-octopole interaction is assumed to be the dominant interaction between the two methane molecules, then n should take the value of 7 . But as it can be seen from the fig. 33, the plot with $n=3$ fits best with the experimental results. However, this cannot be taken too seriously as the equation (5.1.8.) is obtained assuming that perturbation theory can be used to

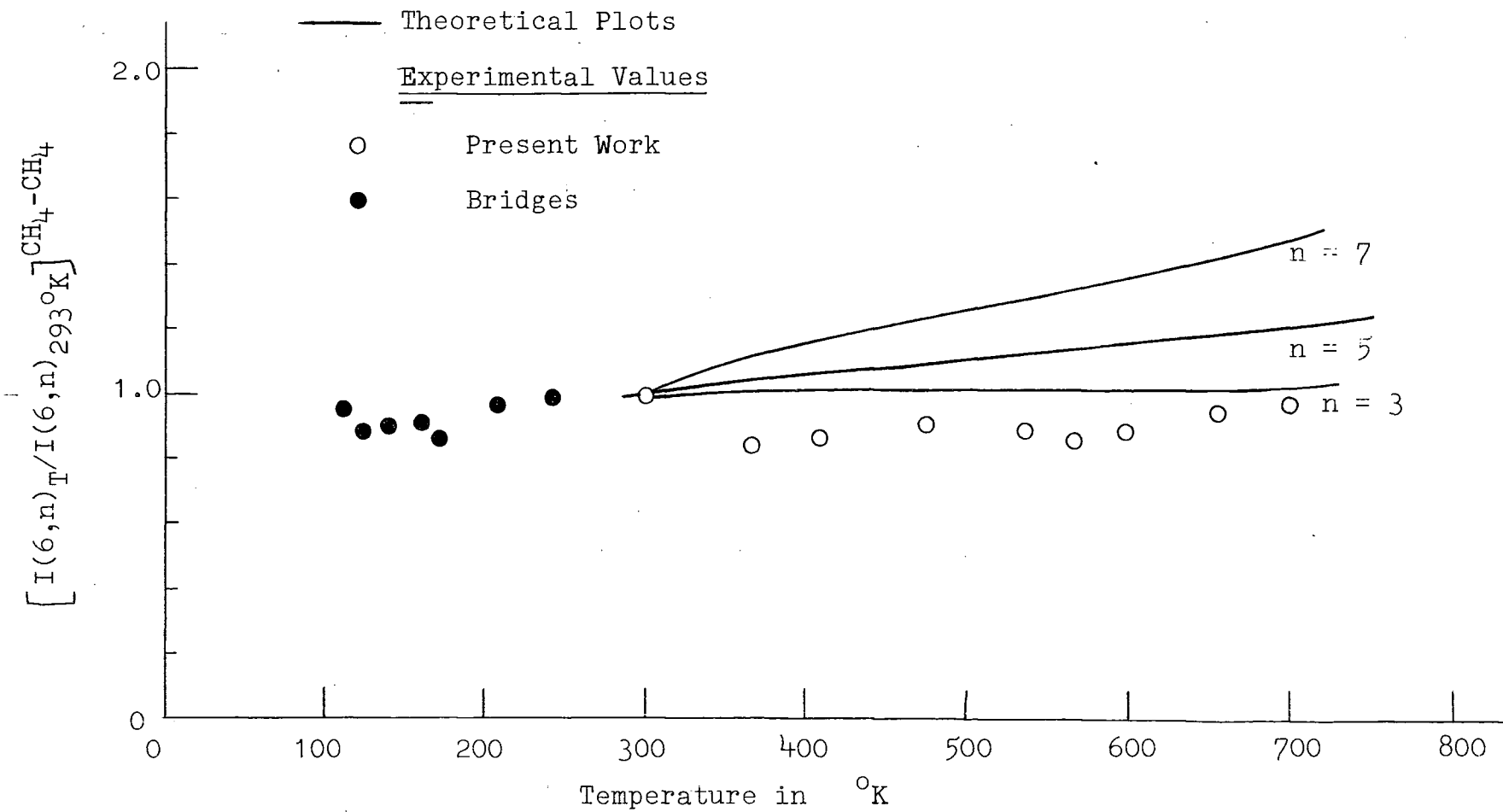


FIG. 33. Comparison of $\left[\frac{I(6,n)_T}{I(6,n)_{293}} \right]^{CH_4-CH_4}$ as obtained from Eq.(5.1.10) with the computed values using the numerical values of the integrals.

evaluate the transition probabilities between the rotational states of the molecule which is not true for this case.

Additional temperature dependence could also be coming from $A(J)$. Hence a more rigorous theory is necessary to understand these results.

5.2. CH₄ - He Mixture.

5.2.1. Results.

T_1 was measured in CH₄ - He mixture as a function of density for five different compositions of the mixture at room temperature and the temperature dependence of mixtures with 30.0% He, 76.0% He and 88.2% He was studied from room temperature up to 700°K. Typical plots of T_1 vs ρ and T_1/ρ vs ρ are shown in figs. 34a and 34b respectively for the mixtures with 88.2% He at room temperature whereas fig. 35a and fig. 35b show similar plots for the same mixture at 730°K. The dependence of T_1/ρ on ρ was linear within experimental errors and the value extrapolated to infinite dilution gives the value of T_1/ρ for dilute gas which will be referred to as T_1/ρ in the following.

$\log (T_1/\rho)$ vs. $\log T^\circ K$ was found to be a straight line for all the mixtures and the slope of the straight line decreased with the increase of the He concentration in the mixture and the values are given below:

30.0% He	- 1.28 \pm 5%
76.0% He	- 1.08 \pm 5%
88.2% He	- 0.82 \pm 5%

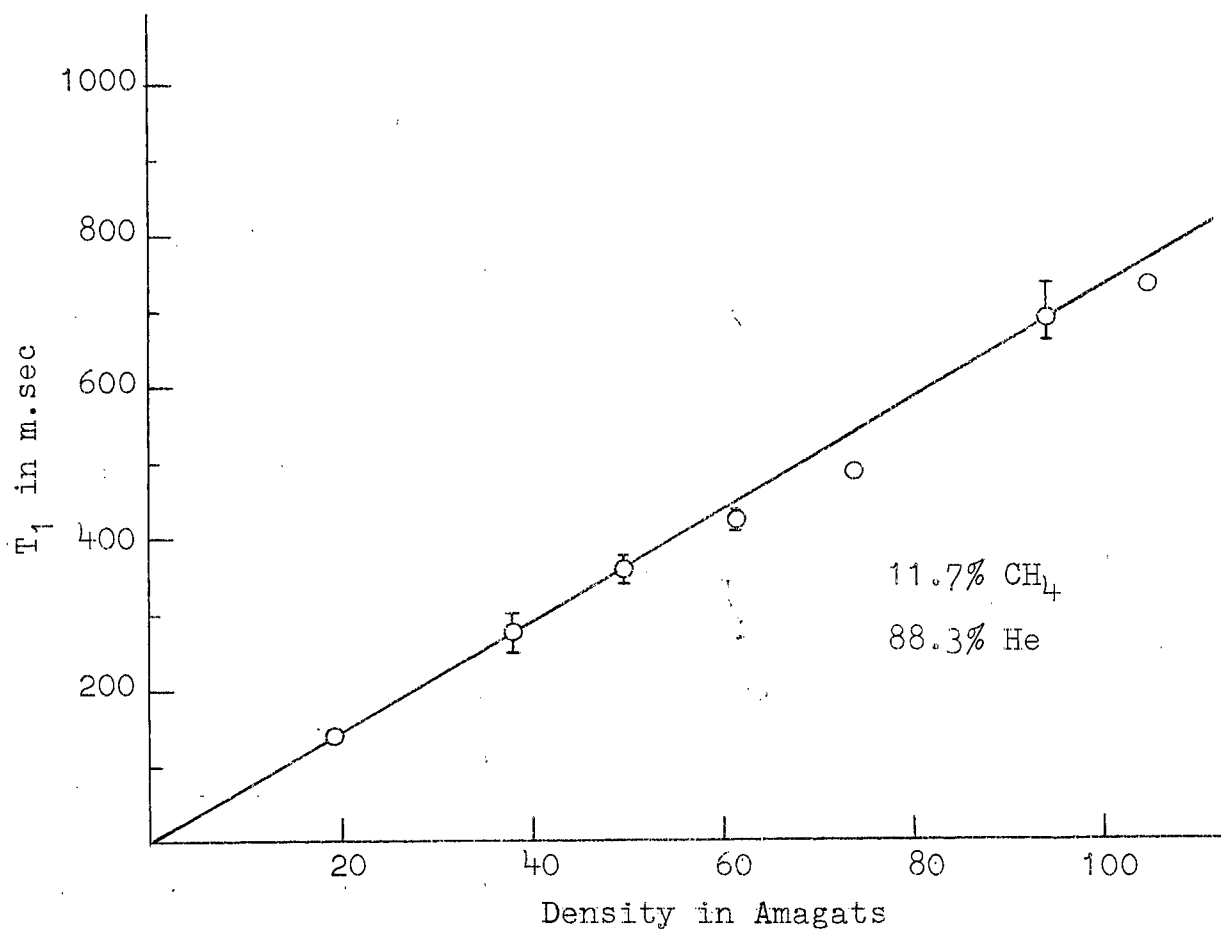


FIG. 34a. Dependence of T_1 on density for CH₄-He mixture at 293°K.

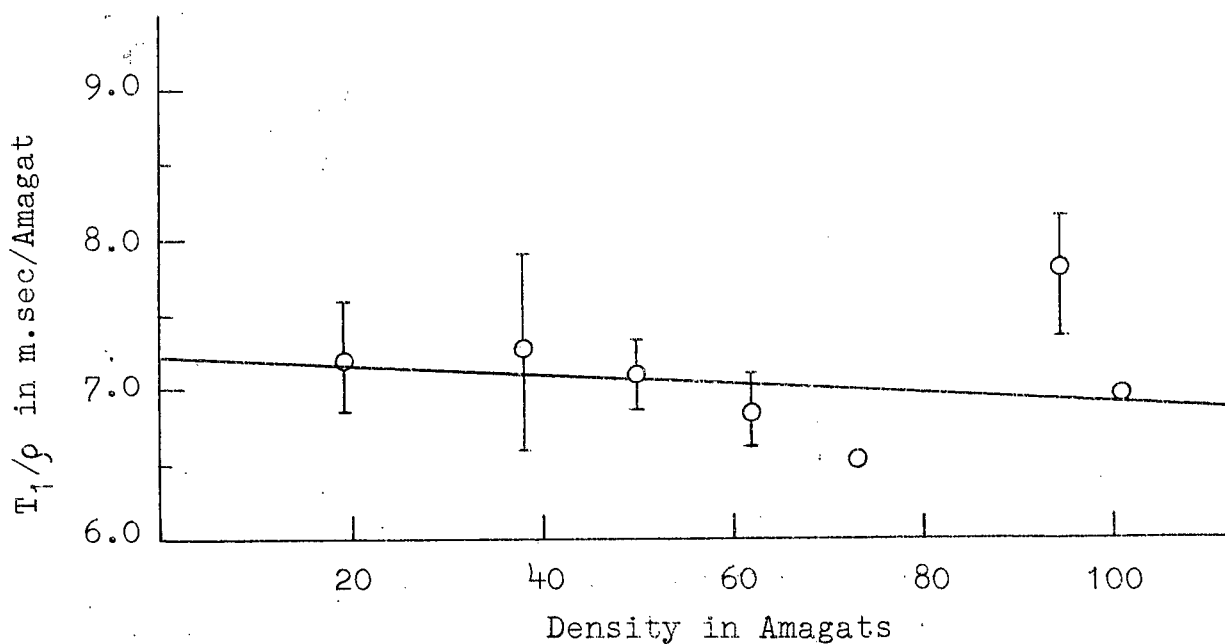


FIG. 34b. Dependence of T_1/ρ on density for CH₄-He mixture at 293°K.

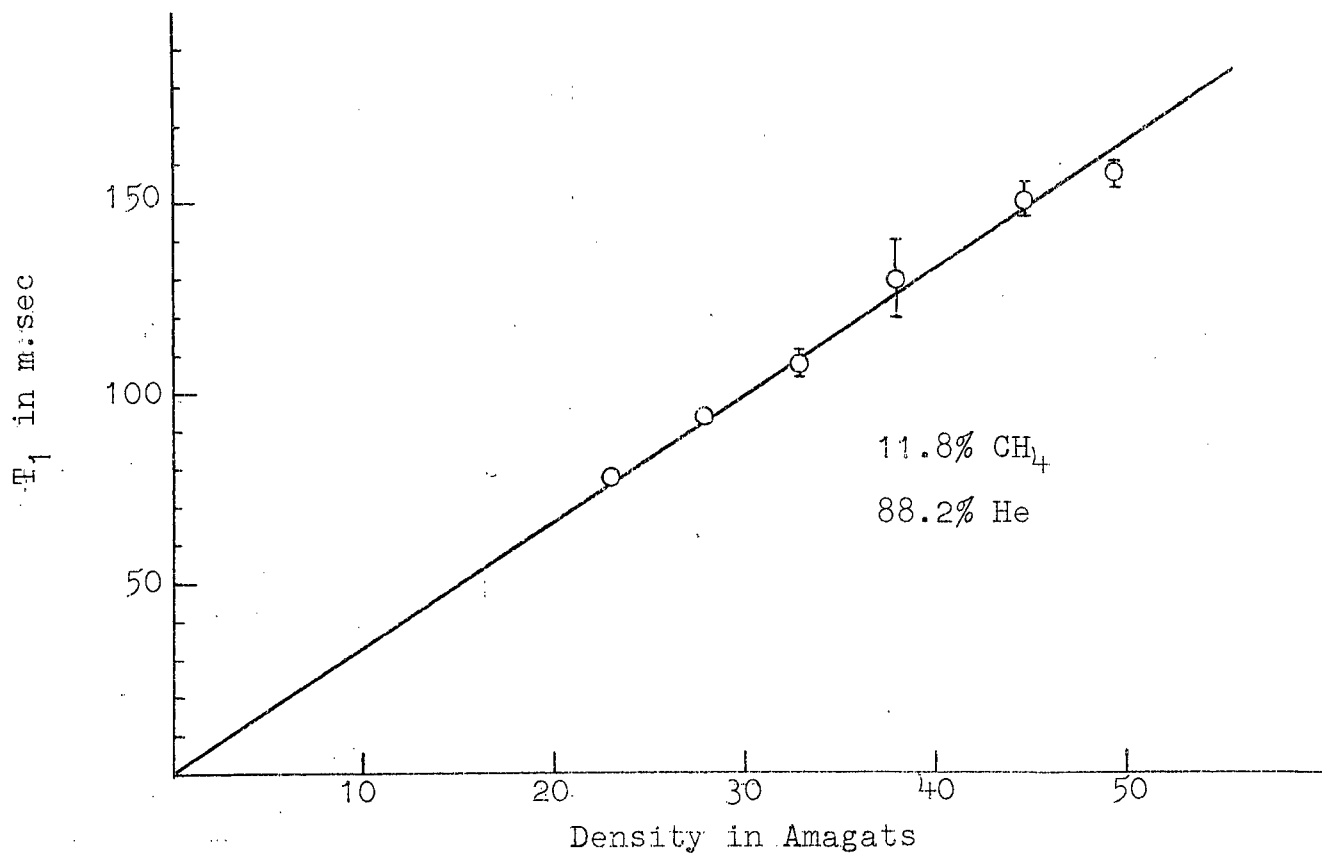


FIG. 35a. Dependence of T_1 on density for CH₄-He mixture at 730°K.

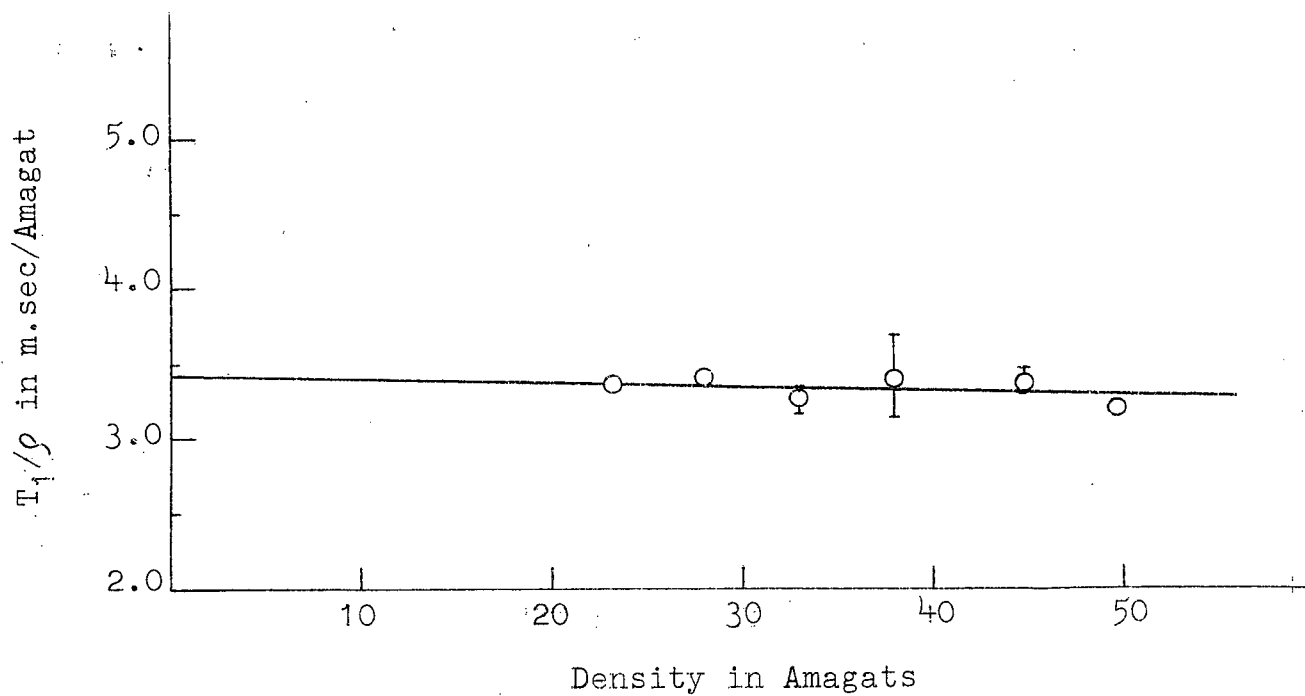


FIG. 35b. Dependence of T_1/ρ on density for CH₄-He mixture at 730°K.

The dependence of τ_1/ρ on the percentage of He at different temperatures is shown in fig. 36. At room temperature the dependence of τ_1/ρ on the percentage of He shows slight non-linearity for smaller percentages of He. In other words when the data of the mixtures is fitted by a straight line and extrapolated to 100% CH₄, the value obtained is about 15% smaller than the actual measured value. There are not enough data for low concentrations of He in the present work to establish this effect definitely. The effect disappeared with increase of temperature and is totally absent above 400°K. Therefore, it is perhaps necessary to do an experiment at around 200°K measuring τ_1/ρ in several mixtures with He concentrations between 0 and 25%. This is only a matter of curiosity and does not affect the purpose of the experiment since the values of interest are those extrapolated to 100% He. The value of τ_1/ρ extrapolated to 100% He gives the contribution due to CH₄ - He collisions alone. $\log(\tau_1/\rho)_{\text{CH}_4\text{-He}}$ vs $\log T$ is a straight line with a slope ≈ -0.8 and is shown in fig. 37.

5.2.2. Interpretation.

In the absence of a detailed molecular theory for the polyatomic gases the analysis of these results will be carried out on similar lines to that presented in Section (5.1.2.) Using the result given by equation (5.1.8.) and remembering that it is derived for the case of diatomic molecules and for the case of no transitions among different J states, τ_1/ρ can be written as

$$\tau_1/\rho \propto T^{-1.5} I(p, n) \quad (5.2.1.)$$

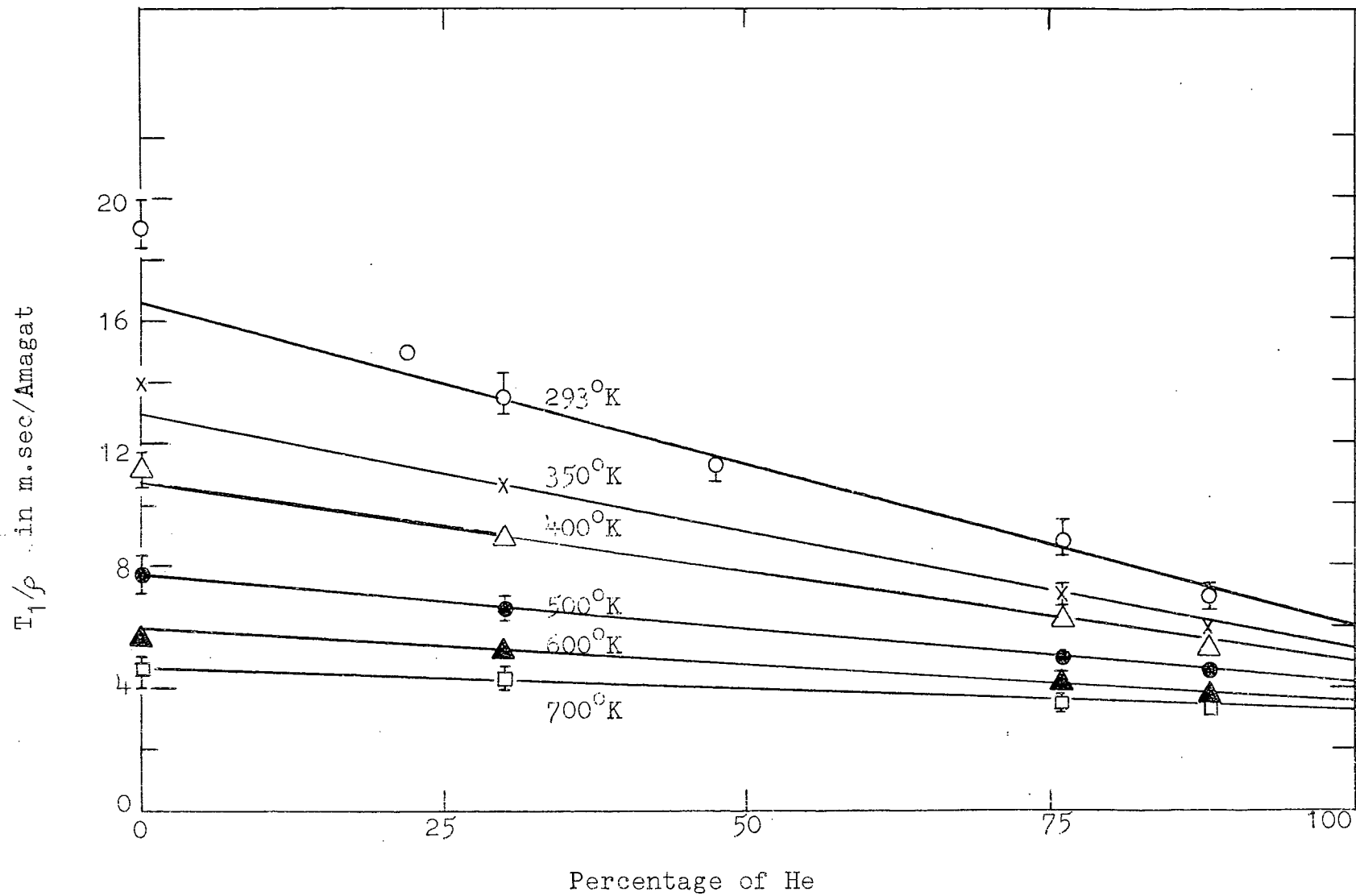


FIG. 36. Dependence of T_1/ρ on Helium concentration in CH_4 -He mixture.

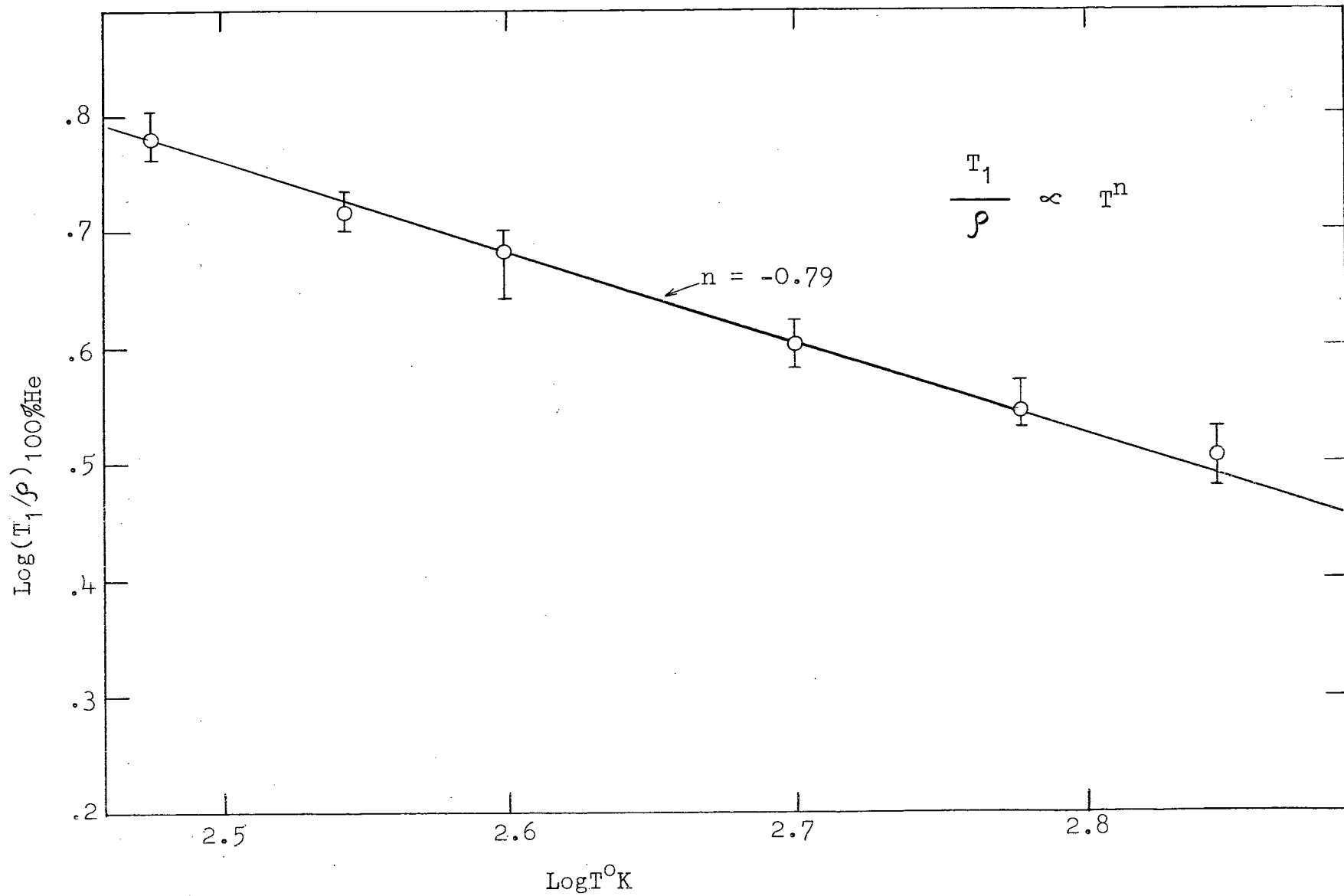


FIG. 37. $\text{Log}(T_1/\rho)_{100\%He}$ versus $\text{Log } T^\circ\text{K}$ for CH_4 -He mixture

Using the experimental result

$$T_1/\rho \propto T^{-0.8} \quad (5.2.2.)$$

the temperature dependence of $I(p,n)$ is obtained as

$$I(p,n) \propto T^{-0.7} \quad (5.2.3.)$$

Using equation (5.2.1.) and experimental value of

$(T_1/\rho)_{CH_4-He}$ the value of $I(p,n)$ is obtained at different temperatures and $[I(p,n)_T / I(p,n)_{293}]^{CH_4-He}$ is shown in fig. 38 as a function of temperature. The theoretical plots of the ratio as a function of temperature are obtained from the tables ⁸ using

$\epsilon_{CH_4-He} = \sqrt{\epsilon_{CH_4} \epsilon_{He}}$ for the cases $n=7$ and 9 . $n=7$ gives better agreement with the experimental results suggesting that the anisotropic intermolecular potential varies as $1/r^7$. However, this result should be considered as a qualitative indication that the interaction is a medium range interaction.

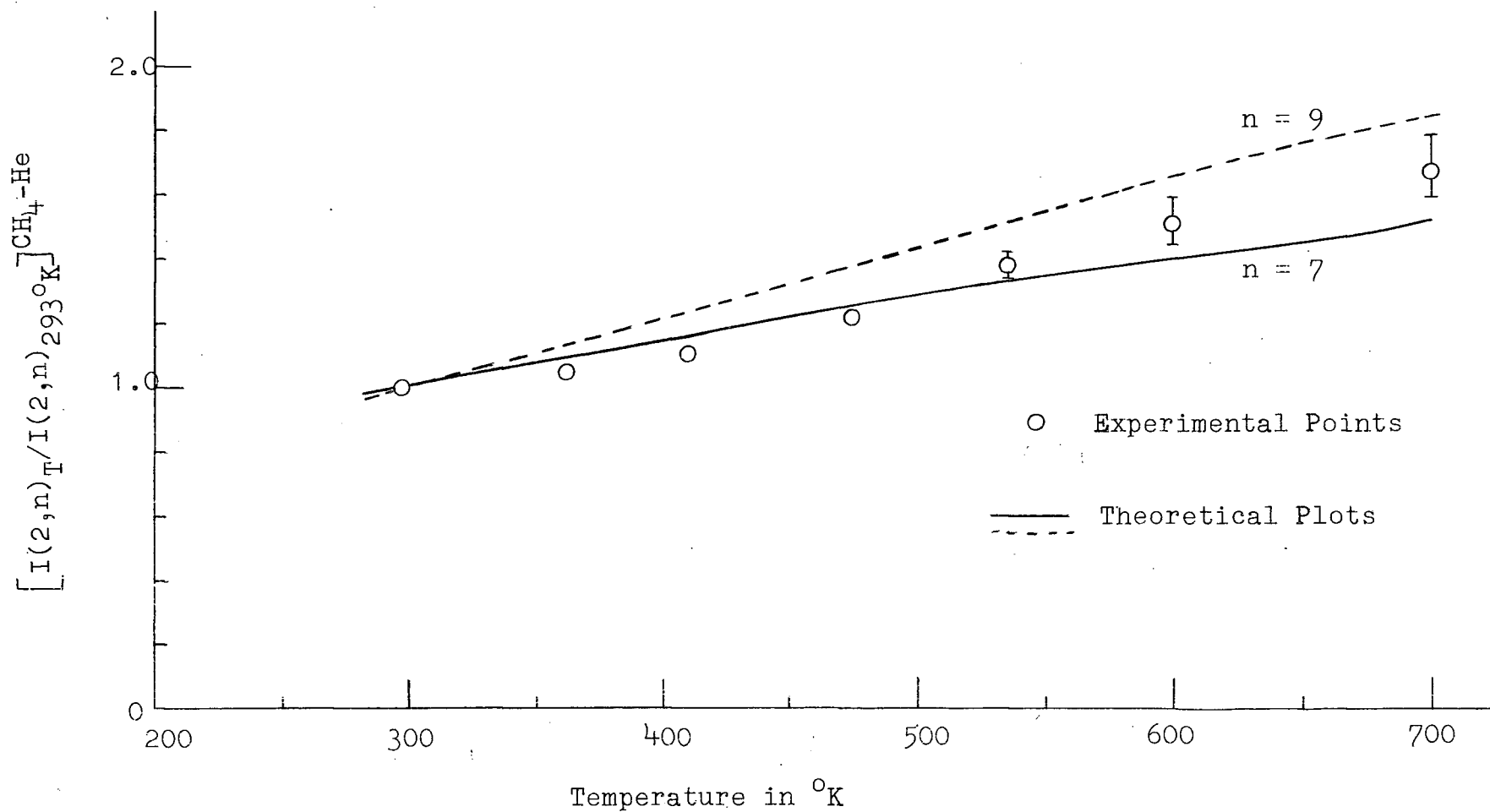


FIG. 38. Comparison of $\left[\frac{I(2,n)_T}{I(2,n)_{293^{\circ}\text{K}}} \right]^{\text{CH}_4\text{-He}}$ as obtained from Eq.(5.2.1) with the computed values using the numerical values of the integrals.

CHAPTER VI

CONCLUSIONS AND SUGGESTIONS FOR FURTHER WORK

The principal interest in the work presented in the preceding chapters is to obtain quantitative information on the anisotropic intermolecular potentials from measurements of the nuclear spin-lattice relaxation time. The results at temperatures below room temperature were interpreted by Bloom, Oppenheim et al.⁸ using a theory which assumed that the transitions between different J states are much less frequent than the transitions among m_J levels of the same J -manifold. Since then the theory has been generalised by Bloom and Oppenheim (to be published) to include the transitions between J states and is presented in Chapter III of this thesis. It was assumed in the analysis of the data that

(i) only two of the rotational states are significantly populated. This assumption is valid in the case of H_2 for temperatures below $500^\circ K$.

(ii) the total rotational angular momentum is conserved.

For H_2 only the ortho- H_2 molecules contribute to the N.M.R. signal. When the colliding molecule is also an ortho- H_2 the collisions in which angular momentum is conserved are resonant and when it is a para- H_2 the collisions are "quasi-resonant". The evaluation of the contribution to $Q_e(JJ')$ from these two types of collisions was discussed in Chapter IV. The analysis of the data at $200^\circ K$ indicates that the "quasi-resonant" collisions contribute about 30% to the effect of quadrupole-quadrupole interaction even though the population of $J=3$ state

is only about 3% at this temperature. It is also seen that the contribution of quadrupole-quadrupole interaction to τ_1/ρ is about 50% at 700°K and greater than that below 700°K. As this analysis gives a reasonably good value for the quadrupole moment of the H_2 molecule it can be tentatively concluded that the quasi-resonant terms can be taken into account in the simple manner as described in this thesis and the other non-resonant terms are insignificant. If $\omega_6^{(1)} = -1.85 \times 10^{12} \text{ sec}^{-1}$; the analysis indicates that $\mathcal{H}_R^{(1)}$ can be adequately described by an attractive part proportional to $1/n^6$ and a repulsive part proportional to $1/n^{12}$. However, it was found that the data can also be fitted by a Lennard-Jones potential in which case the value obtained for $\omega_6^{(1)}$ is $-3.3 \times 10^{12} \text{ sec}^{-1}$.

Since Lipsicas' results in normal H_2 are about 25% higher than the values obtained by other investigators it is possible that his values of $(\tau_1/\rho)_{0,0}$ and $(\tau_1/\rho)_{0,P}$ are also higher in the temperature region 150°K - 300°K. As this information is of fundamental interest it would be worthwhile repeating these measurements and extending the temperature range. Such a study would be able to establish conclusively whether or not the interaction between two H_2 molecules which depends on the orientation of both the molecules is adequately represented by quadrupole-quadrupole interaction.

For the H_2 - He mixture the theory predicts that the dependence of τ_1/ρ on $\tilde{\rho}_{He}$ is non-linear. Though the data at room temperature indicated this non-linearity, it is not enough to establish this effect definitely. As this effect is

a manifestation of the transitions of the H_2 molecule between different J states, one could not expect this effect to be present below $100^\circ K$ where all the ortho- molecules are essentially in $J=1$ state. The theoretical plots indicate that the deviation from linearity becomes smaller at higher temperatures. Therefore room temperature is perhaps the most suitable temperature to look for this effect. The analysis of the data indicates that the intermolecular anisotropic interaction between H_2 - He molecules can be adequately represented by Lennard-Jones potential.

For the H_2 - CO_2 mixtures the experiments were carried out only up to $500^\circ K$ because chemical reaction between the two gases prevented going to higher temperatures. The number density of the mixture was determined experimentally as described in Chapter II. The analysis of the results indicate that the dominant interaction between H_2 and CO_2 molecules can be represented by quadrupole-quadrupole interaction. In view of the chemical reaction H_2 - N_2 mixture would be a better system in which to study the quadrupole-quadrupole interaction between unlike molecules at high temperatures.

For CH_4 quite a large number of rotational states are populated even near room temperature and hence the theory for two-level system could not be used. In the absence of a rigorous theory for polyatomic gases, the result obtained for diatomic molecules with the assumption of no transitions between J states were used to obtain some information about the intermolecular potentials. T_1/ρ was found to be proportional to $T^{-1.5}$ for CH_4 which would be the case if the contributions from $I^{(q)}(\rho)$ to T_1/ρ is temperature independent. If the isotropic

part of the intermolecular potential is assumed to be given by hard sphere potential then the integrals $\int^{(v)}(\rho)$ are independent of temperature. This model predicts that $T_1/\rho \propto T^{-1.5}$ for other systems like $\text{CH}_4 - \text{X}$ as well. For the case when X is He it was found that $T_1/\rho \propto T^{-0.8}$. Therefore, a more realistic potential was assumed for the isotropic part of the intermolecular potential, namely the Lennard-Jones potential. The analysis of the temperature dependence of T_1/ρ suggests that the anisotropic intermolecular potential is proportional to $1/r^3$ and $1/r^2$ for $\text{CH}_4 - \text{CH}_4$ pair and $\text{CH}_4 - \text{He}$ pair respectively. However, these results should be considered more as qualitative than as quantitative and the anisotropic intermolecular interaction can be described as a medium range interaction.

As T_1/ρ vs $\tilde{\rho}_{\text{He}}$ in $\text{CH}_4 - \text{He}$ mixtures appears to be non-linear for smaller concentrations of He at room temperature, it may be interesting to investigate this effect. Since this non-linearity seems to increase with decrease of temperature it may be easier to study this at around 200°K. However to understand any of the results in polyatomic gases the molecular theory has to be improved.

APPENDIX A

CIRCUIT DIAGRAMS

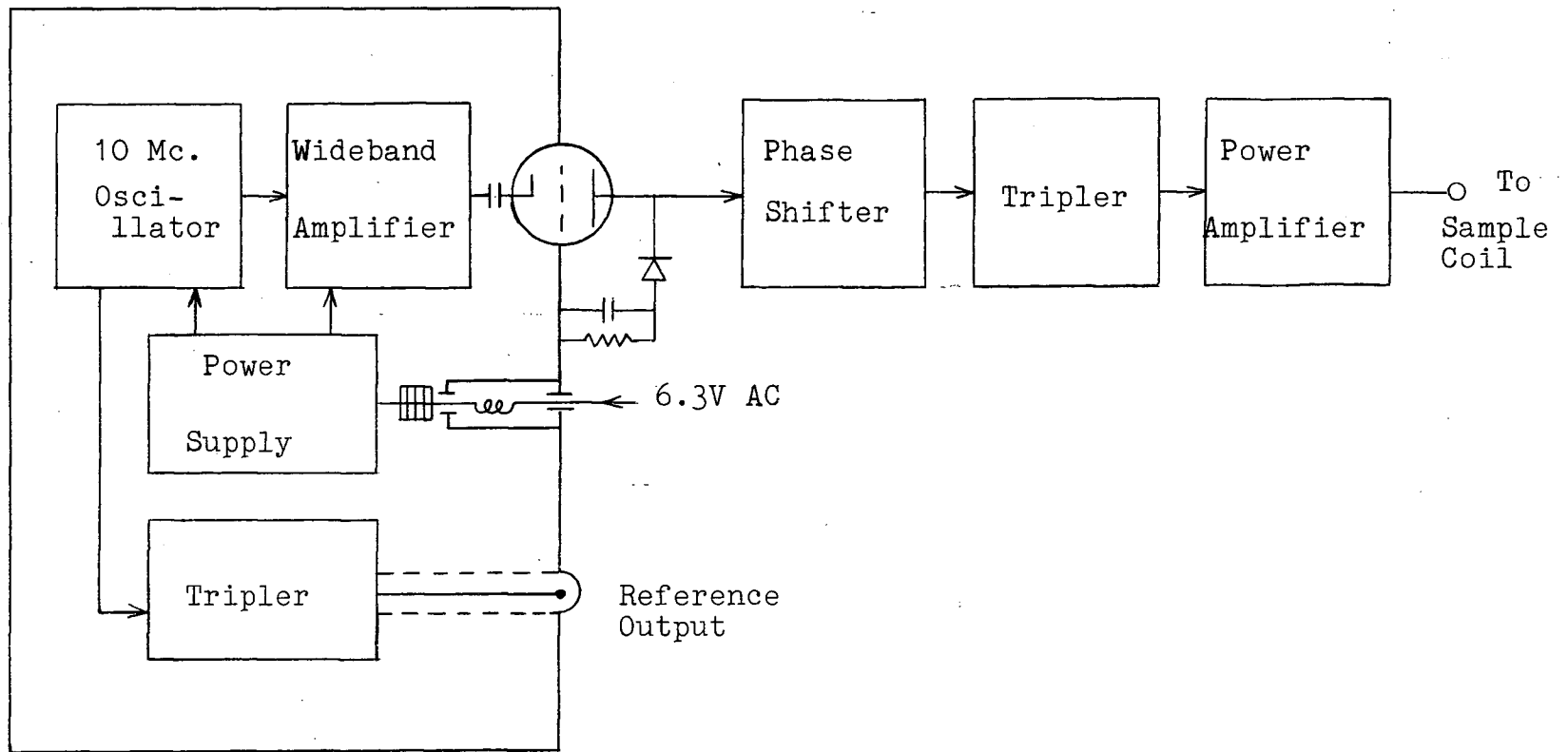


FIG. A1. TRANSMITTER.

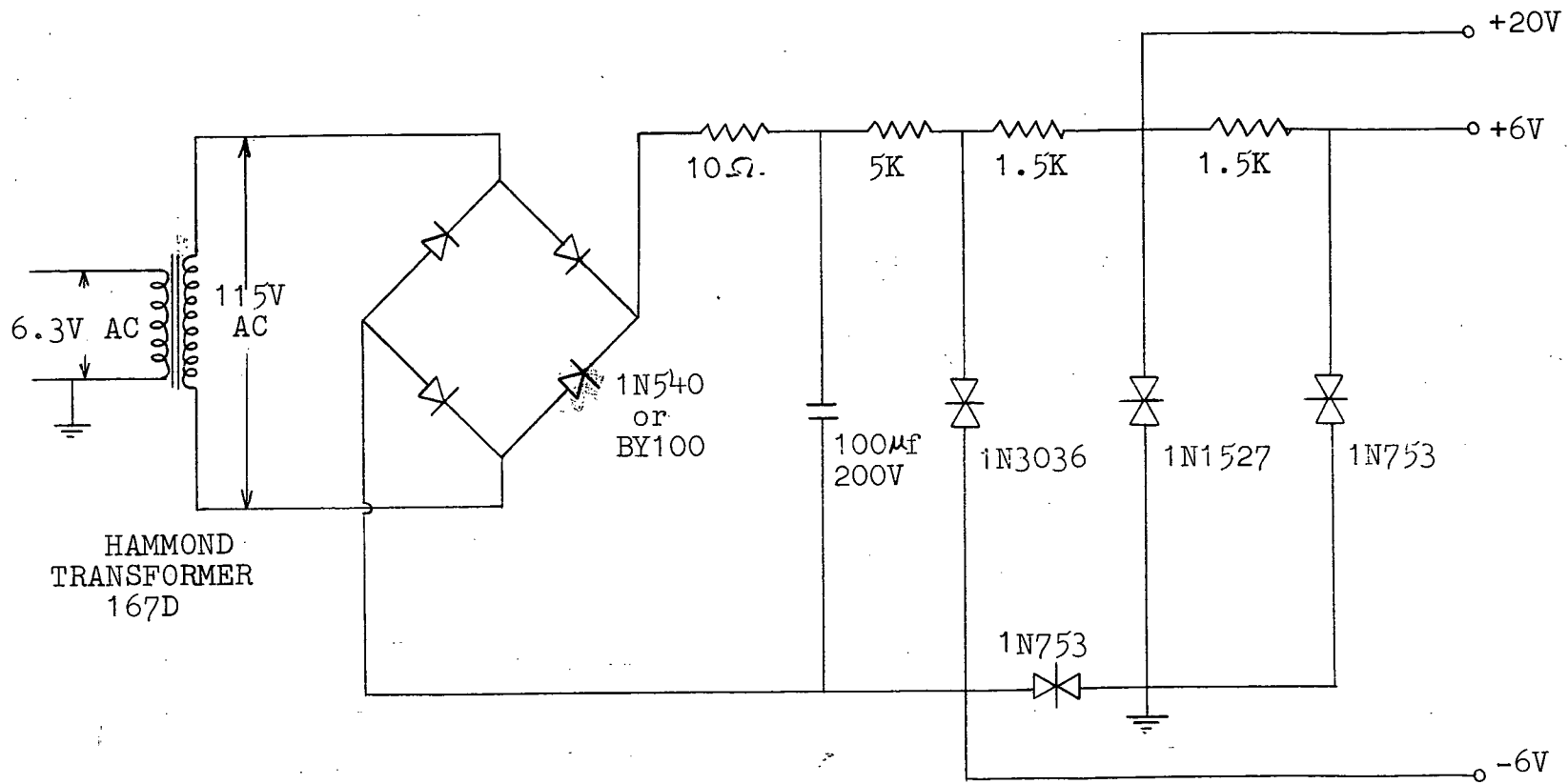


FIG. A2. POWER SUPPLY.

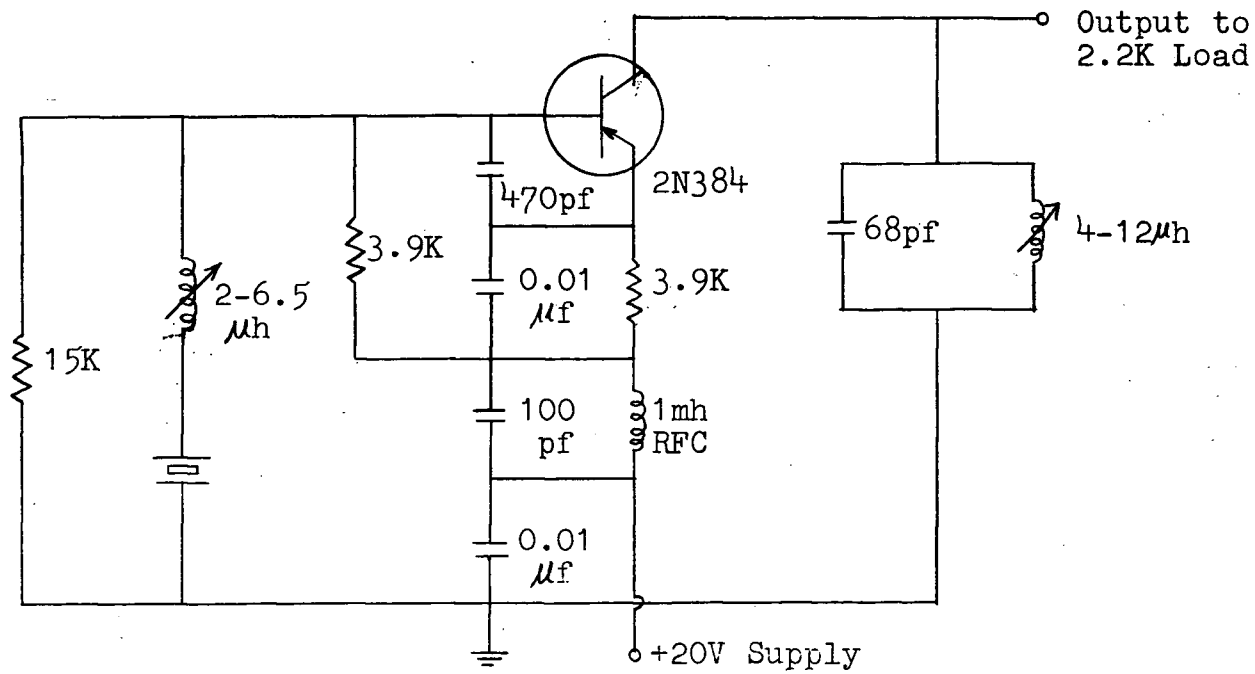


FIG. A3. 10Mc. CRYSTAL STANDARD OSCILLATOR.

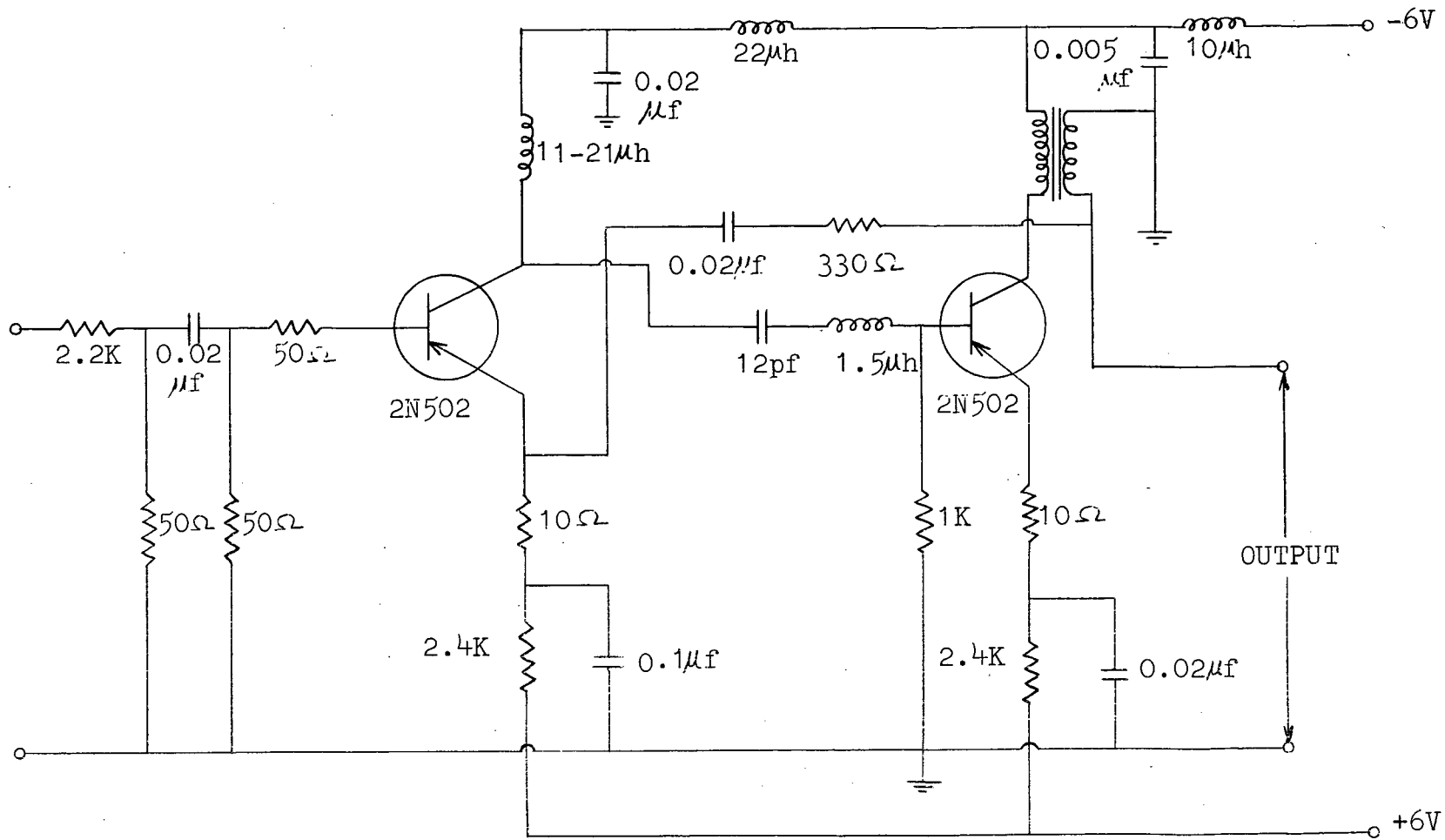


FIG. A4. WIDEBAND AMPLIFIER.

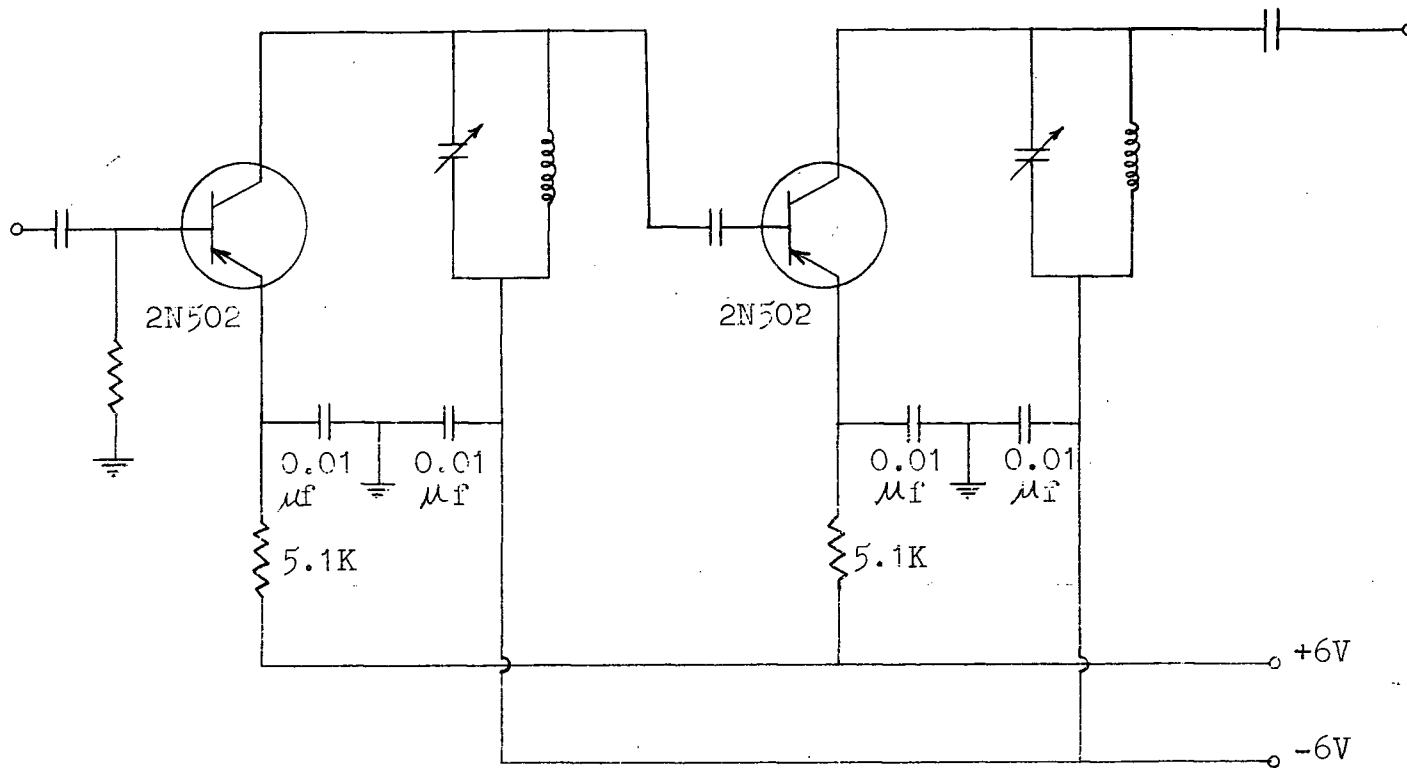


FIG. A5. 30Mc. TRIPLER.

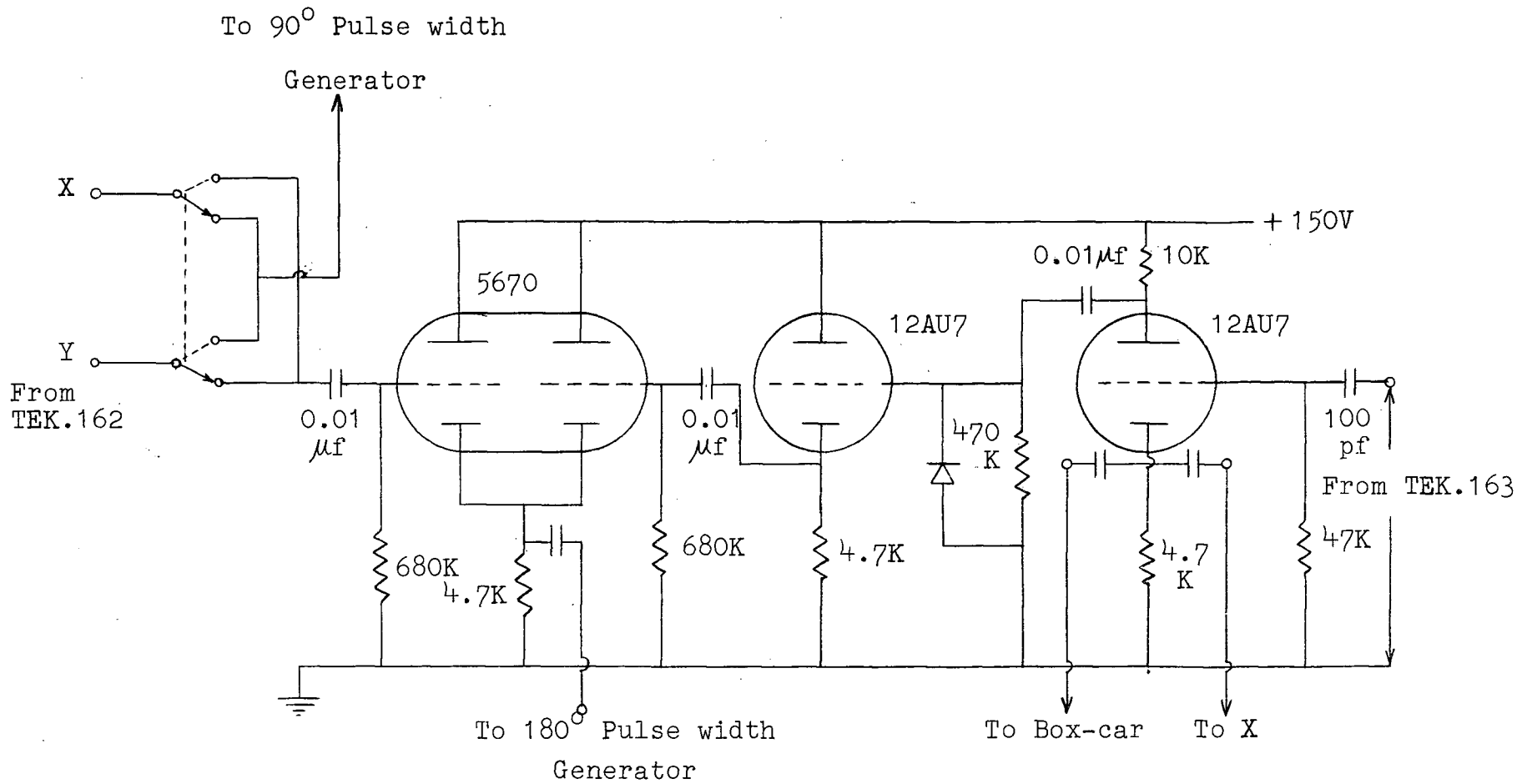


FIG. A6. PULSE SEQUENCER.

BIBLIOGRAPHY

1. A. Abragam: The Principles of Nuclear Magnetism, Oxford University Press, 1961.
2. F. Bloch: Phys. Rev. 70, 460, (1946),
3. N. Bloembergen,
E.M. Purcell &
R.V. Pound : Phys. Rev. 73, 679, (1948),
4. G.T. Needler &
W. Opechowski: Can. J. Phys., 36, 870, (1961),
5. G.S. Johnson &
J.S. Waugh : J. Chem. Phys., 36, 2266, (1962),
6. M. Bloom &
I. Oppenheim: Can. J. Phys., 39, 845, (1961)
7. M. Bloom &
I. Oppenheim: Can. J. Phys., 41, 1580, (1963),
8. M. Bloom,
I. Oppenheim,
M. Lipsicas, : J. Chem. Phys., 43, 1036, (1965),
C.G. Wade &
C.F. Yarnell
9. M. Bloom &
I. Oppenheim: To be published.
"Advances in Chemical Physics", a
volume on Intermolecular Forces,
edited by J.D. Hirschfelder (Interscience)
10. E.L. Hahn: Phys. Rev., 80, 580, (1950),
11. H.Y. Carr &
E.M. Purcell: Phys. Rev., 94, 630, (1954),
12. R. J. Blume: Rev. Sci. Instr., 32, 1016, (1961),
13. J.D. Noble: Ph.D. Thesis, University of British
Columbia (1965),
14. W.N. Hardy: Ph.D. Thesis, University of British
Columbia, (1965),
15. W.G. Clark: Rev. Sci. Instr., 35, 316, (1964),
16. P.W. Bridgmann: "The Physics of High Pressure",
G. Bell and Sons Ltd., London, 1949,

17. G.B. Benedek: "Magnetic Resonance at High Pressure" Number 24, Interscience Tracts on Physics and Astronomy.
18. H.W. Wooley,
R.B. Scott &
F.G. Brickwedde: Journal of Research of the National Bureau of Standards, Research paper RP 1932, 14, 379, (1948),
19. M.E. Rose: "Elementary Theory of Angular Momentum", John Wiley and Sons, Inc.
20. J. Van Kranendonk: Can. J. Phys. 41, 433, (1963),
21. D.Ll. Williams: Can. J. Phys., 40, 1027, (1962),
22. M. Lipsicas &
M. Bloom: Can. J. Phys., 39, 881, (1961),
23. Armstrong: Private Communication.
24. J.W. Riehl: Ph.D. Thesis, Massachusetts Institute of Technology (1966),
25. M. Lipsicas &
A. Hartland: Phys. Rev., 131, 1187, (1963),
26. J.O. Hirschfelder,
C.F. Curtiss &
R.B. Bird : "Molecular Theory of Gases and Liquids" John Wiley and Sons.
27. W.M. Graven &
F.J. Long : J. Am. Chem. Soc., 76, 2602, (1954),
28. American Petroleum Institute Project 44, Vol. III, Table I.
29. F. Bridges, M.Sc. Thesis, University of British Columbia, 1964.
30. M. Bloom,
M. Lipsicas &
B.H. Muller : Can. J. Phys, 39, 1093, (1961),
31. C.S. Johnson &
J.S. Waugh : J. Chem. Phys., 35, 2020, (1961),
32. N.J. Trappeniers,
C.J. Gerritsma &
P.H. Oosting : Physica, 31, 202, (1965).